POLITECNICO DI TORINO

Mechanical Engineering

Master's Degree Thesis

Aeroelastic instability of composite panels in supersonic regime/Instabilità aeroelastica di pannelli compositi in regime supersonico

supervisors
Prof. CARRERA ERASMO
Prof. PAGANI ALFONSO
Prof. ZAPPINO ENRICO

candidate
HUIFENG TAN

A.Y.2020-2021

Contents

List of Tables

List of Figures

Abstract

To study the aeroelastic instability of composite laminated panel under supersonic airflow, in order to analyze it by solving the generalized eigenvalue problem through aeroelastic properties. And generally by calculating the natural frequency of the laminated structure at different incoming flow speeds, the critical instability velocity of the laminated panel under the action of airflow is obtained, because the rigidity of the laminate structure decreases, resulting in the structure instability.

The structural parameters should be reasonably designed according to the mechanical environment of the composite panel to avoid structural instability problems under the action of airflow.Piston theory was originally developed by Lighthill, on the basis of the extension of Tsien's hypersonic similitude by Hayes.In the study of panel flutter, many researchers have proposed various aerodynamic computational models in order to better simulate the actual aerodynamic change process, However, the shortcoming of this aerodynamic model lies in the consideration of more complex boundary conditions, so the solution process of the equation is quite complex.

In the framework of structural mechanic,a two-dimensional models have been used in the derivation of refined aeroelastic models able to predict panel flutter of advanced structure in supersonic range with Piston theory.Piston theory has been used broadly to a number of aerodynamic models,which provides a quasi-steady, point-function relationship between the surface downwash and aerodynamic pressure at a point on a body. This renders piston theory a computationally inexpensive aerodynamic model.

In this thesis, The high-efficiency of the CUF tool allows any order model to be derived,Carrera Unified Formulation allows any models to be derived using a compact and unified formulation.A strong form solutions and the finite element approximation of the proposed CUF models.In the paper,the derivation of the characteristic matrices of the FEM for two-dimensional models,the fundamental nuclei allow the matrices to be derived using an automatic procedure. The Finite Element Method (FEM) still deserves important attentions due to its versatility and numerical efficiency. The various problems of the mechanics have been addressed, including static, free vibration and dynamic response problems. in order to analyze it by solving the generalized eigenvalue problem through aeroelastic properties,and many parameters have been considered to investigate their effects on flutter boundaries.

Keywords: *Finite Element Method,Piston theory,aeroelastic instability,aeroelastisity,Carrera Unified Formulation,supersonic,composite laminated panel.*

Acknowledgement

During the year of doing the thesis, I will not forget the help of Professor Pagani Alfonso and Professor Zappino Enrico. They both encouraged me to move forward from different angles and treated me bravely exploring the potential and the unknown during my study abroad. Professor Pagani once again accepted my shortcomings and gave me light every time I fell into confusion and life. This makes me grateful. Professor Zappino is optimistic and sunny, which is what I like most about him. He will always share his research experience generously and explain what I don't understand. His attitude towards research is the best lesson for me. There is also Professor Carrera Erasmo. Because of the two young and outstanding professors he brought out, he must also be a humorous and generous person. At first, I was shy and unconfident. It was him who silently accepted my shortcomings once. And one sentence awakened the direction of my thesis, which could let me persisted until now. I am fortunate to get teached from Professor Carrera Erasmo. Although I am not your phD student for the time being,but the direction in aerospace of aeroelastisity will become part of my knowledge reserve.
The past few years of studying and living in Italy was been difficult, but I am optimistic. Everything experienced here will be a very precious treasure. I am also very grateful for the encouragement and support from my family far from China, whom I haven't seen for many years. and Matteo.Z in Italy, His love makes me what I am today.
If a person can endure loneliness and endure the test of life, he will be the best himself. Come on, keep working hard.

Torino,Februry 20,2021

TAN HUIFENG

Chapter 1

Introduction

1.1 Panel flutter

Panel flutter is a self-excited vibration phenomenon that occurs on the surface of the aircraft during supersonic and hypersonic flight under the coupling action of aerodynamic, inertial and elastic forces. Although panel flutter is not as certain as wing flutter to cause serious flight accidents, severe panel flutter will have a very adverse effect on the fatigue life of the panel structure and even the flight performance of the aircraft. The research on panel flutter began in 1950s, and a lot of theoretical analysis and experimental research have been done on this phenomenon [1, 2].

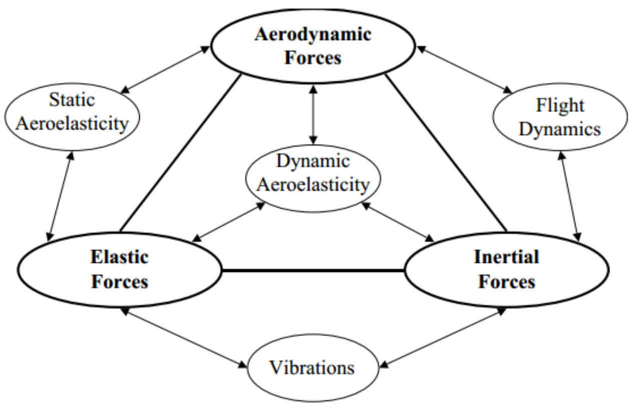

Figure 1.1: Aeroelastic triangle of forces

Study method of panel flutter

research contents

Due to the particularity of the panel structure, the panel flutter usually presents as nonlinear amplitude vibration, that is, limit cycle flutter. Therefore, the analysis of panel flutter needs to solve two problems: one is how to avoid the occurrence of flutter, and the other is the high cost of flutter when flutter cannot be avoided or cannot be completely avoided. so how to suppress the amplitude of the response [3],is that the panel in the design of the fatigue life will not be too violent of nonlinear flutter caused by fatigue failure.Therefore, from the point of view of aeroelastic mechanics [4], the first case can be attributed to aeroelastic stability problem [5], while the latter one is classified as aeroelastic response problem. Correspondingly, the panel flutter analysis includes two research contents:

- boundary of Linear panel flutter

The keypoint of panel flutter boundary analysis is to determine the critical conditions for the occurrence of panel flutter. On this basis, the influence of flow parameters, structural parameters, temperature distribution [6], surface stress distribution and other factors on the panel flutter boundary is analyzed, and the general law of various parameters affecting the critical velocity of panel flutter is summarized.

- Nonlinear flutter response analysis

The purpose of nonlinear flutter response analysis is to determine the magnitude of internal stress and the period of stress cycle, so as to determine the fatigue load spectrum of the panel. In addition, the transformation of nonlinear flutter response properties should be analyzed, because when the nonlinear flutter properties change, the periodic limit cycle flutter changes into chaotic flutter [7].The change of amplitude and frequency maximum probability of nonlinear flutter response, in which case the fatigue life of the panel is not continuously changing, such case should be classified into the structural fatigue theory.

In the study, it is found that the flutter problem of the panel is similar to the flutter problem of the wing structure [8], but it also has a unique property: as the local structure of the aircraft surface, the airflow only acts on one surface of the panel, and the panel is generally fixed on a solid frame. The bending deformation of the panel is constrained by strong structural geometric boundary, and the flutter amplitude is usually of the same magnitude as the thickness of the panel. Therefore, the flutter of the panel generally does not cause rapid structural damage, but more often causes fatigue damage to the structure.In the case of large deflection, the amplitude of flutter is related to the geometric nonlinear effect of the panel structure. This is the most obvious feature of the panel flutter problem that distinguishes from the wing flutter problem, especially when the panel is subjected to thermal loads.

Considering the diversity of structure in engineering practice, the panel model applied in mechanical analysis is also very diverse. There are many ways of categorizing from different aspects. It is divided from whether to consider the aspect ratio effect: when the length of the panel is much longer in other direction, the two-dimensional panel model [9] based on the assumption of infinite spread length can be adopted; if the aspect ratio effect of the panel is obvious, the three-dimensional panel model [10] should be adopted. From the materials of the panel are divided into: isotropic panel model [11], anisotropic panel model [12], composite panel model [13], viscoelastic panel model [14] and functionally graded panel model [15], memory alloy panel model [16], and metal wire composite panel model [17]. From the panel shapes are divided into: flat panel model [18], curved panel model [11], rectangular panel model [19], circular panel model [20], cylindrical shell panel model [21], irregular panel model,etc. From the boundary conditions,they are divided into: simply supported panel model [22], fixed supported panel model [23], elastic supported panel model [24]etc. Of course, the academic community has developed a lot of panel models to adapt to various complex situations in engineering.

But it is almost impossible to consider all cases in a model and run out an analytic solution. With the emergence of numerical analysis technology, especially the development of finite element technology, the establishment of three-dimensional finite element model of panel and the use of numerical methods to analyze the impact of various panel shapes, structural layout, boundary constraints and other factors on the flutter characteristics of panels are the most extensive research methods at present.

1.1.1 Aerodynamic theory

It is necessary to accurately calculate the aerodynamic force on the panel surface when studying the mechanical properties of the panel in airflow. At present, there are mainly four types of aerodynamic models applicable to the analysis of panel flutter, and they are based on different aerodynamic theories, namely potential flow theory, piston theory, aerodynamic theory based on Euler equation and aerodynamic theory based on N-S equation. The aerodynamic model adopted in the study is determined by the airflow condition on the panel surface.

Early research on the potential flow theory, analysis of aerodynamic force on the surface of the plate [25], based on the isotropic,irrotational and no sticky assumption, in the acceleration velocity potential equation, could be capable of embodying the of the air space three-dimensional unsteady effect and time effect, so in theory through the velocity potential equation and acceleration potential equation could obtain the information such as air pressure, velocity and density at any panel surface. However, because the details of the flow field are too complex, the aerodynamic expression can only be obtained after the potential flow equation is linearized. This aerodynamic calculation method is also known as the linearized potential flow theory.The linearized potential flow theory can only be applied to the calculation of the aerodynamic forces on the panel in the low-subsonic and low-supersonic flows if the nonlinear factors of the flow are not very strong. With the development of numerical analysis technology, some numerical analysis methods, such as finite difference method, finite element method or Mach box method, can be used to solve the potential flow equation [26]. However, due to the need to consider the influence of adjacent points in the numerical integration, the aerodynamic analysis method based on the potential flow theory has a low efficiency.

1.1.2 Piston theory

In potential flow theory, the panel surface at any point of the dynamic balance of the air mass should follow assumptions, this method of aerodynamic calculation is too concerned about the details of the flow field, because if assumes that the flow field in the group of particle momentum to the time rate of those changes in size and direction are the same as the forces acting on the particle, according to the law of conservation of momentum, the aerodynamic force on the plate is deduced, thus effectively simplify analysis and calculation. Piston theory is such a kind of simplified analysis method, the theoretical analysis of the process can be briefly as follows: assuming that supersonic airflow disturbance to other points in the content of a point on the surface of the influence can be neglected, which is to think that the interference of stress associated with the mean field of point only, like the piston movement in a pipeline pressure only related to the piston movement speed.Then according to the motion of the object surface, the parameters of each point can be obtained, and then the pressure distribution and aerodynamic force on the object surface can be further obtained. Obviously, the first-order piston theory does not consider the ternary effect, so can be used only in the case that the Angle between the Mach line and the free flow direction is very small in the supersonic flow, that is, the velocity increment in the flow direction is very small but the velocity increment perpendicular to the flow direction is very large. Thus,the disturbance generated on the surface approximately propagates along the normal direction of the object. The disturbance generated by one point on the panel surface has a very weak influence on other points. The piston theory omits the interaction between points on the surface of the panel and assumes that disturbances at each point on the surface of the panel propagate along the normal direction of the point, as disturbances propagated by pistons in a cylinder. The three available conditions of piston theory are: $\omega^{*2}Ma^2 >> 1$,$\omega^{*}Ma >> 1$, $Ma^2 >> 1(\omega^*$

Is the reduction frequency,Ma Is the Mach number of airflow).The piston theory is suitable when the Mach number of the flow is high or the vibration frequency of the object is high. In general wing flutter analysis, the Mach number range of piston theory is $Ma >> 2.5$ [26]. In the analysis of panel flutter, because the panel is a local structure, the frequency of flutter is generally high, so the lower limit of the applicable scope of piston theory can be extended to $Ma = 1.5$ about in Subsonic stage [27].

In the process of research, many researchers continue to improve the piston theory.Lighthill and Ashley et al. used piston theory to calculate unsteady aerodynamic forces in the 1950s[28],[29].In 1990, Chen Jinsong proposed the of local piston flow theory[30],in this theory, the reference velocity is set as the local flow velocity of the wing surface, which makes the unsteady aerodynamic force calculation of the surface with large relative thickness and Angle of attack solved.Yang Bingyuan[31] Based on local piston theory and deduced the unsteady aerodynamic equation and flutter analysis of the supersonic model with large Angle of attack, and the correctness of the analysis results is verified by wind tunnel test,but the shock expansion wave method in used is still an engineering method, which can not accurately calculate the aerodynamic force of complex shape.In 2005, Zhang Weiwei et al. used CFD method to calculate local flow parameters, creating a precedent for the combination of CFD technology in engineering method[32],its result is the limitation of local piston theory on shape, Mach number and Angle of attack is greatly reduced, but the method of modeling aeroelasticity in literature is difficult to carry out stability analysis.Ye Zhengyin et al. [32] developed local piston theory based on steady CFD technology, and used the local piston theory to calculate unsteady aerodynamic force and coupled the motion equation of the structure, so as to realize time domain simulation of hypersonic aeroelasticity.In 2011, Yang Bingyuan et al. [33] further extended and developed the local piston theory, and proposed a new method that can be used to calculate the flutter at large Angle of attack of three-dimensional complex structures such as wing-body complexes.In 2018,Guo J et al.[34] Based on the third-order local piston theory developed the unsteady aerodynamic equation of the lift surface and the nonlinear dynamic elastic response analysis,the software based on PCL and DMAP languages were developed by them, and analyzed the nonlinear dynamic elastic responses of the composite panel at room temperature and with temperature gradient.

1.1.3 Computational fluid dynamics,CFD

Gordnier [35] compared the piston theory with CFD analysis method of computational fluid dynamics, and found that when the Mach number was 1.2, the aerodynamic distribution on the panel surface obtained by the third-order piston theory was consistent with the aerodynamic calculation results based on the Euler equation, indicating that the piston theory had a high analytical

accuracy under certain conditions.
In order to analyze the aerodynamic force on transonic airflow panel, the commonly used method in recent years is the CFD method. CFD methods are commonly used in the study of panel flutter. One is to calculate the unsteady aerodynamic force on the panel based on the Euler equation assuming that the airflow is non-viscous, and the other is to calculate the aerodynamic force on the panel based on the N-S equation considering the viscosity effect of the air. In the hypersonic stage,in which the Mach number is above 10, There is a significant difference [36] between the aerodynamic force of the panel surface calculated by CFD method based on the N-S equation and that calculated by the piston theory. This method is conductive to a more comprehensive consideration of various influencing factors in the airflow.
Gordnier et. compared the piston theory with CFD analysis method of computational fluid dynamics, and found that when the Mach number was 1.2, the aerodynamic distribution on the panel surface obtained by the third-order piston theory was consistent with the aerodynamic calculation results based on the Euler equation, indicating that the piston theory had a high analytical accuracy under certain conditions.
The classification is summarized as follows:

CFD/CSD coupled aeroelastic time domain calculation method

In the high subsonic and transonic stages, the compression ratio effect of the flow is relatively significant, and the unsteady and nonlinear effects of the flow are very strong. Lucia[37],DeBortoli[38]nd Selvam[39] analyzed the aerodynamic force on the panel surface based on the Euler equation, while Atsushi [40] alculated the aerodynamic force on the panel and analyzed the nonlinear flutter response of the panel based on the N-S equation.
Visbal [41] provides a new physical explanation for the principle of panel flutter in subsonic airflow. Based on the nonlinear Von Karman theory, the structural equation of the panel is established, and the completely compressible N-S equation is solved to determine the aerodynamic force of the panel surface. In order to eliminate lagging errors, implicit iteration is adopted to solve the aeroelastic equation of the panel. The aeroelastic characteristics of the panel in the flow with a Mach number of 0.8 were analyzed, and it was pointed out that the static instability of the panel occurred first, followed by the Traverling Wave flutter (TWF). The frequency and wavelength of this wave have the characteristics of Tollmien-Schlichting wave (a disturbance wave formed during laminar boundary layer instability). Therefore, Visbal believed that the limit cycle flutter of the panel was due to the coupling of Tollmien-Schlichting wave and high-order elastic modes of the panel, so it would not occur at a small Reynolds number.

The research on panel flutter in supersonic flow began in the 1950s [42]. It is shown that 2D panel flutter in supersonic flow usually results from the coupling of the first two modes, and the flutter frequency is between the first two natural frequencies and closer to the second natural frequency[43]. Dowell [25] early study, such as using the galerkin method of nonlinear flutter analysis panel response, should take at least six order harmonic mode in order to get more accurate flutter response amplitude as a result, the analysis is in the panel stress conditions, due to the aerodynamic heating effect in the supersonic and hypersonic flow, plate temperature change will produce in-plane thermal stress, so panel temperature change is affecting on thermal flutter boundary and the thermal flutter response,which is an important factor. The critical velocity pressure of thermal flutter decreases with the increase of temperature.Cheng et [44] studied the influence of temperature distribution on the thermal flutter characteristics of the panel, and pointed out that the thermal bending moment caused by the temperature field distributed along the direction of the thickness of the panel causes the deformation and improves the equivalent bending stiffness of the panel, thus increasing the critical velocity pressure of the flutter. In this analysis, Librescu et [45] assumed the curve of elastic modulus and thermal expansion coefficient changing with temperature, and found that under some parameters, the decline of material elastic modulus caused by temperature rise would greatly reduce the critical flutter velocity of the panel.The results show that under the combined action of supersonic aerodynamic force and in-plane thermal stress, there are four kinds of dynamic responses to the disturbed panel in supersonic flow: attenuating oscillation and convergence at the initial equilibrium position, attenuating oscillation and convergence at the large deflection buckling position, limit cycle oscillation and chaotic oscillation. when the flow velocity Reaches a critical value, panel response amplitude from convergence to divergent, until structural damaged, in fact due to plate produced by the vibration of nonlinear surface tension can have the effect of hard spring in vibration, that is, with the increase of amplitude of surface tension the equivalent stiffness in the system increase, then reaches the critical value, when the flow velocity of the response amplitude is not divergent immediately, but there is a speed range, in this range when the flow velocity, plate continuous vibration, it is a kind of nonlinear vibration, the response in the phase space take the form of an isolated closed track, It's called limit cycle vibration. This is a form of vibration independent of the initial conditions, and the amplitude of vibration will increase with the increase of the incoming flow velocity.

Surace et [46] found that the impulse excitation or step excitation would affect the limit cycle shock response of the heated panel by changing the initial value of disturbance, which indicated that the panel aeroelastic system had strong nonlinear behavior.

Mei et proposed the concept of aeroelastic mode in the early stage of improving the computational efficiency of finite element analysis of panel flutter, and developed the frequency-domain analysis method LUM/NTF [47]. The McIntosh[48] and Eastep[49] were the first to combine the structural nonlinear effect and aerodynamic nonlinear effect to study the panel flutter in hypersonic airflow.The nonlinear flutter response of the panel is obtained by solving the differential equation of the flutter motion using Rayleigh-Ritz method and numerical integration method. The influence of the aerodynamic nonlinear effect on the flutter characteristics of the panel is analyzed in detail. It is concluded that the effect of aerodynamic nonlinear effect on the flutter characteristics of the panel and the effect of "soft spring" of geometric nonlinear effect of the structure reduce the equivalent stiffness of the flutter system with the increase of amplitude, which usually also reduces the critical velocity of the flutter. Friedmann has applied Euler equation aerodynamic theory, N-S equation aerodynamic theory, and piston theory to the analysis of panel flutter in hypersonic flows. In the stage of hypersonic flow Mach number of 10, nonlinear effect is very strong, plate amplitude value and the calculated results are obtained by the first-order piston theory by limit cycle flutter based on the theory of the third order piston to vary between $5\% - 7\%$, turbulence viscosity effect is very strong at the same time, based on the Euler equation of aerodynamic force and panel surface aerodynamic theory higher than aerodynamic calculation results based on navier-stokes equation. However, the computational efficiency of the CFD method based on Euler equation and N-S equation is low and time-consuming.In 1970 one of the authors observed an early finite element analysis where in the airframe of the F-111 aircraft was modeled with a 5,000 degree-of-freedom system and the computations carried out by an IBM 360 computer with computation time of one week. Today that same simulation would be carried out on the personal computer with computational time of a few seconds. Conventional FEA models contain millions of degrees of freedom with modeling of multiple physical phenomena.

J.J. McNamara et [50]tried to introduce system recognition methods into time domain analysis and compared three methods for time domain frequency and damping recognition, including Moving Block Method (MBA), Least Square Curve Fitting Method (LSCFM) and Autoregressive Moving Average (ARMA). The calculation of the example model shows that the introduction of system identification method and coupling calculation can effectively improve the computational efficiency and reduce the computational cost. ARMA shows higher computational efficiency, and its computational cost can be reduced by nearly 75% compared with MBA method.

At present, there are many researches on the vibration analysis of panels, but most of them focus on classical boundary conditions. This means that when the panel is heated, no deformation is allowed at the boundary, leading to a generally low critical buckling temperature rise of the panel. However, this is not in line with the reality, because it is mainly based on two points:

first, the support structure has a certain degree of flexibility, and the in-plane deformation cannot be completely restricted. Second, considering the heat conduction effect, the panel support and other structural parts will also be heated to expand, so as to reduce the thermal stress on the panel.

In fact, the real boundary conditions of the aircraft surface panel are much more complicated, and it is difficult to describe them accurately with classical boundary conditions. In contrast, elastic boundary conditions are more universal and flexible, and can be reduced to classical boundary conditions. In recent years, Li et [51] proposed a modified Fourier series method to analyze the vibration of beams and plates under arbitrary boundary constraints. The calculation results show that the modified Fourier series method has good convergence and accuracy. However, the structural models used for flutter analysis of panels are generally isotropic panels with simple classical boundaries, while the studies on elastic boundary panels are mainly free vibration studies. At present, it is rare to directly combine the vibration analysis of elastic boundary plate with aerodynamic force. Zhou [52] proposed a flutter analysis method for Mindlin plate in supersonic flow with elastic boundary conditions, and analyzed the influence of flow deflection Angle and temperature on the flutter characteristics.

The use of materials for panel flutter has been developed for half a century. At present, intelligent material structure technology is one of the starting points for the control direction of panel flutter in the past years. It has been used in wind tunnel test for a long time. After placing the piezoelectric brake on the front edge of the panel and optimizing the control, the critical flutter velocity pressure of the composite panel in supersonic airflow can be increased by 20%-30%. [53]

Nowadays, the hypersonic panel need much higher requirement under the higher speed, greater pressure load, higher temperature and thermal load, and the large deflection of the composite. the structure of the panel is more of a thin-walled structure was adopted in the design of aeroelastic analysis, which is particularly important study. And the theory of panel flutter analysis has been gradually mature and systematized. It is an important task for aeroelastic researchers to learn from previous experimental results and design more optimized wind tunnel tests to verify the theoretical analysis of panel flutter.

1.1.4 Aeroelastic Stability Analysis of Composite Plate

The structural model used for flutter analysis of panels is usually a simple classical panel with isotropic boundary, while the research on elastic boundary panel is mainly about free vibration.As mentioned above, the Mach number range of airflow generally applicable to the test of panel flutter is from subsonic to supersonic.Therefore, it is of great significance for the dynamic analysis and design of vehicle structures to study the vibration characteristics of composite laminates panel under specific airflow and to calculate the critical instability velocity of the structures.

Many scholars have done a lot of meaningful work on aeroelasticity, but most of them focus on supersonic aeroelasticity.For example,Song et[54] studied the aerothermoelasticity of composite sandwich panels in supersonic airflow, analyzed the influence of different sandwich parameters on the aerothermoelasticity of the overall structure by using the frequency domain method, and compared the aerothermoelasticity of the structure when two-dimensional sandwich panel and three-dimensional sandwich panel were adopted.Mahmoudkhani et [55] studied the aerothermoelasticity of composite laminated cylindrical shell in supersonic flow and considered the influence of pre-strain on the stability of shell. Vedeneev[56] studied the aeroelasticity of semi-infinite flat plate under the action of unilateral supersonic flow by discussing the eigenvalue problem.

For subsonic aeroelasticity,Many scholars have studied the aeroelastic stability and nonlinear vibration of two-dimensional plate structures by using the subsonic two-dimensional plate aerodynamic model of Bisplinghoff et[57] study. Dugundji et[58] used Galerkin method to study the critical instability and flutter problems of two-dimensional thin plates with elastic support on opposite sides under subsonic conditions. Tang et[59] used the vortex lattice aerodynamic model based on the theory of lift surface to study the limit cycle motion of two-dimensional thin plates with fixed supports at the lower end of subsonic conditions and free supports at the other end. Zhao et[60] studied the modal changes of the cantilever plate after aerodynamic instability, and compared with the experimental results. Korbahti et[61] studied the aeroelastic stability of orthotropic plates in subsonic flow field based on the compressible aerodynamic model of linear potential flow theory, and discussed the influence of different ratio of length to thickness on the instability velocity of plates. Yao et[62] studied the dynamic stability and nonlinear vibration of four-sided simply supported two-dimensional composite laminates under subsonic airflow.

At present, the existing researches mainly focus on the aeroelasticity analysis of the supersonic lower plate and shell structure, but the research on the subsonic aeroelasticity of the three-dimensional plate and shell structure is relatively few.

On the basis of experiments in the above literatures, some scholars found that the different structural parameters of the panel have a certain influence on the critical instability velocity. As the width increases, the critical instability velocity of the plate decreases gradually. When width approximates 30m, the difference between the critical instability velocity and the result in literature [63]is less than 0.1%. At the same time, with the increase of the incoming flow velocity, the fundamental frequency of the structure decreases gradually. When the fundamental frequency decreases to 0, the corresponding incoming flow velocity is the critical instability velocity of the structure. The specific critical instability should be related to the set boundary conditions of the panel, the geometry of the panel, the material performance of the panel, the laying Angle of each layer of the composite panel and the inflow velocity of the airflow. The experiment shows that the larger the width of the laminate is, that the closer it is to the two-dimensional plate, so the lower the critical instability velocity of the structure, the more likely the structure is to be unstable. Also with the gradual increase of the laying Angle of the laminated plate, the critical instability velocity of the plate first increases and then decreases, indicating that there is an optimal laying Angle.The optimal laying Angle of laminate is related to its own structure size. One possible conclusion is that the optimal laying Angle can be determined by calculating the curve of the critical instability incoming flow velocity with the laying Angle of the laminate.

1.1.5 Flutter Suppression active control

When the flight speed reaches the critical flutter speed, the self-excited vibration will lead to catastrophic results. The active flutter suppression technology is to transform the previously unstable mode into stable mode through closed-loop control.

Active flutter suppression is not a new idea.Active flutter suppression is an alternative to passive flutter solution. An active system offers a means of artificially stiffening and damping the aircraft structure to increase the flutter speed by using aerodynamic control.In the study of active flutter suppression, intelligent materials such as piezoelectric electromagnetostrictive materials and shape memory alloys have been paid more attention. However, shape memory materials are mostly used in adaptive wings, focusing relatively on aeroelastic control (improvement of lift-drag ratio, etc.), while the research on flutter suppression is still in the in-depth exploration stage.

Shape memory alloy has the advantages of high damping, large restoring stress, large strain capacity and strong anti-fatigue performance, so it will play a great role in the future flutter suppression application research. A few years ago, a device called dynamic vibration absorber was used to suppress the vibration of two-dimensional wing limit cycles[64, 65].After that, many scholars have tried to suppress the flutter of the panel of hypersonic vehicle based on dynamic vibration absorber.Not only the geometrical nonlinearity of the structure, but also the aerodynamic nonlinearity is considered.The experimental results show that the flutter suppression is effective and the critical flutter velocity is improved.

1.2 Composite materials

With the rapid development of high-speed carrier vehicles and aircraft, Especially the rapid development of material science since the 1980s,most of the materials used in high-speed aircraft are composite materials.This is because the composite material has high specific strength and high specific stiffness, but its lightweight and low damping characteristics make the aeroelasticity problem of aircraft structure more prominent. Therefore, the study on aeroelasticity of modern aircraft will be of more and more important significance.The application of composite materials has been extended to various fields such as transportation vehicles, medical devices, construction engineering and new energy manufacturing, etc.And composite material components are required to maintain high stability and reliability in complex working environments and emergencies.single-track composite laminates have two different mechanical properties in transverse and longitudinal directions, so they have the characteristics of orthogonal anisotropy. When the Layer Angle changes or the laying position of damping layer changes, composite materials will show more comprehensive mechanical properties than traditional materials.There are many types of composite materials and their mechanical properties differ greatly.

Two-dimensional Laminate Theory has been widely applied due to its high computational efficiency. For example, Classical Laminate Theory (CLT) [66] based on Kirchhoff-Love hypothesis can achieve better results for thinner laminates, but higher results for thick plates.In order to use the same formula for the calculation of thin and thick laminated plates, the laminated plate theory with shear deformation is applied.The first order shear deformation theory (FSDT)[67] based on Reissner-Mindlin hypothesis introduces shear correction factor, which is suitable for the calculation of thin and thick laminated plates.Shear correction factor can be obtained by shear strain energy prediction [68] and correction method[69].The zig-Zag theory can be obtained by adding the redefined FSDT theory of zig-Zag function and the redefined HSDT theory (RHSDT)[70], respectively. The above laminated plates theory only has analytical solutions in a few cases. For most engineering problems, finite element method is needed for numerical analysis.

In earlier study, Dixon[71] with the limit cycle vibration of rectangular composite laminates is studied by using a plate element with 24 degrees of freedom.Gray et,al.[72][73] studied the nonlinearity of composite laminates in hypersonic flow, as well as the layering Angle and sequence of the laminates, which will affect the stability and flutter mode shape of the laminates.Jehad[74] and Kouchakzadch[75] studied the nonlinear flutter of composite laminates by means of the Galerkin method.Kouchakzadeh et al. [76] studied the nonlinear aeroelasticity of composite laminates in high-speed flow field, and analyzed the influence of in-plane load, static pressure difference, fiber direction and aerodynamic damping on the nonlinear aeroelastic characteristics of plates.The results show that the fiber direction has a significant effect on the dynamic characteristics of the plate and the asymmetric characteristics of the plate change the vibration performance of the limit cycle.Abdel Motaglay et al.[77] proposed a finite element formula for the effect of arbitrary directional inflow on the large amplitude supersonic flutter of composite plates, and analyzed isotropic and orthotropic composite plates in yaw supersonic flows.Singha and Ganapathi [78] used shear deformation finite element method to study the influence of system parameters on supersonic flutter characteristics of composite laminating plates. The influence of aerodynamic force, structural damping and thermal load on the critical dynamic pressure is analyzed.Yang Chun et al. [79]studied the thermal flutter of composite panels by using a step-by-step solution method, and obtained the relationship between the critical flutter velocity and temperature rise of three different layers composite panels.Yang G et al.[80] applied finite element method to study the influence of airflow deflection Angle and thermal load on the flutter characteristics of composite panels of different shapes, and analyzed the variation of critical dynamic pressure of composite panels of different shapes with temperature rise and airflow deflection Angle.

1.3 Goal of this thesis

In the paper, a large review of the remarkable results found in literature related to panel flutter study in Piston Theory and WT test have been studied. Aeroelastic phenomena is a multidisciplinary problem,not only one solution for certain one case.During the Aeroelastic instability study,many parameters have been considered to investigate their effects on flutter boundaries at different flow regimes, also a preliminary computational analysis in numerical results have been analysed in supersonic range.At the same time, this article summarizes and sorts out the effective theoretical computational methods and experimental basis for future research on aerodynamic methods for the analysis of panel flutter phenomena.

Chapter 2

State of the Art

Aeroelasticity of panel flutter has been studied for a long time.Panels are normally designed to avoid flutter. It occurs most frequently in a supersonic flow. At subsonic speeds, the instability more often takes the form of a static divergence or aeroelastic buckling. In a linear theory, the critical flutter condition represents a sustained harmonic oscillation. On the unstable side of the flutter boundary, the amplitude of oscillation increases exponentially with increasing time, while on the stable side of the boundary it subsides exponentially. Experimentally, however, a different situation usually arises. The panel lies in a flow that is turbulent so that on the stable side a random oscillation of small amplitude, is observed; on the unstable side, the growth in amplitude of oscillation is limited by the nonlinear effects of membrane tension so that a steady limit cycle oscillation is normally observed ,cited from NASA report[81].This is a form of vibration independent of the initial conditions, and the amplitude of vibration will increase with the increase of the incoming flow velocity.In general, catastrophic structural failure will not occur immediately after the occurrence of flutter, but often takes the form of limit cycle vibration, which is a kind of stable limit cycle flutter.This stability limit cycle flutter often leads to fatigue failure of the structure (also mentioned above in Introduction).

So the study of panel flutter is helpful to deepenly understand the aircraft structure mechanism.Therefore,the design parameters on the stability boundary of panel flutter can be found to guide the aircraft study during the course of the highspeed aircraft panel design work. On the other hand, the research content of panel flutter involves some basic theories of fluid-solid combined vibration, including analysis method, modeling method and control method. It is widely used in those fields, including wing flutter and wind engineering, such as air flow around long-span bridge Beam, cable, flow of high-rise buildings, mechanical engineering such as flow of fluid in elastic pipes, turbine winding internal flow of machine blades and nuclear engineering such as flow around heat exchanger blades. So the further study of the fluid-solid combined vibration and its stability is not only of great theoretical significance but also of great importance application value.

2.1 research background

An American fighter aircraft in flight crashed in the 1950s, according to a survey, is caused by the wall panel flutter hydraulic line near the fracture is the main cause of the accident of the 50s, NASA (National Aeronautics and Space Administration, NASA) technology demonstration machine X-15 (a rocket booster can flying under high altitude 90000 meters, Mach number is seven of hypersonic flight vehicle) on the tail part of the first flight of elongated panel plate and the fuselage side fairing wainscot have experienced violent flutter phenomenon.The test results show that the flutter of fairing wainscot at the dynamic pressure of 0.305 atmospheres has aroused wide concern in the aviation engineering field about the safety of the panel flutter of supersonic aircraft.Later in the 1960s ,the Saturn rocket (Apollo project) and Atlas Centaur in the research of carrier rocket, and the U.S. air force pneumatic thermal Elastic structure system environment test project, ASSET.A considerable amount of manpower and material resources have been invested in the research of panel flutter.In the 1970s and 1980s, the United States put forward the design requirements to prevent the flutter of the skin panel in the issued «NASA spacecraft design specification » and « aircraft structure general specification ».

Flight practice before the 1970s shows that panel flutter usually occurs during supersonic flight. This was related to the material selection and structural arrangement of the aircraft at that time.In traditional metal aircraft, panel flutter is a classic supersonic aeroelastic phenomenon. However, with the application of modern new materials and the updating of aircraft design concept, new characteristics begin to appear in the problem of panel flutter.In 1992, about half of the composite skin of the F-117A stealth aircraft was cracked due to panel flutter during a test flight.On the other hand, the design of the second generation reusable Launch Vehicle (RLV) proposes a new concept for the thermal structure.This design, which combines bearing structure with thermal protection System (TPS), enables the panel structure to withstand the thermal load caused by aerodynamic heating, resulting in the thermal flutter on the panel at the hypersonic stage.Since the 1990s,some aerospace Vehicles and High performance plane has been developed by the US National Aerospace Plane (NASP), Space Launch Initiative (SLI), High Speed Civil Transport (HSCT), technology demonstrator Aircraft X-33, X-34, X-38 and high-performance fighter aircraft YF-22,JSF.At that time, there was a new wave of research and development in the engineering field for the

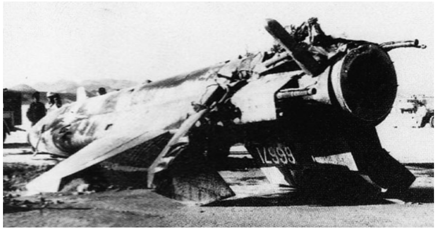

(a) X-15

(b) X-20

(c) S-IVB

(d) F-117A

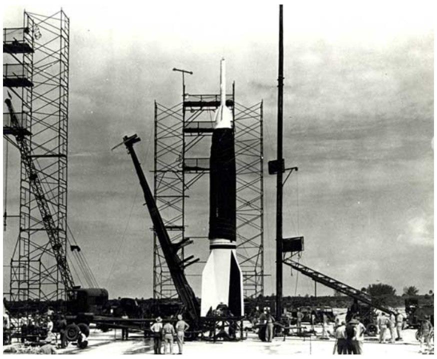

(e) V-2 bomb

(f) Saturn rocket V-5

Figure 2.1: Aircrafts with panel flutter during flight test

thermal flutter of panels and the flutter of composite panels.
In 1970s,panel flutter has occurred on the X-15 during flight operation[82],

during wind tunnel tests in the development program of the X-20 [83, 84, 85], on Titan I1 and I11[86], and on the S-IVB[87].The structural damage resulting from panel flutter was judged destructive on the X-15,and the X-20. The structure of these vehicles was stiffened to prevent panel flutter throughout the flight envelope. For the Titans and S-IVB, the flutter was judged non-destructive because it was determined that the severity and duration of the flutter would not be great enough to degrade unacceptably the structural integrity of the panel. Hence, no stiffening was added (no weight penalty incurred) to prevent flutter of these panels.

(a) X-33

(b) X-34

(c) X-38

(d) YF-22

Figure 2.2: development of research in the engineering field for the thermal flutter of panels and the flutter of composite panels

The occurrence of flutter in a particular panel configuration depends upon the mass,damping, and stiffness of the panel; local Mach number, dynamic pressure, density;in-plane flow angularity; boundary layer profile and thickness.

The parameters affecting panel stiffness which are reflected in panel natural frequencies include the panel length, thickness, material modulus, length-to-width ratio, edge conditions, curvature, orthotropy(variation in stiffness with direction),in-plane loads, transverse pressure differential across the panel, and

acoustic cavity (closed-in space) beneath the panel.
Therefore, in flight test, the timely prediction of panel flutter, the design of panel flutter prevention and the evaluation of the severity of panel flutter are particularly important.In other words, vibration test and wind tunnel test are carried out for the panel under different airflow conditions, and effective analysis is provided for the design of the aircraft panel.Related NASA design criteria monographs include those on natural vibration modal analysis[88] and structural vibration prediction[89].

2.2 The research method of panel flutter

Most of the panel flutter phenomena occur in supersonic airflow, and the structure in which such phenomena occur is the thin-walled structure of aircraft. Therefore, most of the research on the panel flutter is to abstract the physical model based on this object for study.The ideal goal of panel flutter analysis is to eliminate flutter, which is often difficult to achieve.Therefore, the problem of how to delay the occurrence of flutter and how to suppress the intensity of flutter is solved. In terms of aeroelastic mechanics, it is usually possible to classify the elimination or delay of flutter occurrence as an aeroelastic stability problem, and the strength of flutter suppression as an aeroelastic response problem.
The aerodynamic force used for panel flutter is generally obtained by the following three methods:
(1) Potential flow theory has been widely used in the early studies on panel flutter. The advantage is that you can get any point of the panel pressure, velocity, density, etc. The disadvantage is that too much attention is paid to the details of the flow field, so it needs to be linearized to aerodynamic expression. It can only be used in low subsonic and low supersonic flows with weak nonlinear factors.
(2) Piston theory is a simplified potential flow theory applicable to supersonic flow. For supersonic flows, It is considered that the interference force of a particle in the airflow is only related to the downwash of the particle, and then according to the movement of the panel surface . In this case, the downwashing of each particle in the airflow can be obtained, and then the aerodynamic load on the plate can be obtained. First order piston theory is commonly used at the supersonic stage, from Mach number 1.5 to Mach number 5.0, the third-order piston theory is often used at the hypersonic stage because during this stage,The first order piston theory can no longer reflect the aerodynamic nonlinear effect effectively.
(3) N-S equation method, which is a numerical method, is used to analyze the panel of transonic airflow with strong nonlinear effect Unsteady aerodynamic force on the plate. At subsonic and supersonic stages, more precise

aerodynamics can be obtained than linearized potential flow theory Force.
Navier-stokes equation:
$\rho\frac{Dv}{Dt} = \rho F - \nabla P + \mu\nabla^2 v$
From left to right are inertial forces, mass forces, pressure and viscous forces.

(4) Euler dynamics equation. This is also a numerical method, based on the assumption that the flow is not viscous, applicable range as the same as the N-S equation.
Euler's dynamics equation:
$\rho\frac{Dv}{Dt} = \rho F - \nabla P$
To study panel flutter, the vibration equation or equations should be obtained first. Panel is a continuous system, panel flutter vibration equation is a multivariate partial differential equation, which is related to both time and space. Equations like this are often extremely difficult to solve. We can set up a continuous system of infinite degrees of freedom by discretizing it into a system of finite degrees of freedom.Thus, A discrete ordinary differential equation that is relatively easy to solve.There are two ways to establish discrete ordinary differential equation. One is to directly establish the partial differential equation of the plate, and then use Galerkin method to discretize it into ordinary differential equation. Second, it is to use the finite element method or finite difference method directly by discretization of the differential equation of the finite element method.The finite element method has a wide range of applications and a very strong Practicality.
Perturbation method and harmonic balance method are commonly used in the analysis of panel flutter. There are also multi-scale method, average method, asymptotic method and so on.The perturbation method is applicable to weakly nonlinear systems by taking the solution of the nonlinear system to a different power of the small parameter. The approximate solution is obtained by row expansion, which is often used to solve periodic systems. The basic idea of harmonic balance method is to describe vibration of the system and the excitation of the system are expressed in terms of Fourier series. The harmonic components of the inertial force and the applied force of the system should be able to balance each other, and therefore can be induced The coefficients of the two ends of the mechanical equation with harmonics of the same order are equal to each other so as to determine the level system of the undetermined Fourier series number. The average method using two different time scales of fast and slow change, the average method equalizes the parameters such as amplitude and initial phase Angle of the vibration in the period of fast change, and then discusses the slow change process. The multi-scale method is a more accurate averaging method, which uses a series of different time scales. The multi-scale method has many advantages over the perturbation method, for example, it can be used not only for analyzing periodic vibration and steady-state analysis, but also for non-periodic vibration and unsteady process. Numerical methods usually use

numerical integration to solve ordinary differential equations. The galerkin method is often used to calculate the frequency domain calculate. Galerkin method is a kind of weighted parameter method, which needs to choose proper shape function and weight function. There are also matrix iterations Method, subspace iteration method, etc. Numerical integration in time domain can be divided into explicit integration and implicit integration. The explicit integral is only necessary to guide the panel motion before time t, and the commonly used methods include central difference method and Runge-Kutta method, etc. Implicit Integral iterative calculation is required, not only need to know the panel movement before t moment , also need to know the next moment of some physical quantities. Houbolt method and Newmark method are commonly used.

2.2.1 The method of solving the panel flutter equation

As the panel structure is a continuous parameter system, the panel flutter equations, which reflect both the temporal and spatial information of the panel vibration. Therefore, the problem of panel flutter is to solving partial differential equations in mathematics. Only in some of the simplest cases can the exact solution be found, while the approximate solution, namely the spatial discretization method, is often used for complex nonlinear panel flutter problems.

At present, the commonly used spatial discretization methods include galerkin method, finite difference method, finite element method, finite volume method, etc. The applications of these methods in the analysis of panel flutter are described below.

(1) Galerkin method has long been used in the study of panel flutter. Dowell used the von Karman plate theory and the first-order piston theory to build the aeroelastic model of two-dimensional panels based on galerkin method. Many studies have shown that at least 6 modes should be used to accurately reflect the flutter characteristics of two-dimensional panel subjected to in-plane stress in supersonic flows.

(2) Finite difference method. from the precision of difference division, there are first order, second order and higher order difference. If the time factor is considered, the method can also be divided into explicit, implicit and explicit alternating finite difference methods. At present, the common methods are the above several combinations, such as the first-order central difference method and the fourth-order central difference method, which have been applied by many scholars to solve the nonlinear flutter equation of panel flutter.

(3) Finite element method.Based on discrete Kirchhoff Theory, the 15-degree-of-freedom triangular plate element is used to analyze the nonlinear flutter characteristics of panel flutter. In this DKT element, there are 5 degrees

of freedom on each node, which can be used to analyze the buckling and thermal flutter of panel.Then, 54 degrees of freedom high order triangular plate elements are developed.In addition, the Mindlin plate unit based on Reissner theory is also suitable for the flutter characteristics analysis of medium thickness and composite panel. In conclusion, in the current finite element analysis of panel flutter problem, there is no rule to follow in the selection of element types. Therefore, based on the basic mechanical model, the accuracy and calculation efficiency of the analysis results should be considered comprehensively, so as to determine the type of panel elements to be used.

Other spatial discretization methods, such as finite volume method, Rayleigh-Ritz method, differential quadrature method.To sum up, galerkin method and finite element method are mostly used to discretization the structure model of the panel, while finite difference method and finite volume method are mostly used to discretization the aerodynamic model.

2.2.2 The Method of solving ordinary differential equations

A set of second order ordinary differential equations is obtained by discretizing the panel flutter equation.In the mathematical analysis and solution of ordinary differential equations,analytical method analyzes the properties of nonlinear systems by solving approximate expressions of steady-state periodic solutions of differential equations.The quantitative analysis methods applied to the study of panel flutter mainly include perturbation method and harmonic balance method.

Another equivalent linear analysis method based on the harmonic balance method is the LUM/NTF method, which uses the iterative method of constantly updating modes to solve the nonlinear stiffness, but cannot be used to analyze the none harmonic panel flutter.

In conclusion, there are many ways to solve nonlinear ordinary differential equations, and each has its own advantages and limitations.If the harmonic limit cycle flutter is analyzed, the LUM/NTF method is a good choice; if the non-harmonic flutter is analyzed, the time-domain numerical integration method is adopted.

2.2.3 The Method of Unsteady Aerodynamic

Strip theory aerodynamics originated in the early 1940s,This aerodynamic method, coupled with the normal mode approach,and the V –g–ω solution technique formed the basis for production flutter analyses in the late 1960s,and this method was the primary aerodynamic tool for flutter analyses for many years.

The doublet-lattice method is accurate enough for production flutter analyses,well the answers are not correct in the transonic speed range.Second, the method produces AICs.This feature allows the method to be cost competitive with simpler methods,such as modified strip theory.Third, the method's ability to model fairly complex geometry.Lifting surfaces are simply paneled with a series of chordwise strips that are further subdivided into boxes. Bodies can be represented using slender-body theory and interference tubes.
The Mach box method is not recommended below a Mach number of 1.414.The method does not compute AICs (aerodynamic influence coefficients),the cost of the method is high relative to doublet lattice or modified strip theory. Mach box method was used for the supersonic flutter studies. In comparison to the doublet-lattice code, this code was difficult to use and could not account for interfering surfaces.
The doublet-point method had the added advantage that a single code could handle both the subsonic and supersonic Mach ranges.
The harmonic-gradient method was shown to not only reduce the number of panels required for these complex configurations but also yielded improved accuracy in all cases evaluated. In addition,improvements to the method were also described as ZONA51C for supersonic flutter analyses.
Modern High-Performance unsteady aerodynamics ZONA Code. First, a new subsonic code, ZONA6 has been introduced as a substitute for doublet lattice. This code is based on the constant pressure panel method, and it has demonstrated improvements in modeling capability, especially for cases of high aspect ratio boxes that can result if high-reduced frequencies are needed. Second,a new supersonic code,ZONA7 has been introduced as an improvement over the previously introduced ZONA51 that is contained in the NASTRAN aeroelastic package. Third, a unified supersonic/hypersonic lifting surface method, ZONA7U that combines ZONA7 with piston theory has been introduced,it has been developed that can account for wing thickness or incidence effects in supersonic and hypersonic flow.
Recently,CFD has made progress as a research tool, it has yet to demonstrateits value in a production environment.Corrections to flutter speeds computed using linear methods are still needed and are usually generated using transonic wind-tunnel flutter model testing.

2.3 Instability analysis

To study the aeroelastic stability of composite laminate structure under different airflow, in order to analyze it by solving the generalized eigenvalue problem through aeroelastic properties. And generally by calculating the natural frequency of the laminate structure at different incoming flow speeds, the critical instability velocity of the laminate structure under the action of

airflow is obtained, because the rigidity of the laminate structure decreases, resulting in the structure instability.
Because of the complexity of the structure considered and the multidisciplinary of the problem to solve, the first activity performed in the present work is a large review of the remarkable results found in literature related to panel flutter. Many parameters have been considered to investigate their effects on flutter boundaries.[90].
The literature overview has been focused on:Identification of the aeroelastic phenomena at different Mach numbers;Effect of the panel configuration (load, BC) on the aeroelastic instabilities;Available computational approach.In fig. 2.3,To perform accurate aeroelastic analysis, it is important to use an appropriate computational model. all possible approaches that can be adopted in the aeroelastic solution are reported. The structural model should be considered non-linear if the LCO has to be evaluated. Complex aerodynamic theory should be used in the transonic regimes while, in the hypersonic range, the non-linearities of the flow cannot be neglected. In fig. 2.4the effects of some panel parameters on the aeroelastic instabilities are reported. In the first column the parameters investigated are given, the increasing of these parameters could have strong effects on the behaviour of the flutter flow parameter (q_f), on the flutter frequency (f_f) and on the LCO amplitude (h_f/t). The up arrow means increasing while the down arrow means decreasing and the empty space means that no information was found in literature. As an example, the increase of the curvature radius R, increases the flutter frequency f_f, while it decreases the critical dynamic pressure q_f.The literature review suggests the following considerations:The choice of the aerodynamic model is crucial to describe properly the whole physical phenomena;The transonic range is the most critical range in which aeroelastic phenomena may occur;The effects of the boundary layer are not negligible and they have a strong influence on the flutter boundary, as consequence a refined aerodynamic model is requested, specially in the transonic and low supersonic regimes.
In one report of Professor Zappino which is related to literature [90] says that:To describe properly the panel flutter phenomenon it is necessary to investigate 3 parameter:Critical flow condition, including critical Mach number M_{cr} and critical flow dynamic pressure q_{cr},those parameters directerly influenced to flutter boundary; Flutter frequency f_{cr},thus we konw flutter cycles;Limit cycle oscillations,(w/h) has a relation with dynamic damping Matrix of analysied system,insuch way we could know each stress on each flutter models.AND those later two parameters together could obtain the computaion on Fatigue life.
Althogh,Despite above parameters we illustraterd,the panel flutter phenomena are influenced by many other parameters in details.A collection of literature significant results is presented in order to describe the effects of:Geometry parameters,including Aspect ration (a/b) fig. 2.5, Curvature (R) fig. 2.6,Con-

strains fig. 2.7; Material parameters,including Mass ratio (μ) fig. 2.8,Orthotropy (E_{11}/E_{22}) fig. 2.9; Load parameter,including Differential pressure (δ_p) fig. 2.10,Temperature (δ_T) fig. 2.11, In plane stress (P_{cr}) fig. 2.12,Boundary layer thickness (δ) fig. 2.13.

Mach range	Structural model	Aerodynamic model
$\sqrt{2} < M < 5$	Linear	Linear piston theory
$1 < M < 5$	Linear	Linearized potential flow
$\sqrt{2} < M < 5$	Non-linear	Linear piston theory
$1 < M < 5$	Non-linear	Linearized potential flow
$M > 5$	Non-linear	Non-linear piston theory
$0 < M < \infty$	Non-linear	Euler or Navier-stokes

Figure 2.3: Models available for the aeroelastic analysis

Param.	q_f	f_f	h_f/t
a/b	↑	↑	↓
R	↓	↑	
$\frac{E_{11}}{E_{22}}$	↑	↑	↓
Δp	↑		
ΔT	↓		↑
P_{cr}	↓		↑
δ	↑	↑	↓

Figure 2.4: Panel flutter parameter influence

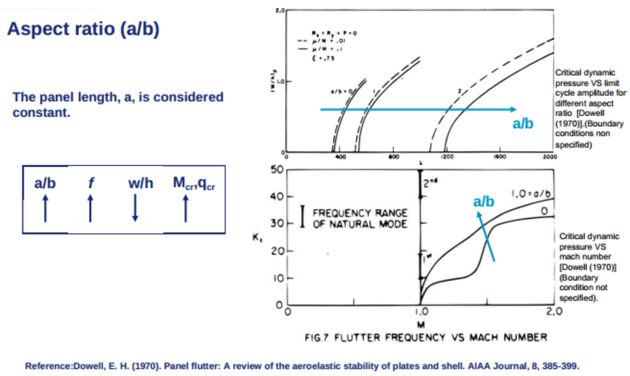

Figure 2.5: panel flutter phenomena parameter: aspect Ratio

Through the eigenvalue equation presented in the previous Chapter 3, the natural frequencies of the structure at different incoming flow speeds can be obtained. It can be seen from the stiffness matrix that when the

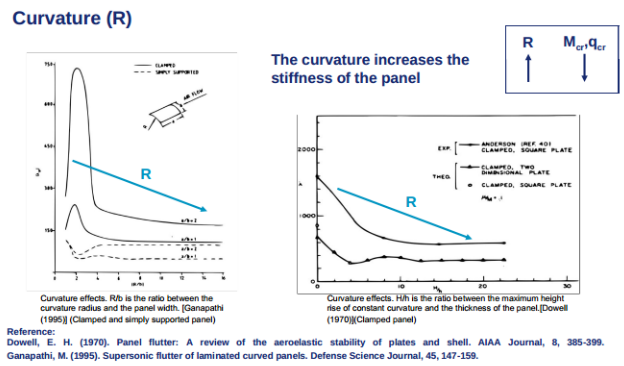

Figure 2.6: panel flutter phenomena parameter: Curvature

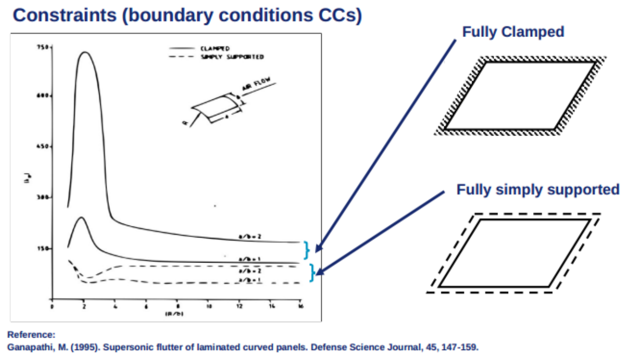

Figure 2.7: panel flutter phenomena parameter: Constraints (boundary conditions)

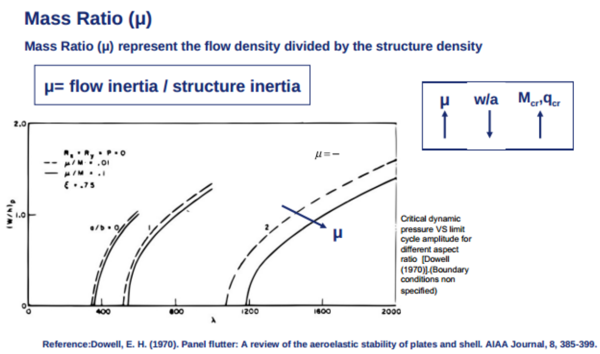

Figure 2.8: panel flutter phenomena parameter: Mass ratio (μ)

aerodynamic pressure is considered, the stiffness of the structure system includes the aerodynamic stiffness term, and the With the gradual increase in speed, the stiffness of the structural system will gradually decrease, which will cause the natural frequencies of the system to gradually decrease. When the fundamental frequency of the structure is reduced to 0, the structure will

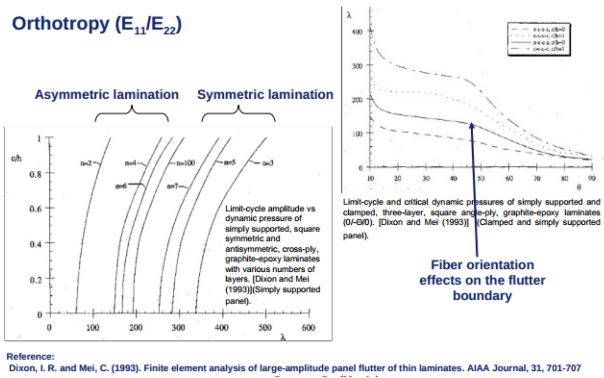

Figure 2.9: panel flutter phenomena parameter: Orthotropy (E_{11}/E_{22})

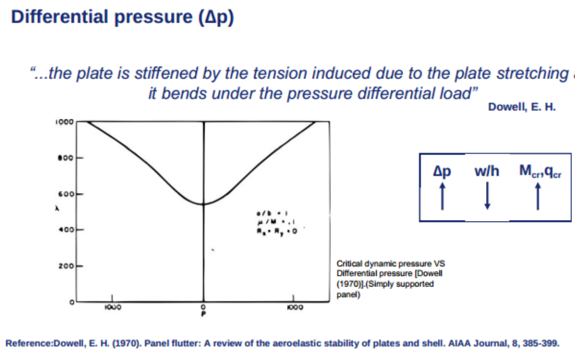

Figure 2.10: panel flutter phenomena parameter: Differential pressure (δ_p)

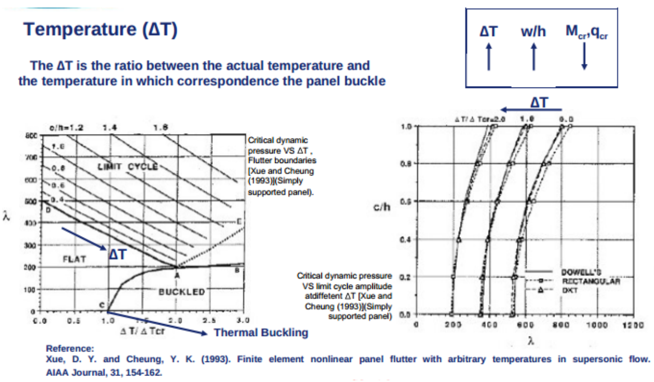

Figure 2.11: panel flutter phenomena parameter: Temperature (δ_T)

be in a critical instability state. The corresponding incoming flow velocity is the critical instability velocity. Therefore, in practical applications, the structural parameters should be reasonably designed according to the mechanical environment of the composite laminate structure to avoid structural instability problems under the action of airflow.

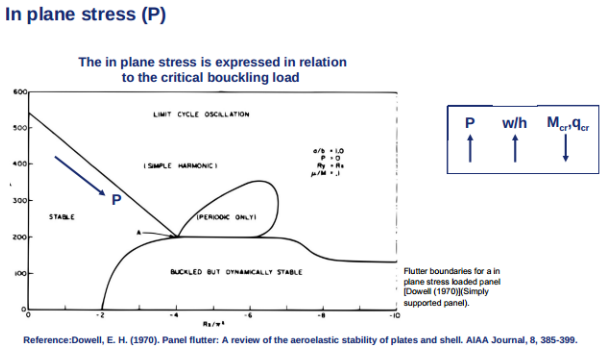

Figure 2.12: panel flutter phenomena parameter: In plane stress (P_{cr})

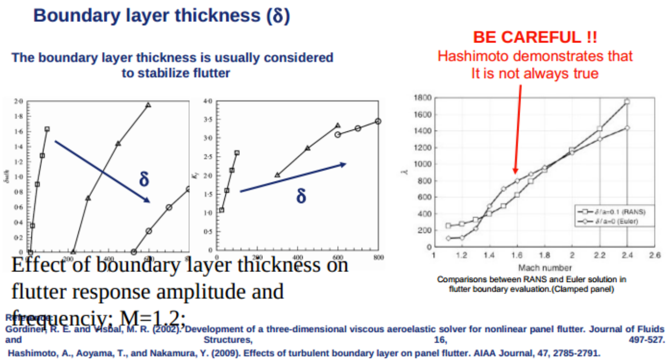

Figure 2.13: panel flutter phenomena parameter: Boundary layer thickness (δ)

2.4 progress of composite structures

With the continuous development of aviation science, especially since the 1980s, with the rapid development of materials science, a growing number of aircraft structures made of composite materials. This is because The composite structure has good designability, high specific stiffness and high specific strength and light, and makes the structure of the aircraft aerodynamic elasticity problem become more prominent, it has been widely applied in the aerospace field.

Highlights

Fiber-reinforced composites are being used in primary structures of flight vehicles ranging from small unmanned aircraft to space launch vehicles.The

Figure 2.14: Application of Composites on Flight Vehicles

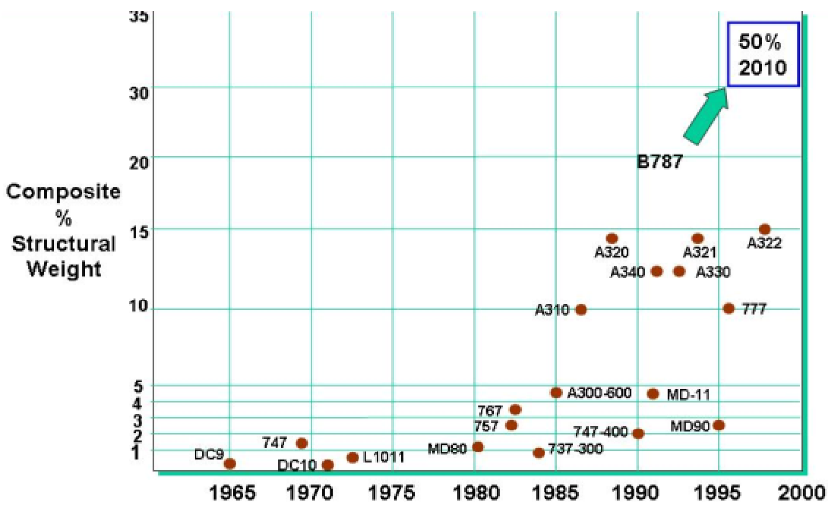

Figure 2.15: Composites in Commercial Transport Aircraft

percentage of structural weight made from composite materials has grown from less than 1% to more than 50% over the past four decades.Primary drivers for expanded use of composites has been weight reduction, stealth for military aircraft, and cost for commercial aircraft.Composite materials have emerged as the materials of choice for increasing the performance and reducing the weight and cost of military aircraft, general aviation aircraft,

transport aircraft, and space launch vehicles. Major advancements have been made in the ability to design, fabricate, and analyze large complex aerospace structures.
In the United States, research on composites has been a combined effort of government laboratories, universities, and industry. The development of high-performance composites for aerospace applications has been spearheaded by the major airframe companies (Boeing, Lockheed, Northrop Grumman, McDonald Douglass (now Boeing), General Dynamics, and others), and by NASA and DOD, with the FAA playing a critical role in the certification requirements for composite flight structures.
Within NASA, Langley Research Center had the lead role for development of composites for airframe applications, and NASA Glenn had the lead role for development of high-temperature composites for aircraft engine applications[91].
Such as the Boeing777,Graphite and hybrid composites have been widely used in large double-engine engine.Different components, such as stabilizer, tail fin and inner and outer plate spoiler, are used on each aircraft approximately 8400 kg Composite material, accounted for the total structure the weight of the 10%.

Figure 2.16: The B-777 Airframe Incorporates Durable Lightweight Composite Aircraft Structures, Including Graphite Epoxy Floor Beams, Flaps and Tail Assembly

F/A-18 wing is designed to be multidisciplinary optimally in assurance. The weight of the structure is reduced under energy 48% The torsional stiffness is reduced 40%.

F-16 Fighter aircraft wing optimization design results when the outer segment stiffness of the wing decreases 25% , the weight of the structure can be reduced 20% ,and at high dynamic pressure, improved control efficiency 10%.
Composite materials are used not only to reduce weight, but also because these materials are corrosion and fatigue resistant and can be tailored to reduce radar cross-section. The modern military aircraft, such as the F-22, uses composites for at least a third of its structures, and future military aircraft are likely to be more than two-thirds composite materials. Military aircraft use substantially greater percentages of composite materials than commercial passenger aircraft, primarily because of more stringent performance requirements and operational issues. The limiting factor in the widespread application of these materials has been the high cost of fabricated structures compared to conventional metals.

Current progress of composite structures

There are many types of composite structures, and their mechanical properties vary greatly. At present, composite structures are commonly used in aircraft structures The composite materials are: laminated composite, fiber-reinforced metal laminated composite, honeycomb sandwich composite, Nanoreinforced Composites.
Laminated composites are referred to as laminated plates for short, is commonly used in engineering composite material structure, such as graphite/Epoxy laminated Plate. Honeycomb sandwich structure is a special composite material structure, it is generally by the upper and lower skin panel and the middle thicker but soft sandwich through the adhesive(Or brazing)constituted.Honeycomb structures have higher strength and stiffness than other Laminated structures, the efficiency of the structure can be improved 15% to 30%.Fibre reinforced metal Laminates,Commonly used are aramid fiber aluminum alloy laminates, glass fiber aluminum alloy laminate, and Carbon fiber aluminum alloy laminate, have been earlier applied in aircraft structures, achieving a good self-weight reduction effect. Such as applied in the lower wing plate of F-27. NASA Langley has conducted research in the general area of nanotechnology for the past several years (2000 to present). Most of the work on Nanoreinforced composites has focused on how to achieve a stable dispersion of SWCN in polyimides, measurement of changes in electrical properties of polyimide composites with additions of carbon nanotubes, and changes in mechanical properties.

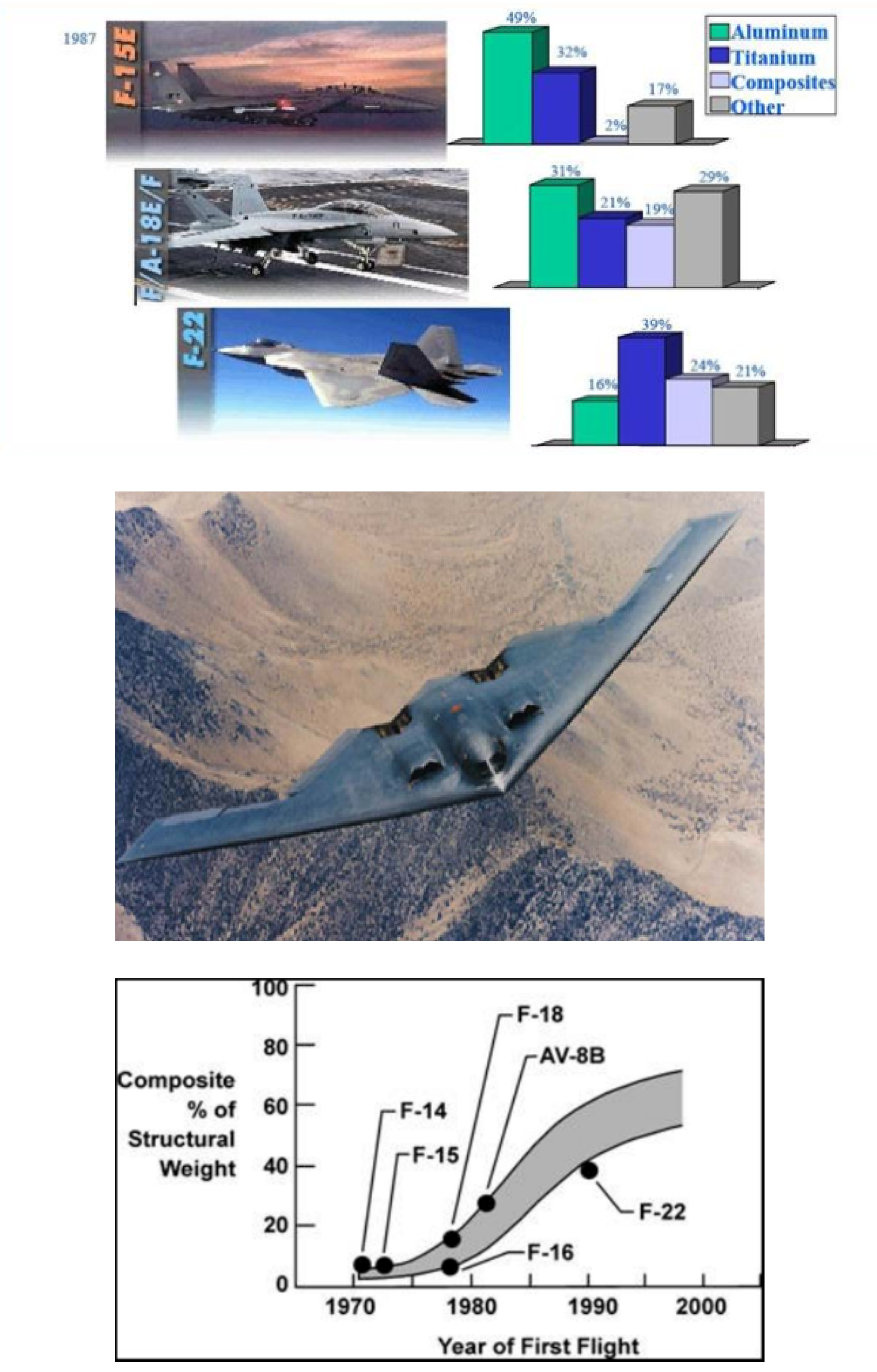

Figure 2.17: Composites in U.S. Fighter Aircraft

The NASA Langley work in nanocomposites began with several efforts that had their roots in a program in multi-scale analysis begun more than a decade earlier. The modeling focused on developing relationships between the atomistic and macroscopic scales[92].Research efforts were undertaken to model the carbon nanotube fiber with a geometry composed of discontinuous carbon nanotubes in a helical geometry appropriate to a twisted geometry[93],[94, 95, 96, 97].These results suggested that such a microscopic fiber would yield stiffness and density properties typical of the high-performance, PAN-based carbon fibers. 1012 single walled carbon nanotubes of aspect ratio of 1000 are required to produce 1 meter of micro fiber[98].
Carbon fiber dimension is a kind of high energy fiber material whose carbon mass fraction is above 95% after high temperature carbonization or graphitization of high polymer materials. It has advantages such as high strength, high modulus and high temperature resistance, etc. Carbon fiber dimension/cyclic oxygen resin composite material has excellent properties such as small density and mechanics, and is widely used in aerospace satellite communication system.

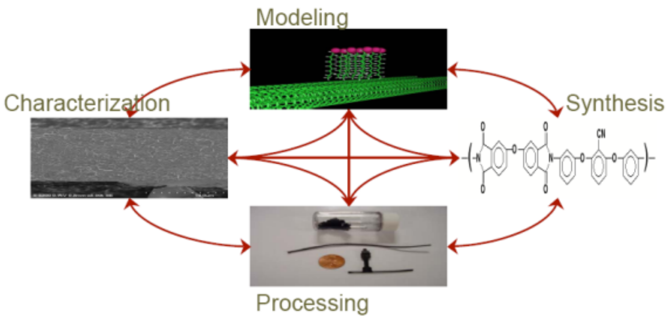

Figure 2.18: General research areas of Nanoreinforced composites

Recent Advancements in the deeply study on nanoreinforced composite is Boron-nitride Nanotechnology.The National Institute of Aerospace have used lasers to create the first practical macroscopic yarns from boron nitride fibers, opening the door for an array of applications, from radiation-shielded spacecraft to stronger body armor.Using this new technique they are able to synthesize high-quality boron-nitride nanotubes (BNNTs).The nanotubes are highly crystalline, have a small diameter, contain few walls and are very long.The researchers say the next step is to test the properties of the new boronnitride nanotubes to determine the best potential uses for the new material. They are also attempting to improve and scale up the production process.

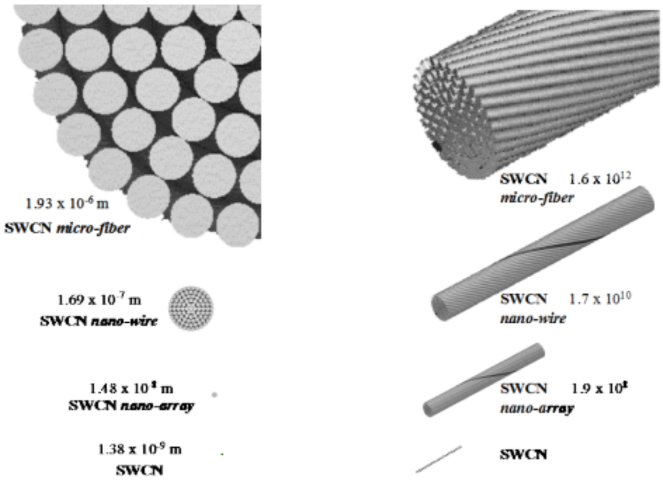

Figure 2.19: a) Self-similar Scales and b) Number of SWCN Per Meter Length

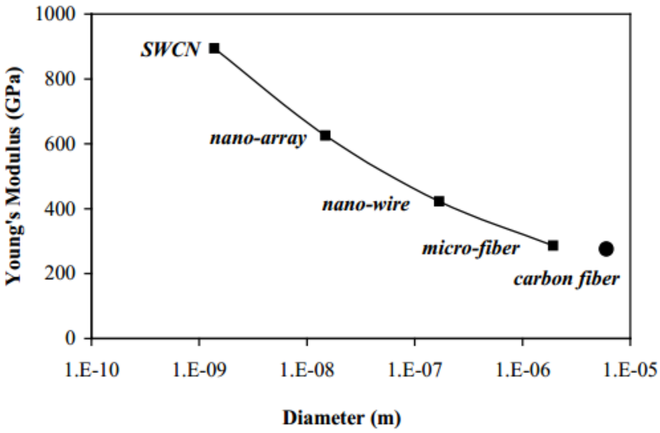

Figure 2.20: Young's Modulus of the Carbon Nanotube Micro-fiber

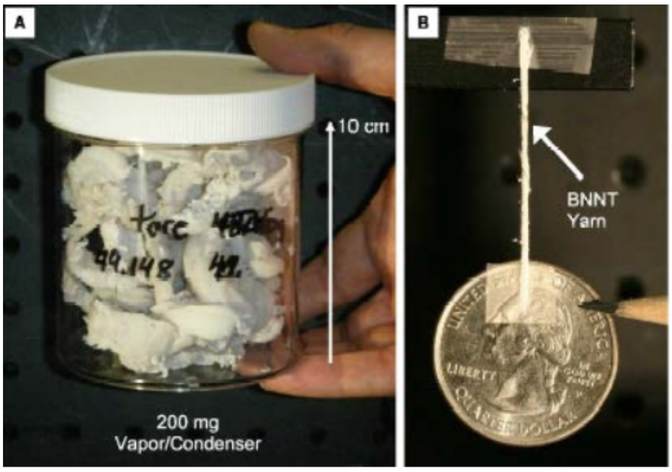

Figure 2.21: A) 200 mg of PVC-grown BNNT Raw Material and Yarn. B) A 1 mm Diameter, 3 cm Long BNNT Yarn Spun Directly from PVC-grown BNNT Raw Material.

Chapter 3

Wind tunnel panel flutter test

Wind-tunnel flutter testing is effected by boundary layer effects and amplitudes, stresses, and frequency of the flutter oscillation. High-Mach number flows are the most difficult to simulate properly because of the high temperatures and low dynamic pressures.Earlier in the 1950s and 1960s, NASA coorporates with U. S. Air Force Laboratory established the hypersonic velocity wind tunnel flutter test technology lab, A large number of hypersonic velocity wind tunnel flutter tests have been developed.Relevant design parameters and flutter properties are studied in the influence of number on the flutter characteristics of rudder airfoil at hypersonic speed.In this paper, only the flutter wind tunnel test data of aircraft panel are summarized, the specific test of hypersonic rudder airfoil is not reviewed in detail[99, 100, 101, 102, 103, 104, 105, 106, 107, 108, 109].

Wind tunnel test equipment is a national aerospace industry development infrastructure in the research and development of new aerospace vehicles in use,it plays an important role in the improvement, test and evaluation of aircraft tests.In general,large wind tunnel test equipment is regarded as a national strategic resource.In the aircraft ,Before the test flight, the wind tunnel flutter test is used to test the results and the flutter by Conducting a trial and provide evidence, and try make flying risk lower.The United States NASA has the world's largest cluster of wind tunnel equipment,These huge sums of money were spent to build the experimental infrastructure into the United States military and civilian use of aerospace aircraft development.

The United States is currently engaged in some important research and development programs, military combat Aircraft, unmanned combat aircraft, missiles and orbital space shuttles will dominate Hypersonic range. Researchers are looking for something similar to blowing off boundary layers, this technology could control the air flow on the plane's surface and to achieve the purpose of the takeoff and landing vehicle to an extremely short vertical distance.

3.1 NASA Wind Tunnel Laboratories

Nasa Langley research center , 16ft(4.8m) transonic wind tunnel

The wind tunnel has a long history,Utilization has been very high,Low Re number and poor quality of flow field.

Nasa Ames 12ft(3.6m) subsonic wind tunnel

The wind tunnel is suitable to meet the needs of all domestic users,high Re number general purpose subsonic wind tunnel for civilian, aerospace and military aircraft Research, development, testing and evaluation.
The tunnel was transformed between 1988 and 1995, but the utilization rate after transformation is still very low, in the test technology competition There is no advantage.

Green 9ft x 15ft(2.7m x 4.5m) propulsion wind tunnel

The wind tunnel is NASA's special propulsion research facility,it has potential for military applications. NASA uses this device for engine exhaust Gas noise reduction studies by the Department of Defense Air Systems Command and the Navy Support from air Force Weapon Systems Department.
high ratio of usage,high technically competitive. Re number is low, it does not have the ability to measure force parameter.So it can't as a universal device, users will instead rely on AEDC-16S for satisfaction their test requirements.

Green 10ft x 10ft(3m x 3m) supersonic wind tunnel

Ma numbers range from 2 to 3.5,Low Re number and no measuring force ability.

Nasa transonic dynamic wind tunnel(TDT)

NASA built the first transonic dynamics wind tunnel specifically designed to study aeroelasticity of aircraft in 1960.It mainly solves the problem of transonic flutter design for aircraft models' Evaluation and verification of transonic flutter simulation.Especially in F-16, B-777, F-18E/F and other aircraft flutter wind test, the data obtained made a great contribution to the development of flutter simulation program.TDT developed a great deal work

of full-mode flutter test with modeling, wind tunnel flow field and support system, etc.
For CFD simulation of transonic flutter, Boeing further developed the NASA CFL3D CFD program based on Euler/N-S equation of transonic flutter simulation, and use the TDT wind tunnel model test results of HSR procedures for later correction, and obtained bigger progress[110], the Boeing company also use CFL3D limit cycles of the B-1 aircraft and took a comprehensive simulation study.[111, 112, 113]

Nasa national aerodynamic center(NFAC)

NFAC is the world's largest full-size wind tunnel.According to the website of «US aviation Week» in June 2017, it was reported on June 19 that NFAC had a panel falling off during the test. The wind tunnel fan blades are damaged onetime.This wind tunnel has complete the compatible with multiple operating systems(Windows, Linux, Apple, Android),and Real-TDS a real-time trial display system was put into use since then.NFAC Developed half-mode wind tunnel interference correction technology and expanded the support mode of the NFAC wind tunnel model and the disturbance of the existing correction ability.
When flutter boundaries are determined by wind tunnel test,all significant flight parameters shall be conservatively simulated by the model and the wind tunnel. If no previous experience exists for a given panel type, natural modes and frequencies under critical environmental conditions, including thermal, mechanical, and pressure loads, shall be determined by vibration tests before flutter analyses or flutter tests are undertaken.For more informations on natural frequency and vibration test modes, see literature[114].

In order to avoid the occurrence of flutter accidents, the development of new aircraft must go through the flutter flight test to determine the stable flight envelope without flutter. For flight flutter is not my case in study ,so not illusmate in detail.
The main content of the flutter test on vibration mode test is to stimulate the aircraft structure at different flight status points at different flight altitudes and speeds, identify the modal parameters such as the flutter frequency and damping of the air dynamic structure according to the dynamic response data, and finally predict the flutter boundary based on the changing trend of damping.Therefore, in vibration model test, how to effectively deal with test data to accurately identify modal parameters has become an important research topic in current flight flutter test.Such study is of great significance to accurately predict the flutter boundary and ensure flight safety.
In the last century, NASA carried out a series of F/A-18 tests to explore of a new method for flutter modal parameter identification.For example, the devel-

opment of a new type of drum type small rotor excitation device[115], In the time-frequency domain wavelet is used to de-noising the test signals[116], and advanced subspace methods are used to identify the modal parameters[116]. These new methods significantly improve the estimation accuracy of the flutter parameters and the accuracy of the flutter boundary prediction.

Flutter test of modern research covers mechanical control information, and other disciplines, has developed into multi-discipline experiment equipment, and rough analysis method has been rapidly developed of the modern flutter test, replaced by sophisticated testing apparatus and precise analysis.So It is necessary to simplify the development of flutter test data processing.

In the last 1940s, testing engineers have gradually realized that the modal frequency and damping coefficient of aircraft structure are the best reference indexes to predict the occurrence of flutter, and extracting these two parameters from the data has become the task of flutter test data analysis.Due to the limitations of the experimental excitation conditions at that time, the modal frequency is usually judged by the amplitude of the response signal of the frequency sweep excitation, and then the damping coefficient is determined by the control surface pulse excitation. Due to lack of computer and maturity of identification algorithm, the modal parameters can only rely on manual during flight clearance, using the logarithmic decrement method analysis of time domain signal attenuation from time to time is the commonly used method for damping coefficient at the same time. due to not have telemetry equipment, test engineers must analyze the test data processing on the plane.In the 1950s, engineers were able to perform data analysis on the ground, thanks to advances in telemetry equipment.For the attenuation response signal of multi-mode, the single mode response is extracted by filter. This analysis method is very effective for sparse mode, but not for dense mode. At the same time, spectral analysis technology has also been used in flutter stability analysis. At that time, its function was limited to judge the resonance frequency and calculate the amplitude value at a certain frequency, but it could not provide specific damping information.until the 1970s, with the progress of computers and the spread of the Fast Fourier Transform,The research of modal parameter identification and flutter prediction has become the main research direction of flutter data analysis in that period.For example, in the development and test of F14 and F15 fighter aircraft of the United States, the new identification algorithm is fully utilized for modal parameter identification, and the parameter identification results under the subcritical state point are applied to the prediction of flutter boundary[117].

Up to now, although there are many new methods used to predict the flutter boundary[118, 119, 120], it is still the most effective method to determine the critical flutter velocity by the trend of damping change.

3.1.1 Flutter test model design

Flutter is a destructive phenomenon of aeroelastic dynamic instability.Wind tunnel test is the main method and means for flutter design research of aircraft.The research on aeroelastic problems mainly involves numerical calculation, wind tunnel test and flight test. The aeroelastic wind tunnel test is highly reliable (compared to numerical calculations) and low cost (compared to flight tests) have become important means for evaluating and verifying the aerodynamic and elastic performance of aerospace vehicles.

The flutter test model usually consists of a load-bearing frame plus a dimensional skin. The scaled flutter test model is obtained by scaling down the original model, and then according to artificial experience or structural optimization.NASA developed the B-52 flutter suppression test model in 1974. The model is made of aluminum alloy frame fuselage and spar to provide model stiffness, and elastic segmented skin to provide accurate aerodynamic profile [?].In 2015, the Truss-Braced Wing (TBW) flutter test model still adopts a similar design idea [?]. The design method has been quite mature after decades of development. With traditional manufacturing and processing technology, it has become a model flutter great contribution to design and analysis.

With the continuous development of active control technology, the use of

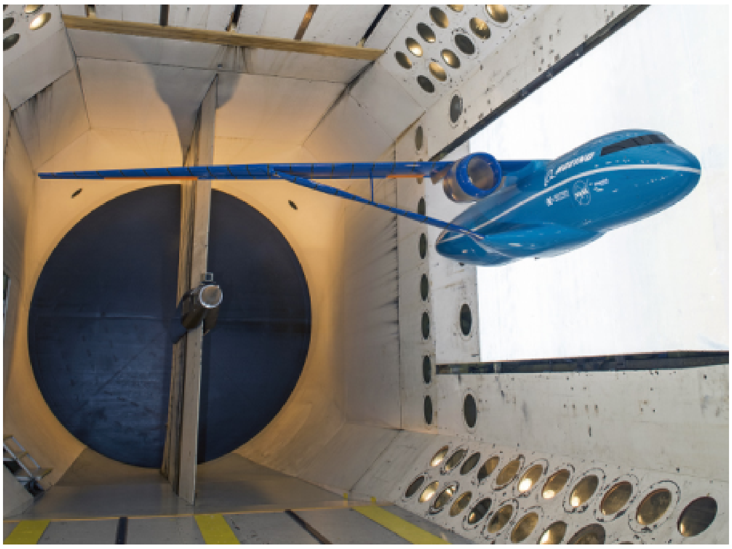

Figure 3.1: TBW test model installed in the TDT wind tunnel

rudder deflection or piezoelectric control to improve the aeroelastic performance of aircraft has become a research hotspot, and the layout of the control system needs to be considered during the design of the test model.In 2008, Bartley-Cho [?] and others introduced the design process of the Northrop-Grumman sensor aircraft aeroelastic active control test model. The main structure of the model is still in the form of a wing box, equipped with 5 control surfaces. The design results are shown in the figure. In 2011, Scott [?] and others introduced the design and production of the Boeing sensor aircraft active control test model. The model is equipped with 14 active control surfaces and 80 data stream channels. The above models have all been tested in the TDT wind tunnel.Research results show that the active control system improves the performance of the aircraft very significantly.

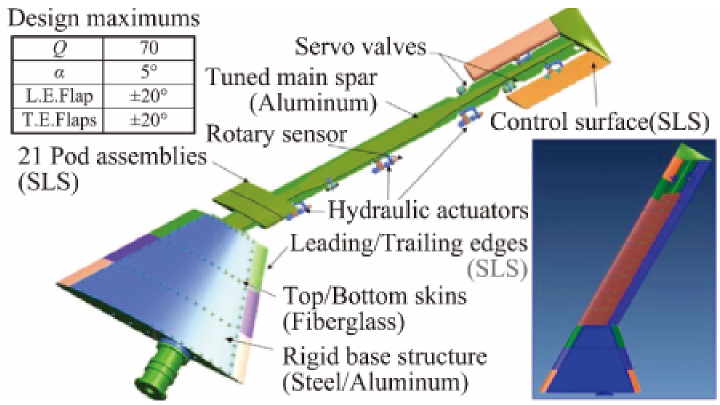

Figure 3.2: HILDA test model

3.1.2 Flutter test signal processing

Flutter test signal processing includes: a, signal preprocessing. Due to the poor quality of the sampled signal, it is necessary to pre-process the obtained data, including de-zero bias, de-trend term, filtering, windowing, etc.Among which signal filtering is the key technology. b, Subcritical response analysis. Identify the parameters (modal damping or other stability parameters) of the preprocessed test signal, obtain the changing trend of the parameters with the incoming flow velocity (speed pressure), and obtain the flutter boundary through extrapolation. In recent years, wavelet transform based on time-frequency analysis has been widely used in flutter test signal processing due to its good time-frequency resolution and band-pass filtering properties.

In a large number of wind tunnel tests, NASA Langley Center found that there is a certain relationship between the spectral peak of the flutter test signal and the incoming flow pressure. In 1975, Foughner proposed the Peak-Hold method on this basis, by establishing the Peak-Hold spectral peak value The relationship between the reciprocal and the speed pressure is extrapolated to obtain the flutter boundary. Doggett applies the Peak-Hold method to the subcritical response of the small aspect ratio delta wing model flutter test, showing high accuracy and reliability This method has gradually become one of the standard methods of signal processing for the TDT wind

tunnel flutter test at NASA Langley Center.Subsequently, the TDT wind tunnel at the NASA Langley Center carried out a root-fixed swept wing flutter test. Four subcritical response analysis methods (random attenuation method, power spectral density method, cross power spectrum method and Peak-Hold method)) Was evaluated. The test results show that, in contrast, the Peak-Hold method and the cross-power spectrum method can obtain reliable results and are suitable for online processing.
In 2009, NASA funded ZONA to develop a set of online flutter prediction tools based on parameter change estimation methods, integrating multiple parameter identification techniques to estimate the damping and frequency of physical modes during wind tunnel testing, including Zimmerman-Weissenburger flutter margin , Tradition methods such as damping trend extrapolation and advanced methods of analysis, provide online processing capabilities for the test. The focus is on method engineering Practical, there is no innovation or breakthrough in theory.

3.1.3 Flutter test model support method

The NASA Langley Center TDT wind tunnel, as a special wind tunnel for aeroelasticity tests, has a variety of test model support methods, including: a variety of pole supports, a variety of sidewall supports, a rotating window (located on the wind tunnel floor), and a double Cable suspension support, one helicopter test equipment, one Tilt-rotor test equipment, and some custom support systems. There are also some special equipment inside the support system. For example, the side wall turning window can be moved at a high frequency by a motor or hydraulic pressure, which is called an Oscillating Turntable (OTT).

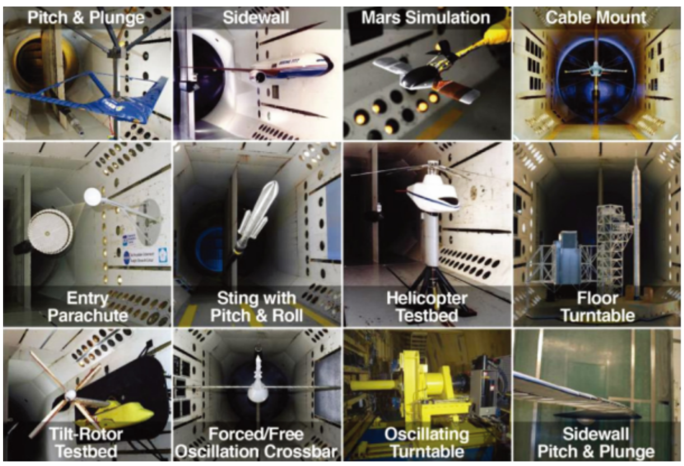

Figure 3.3: TDT model mount systems and unique models

3.2 Panel flutter Wind Tunnel test

In the above report, the basic conditions and wind tunnel test methods of NASA's wind tunnel flutter test have been sorted out. In the following, we will use Professor Carrera E. and Enrico Z. as references to further understand the instability characteristics of panel flutter and the analysis of boundary parameters on the basic specification requirements of conventional wind tunnel tests in the supersonic regime.
Because of the complexity of the structure considered and the multidisciplinary of the problem to solve,the first activity performed is a large review of the remarkable results found in literature related to panel flutter.Many parameters have been considered to investigate their effects on flutter boundaries,including identification of the aeroelastic phenomena at different Mach numbers,Effect of the panel configuration (load, BC) on the aeroelastic instabilities,available computational approaches.In Chapter 2 ,we have illustrated all those identifications in advance.Also a more accurate computational approach has been used in some WT tests in order to assess the computational tool more accurately. In order to have a better understanding on computational approach, we take a note below on such topic.

3.2.1 Computational aeroelasticity approach

To investigate the flutter boundary of the full scale model, we use computational aeroelasticity approach. In professors' report, two two different approaches are depicted. In LKE approach, the structural solution is pro-

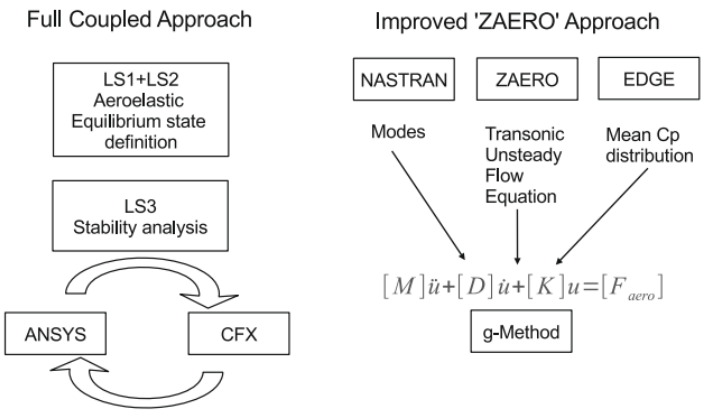

Figure 3.4: Two Computational aeroelasticity approach,LKE approach and VZLU approach

vided by the commercial FE code ANSYS, the flow solution is provided by the CFD code CFX.Firstly,the structure is considered rigid,the flow field is

evaluated at the given M number in its steady condition. Secondly,the structure is considered flexible,also take int account effects of the external load. Thirdly,equilibrium condition in last phase is change into perturbed,then investigate its stability.This solution is computed in the time domain.
In VZLU approach fig. 3.4 above,three softwares were combined for aeroelastic analysis. ZAERO code based on potential flow theory,to predict the flow perturbation (δ_{Cp}) around a steady condition. EDGE CFD solver is used to evaluate the mean Cp distribution in the steady condition. NASTRAN,an FE code,is used to evaluate the dynamic properties of the structures: modes, frequencies, modal masses. Those information from NASTRAN and EDGE is used by ZAERO to evaluate the aerodynamics coefficients collected in the aerodynamic matrices. The solution is computed in the frequency domain by means of the g-method.

3.2.2 wind tunnel test

It was not possible to test the full-scale panel in the WT facilities provided by VZLU.a scale of 1/60 the model was introduced to have reliable WT results. To assess of the fluid field. Two rigid models were build: the first with a 1/2 cylinder geometry, the second with a 1/8 cylinder geometry. The models was used to evaluate the quality of the flow over the panel and the noise level of the WT facility.And the percentage pressure difference between the WT test results and the CFD computational analysis on different Mach regimes are also reported.The results show that the flow field can be considered uniform on the model and the real M number is very close to the reference one. The comparisons with the computational tool show that the CFD analysis is able to predict properly the flow field in the WT and so the fluid model can be considered reliable enough for the aeroelastic computation.
The 1/2 active model aim to assess the fluid structure interaction (FSI)

M	1/2 RM (%)	1/8 RM (%)
0.776	−1.36	−1.46
1.529	−19.29	−20.08
1.729	−8.76	−6.88

Figure 3.5: Maximum pressure difference (%)between WT test results and CFD model

capabilities of the computational tool. The flexible model was activated by an actuator put on the bottom of the panel, the oscillations of the panel created some perturbations on the flow field, The test aims to predict numerically perturbations by means of the unsteady aerodynamics model used in the FSI solution.For this analysis the random excitation has been imposed as external loads, the load spectra have been provided by VZLU and it was derived by the WT test.At the regime at Ma equal to 0.86, the results from the WT test showed that the model was able to predict some aeroelastic instabilities with a frequency equal to 10 KHz.The results show that Aeroelastic instabilities has been imposed as external loads, and the computational tool is able to predict the aeroelastic behaviour observed in the WT test.

The 1/8 cylinder aeroelastic model was devoted to the flutter analysis

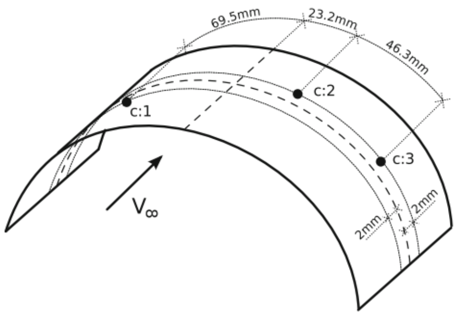

Figure 3.6: Pressure sensors position (c:1,c:2 andc:3) on the active panel

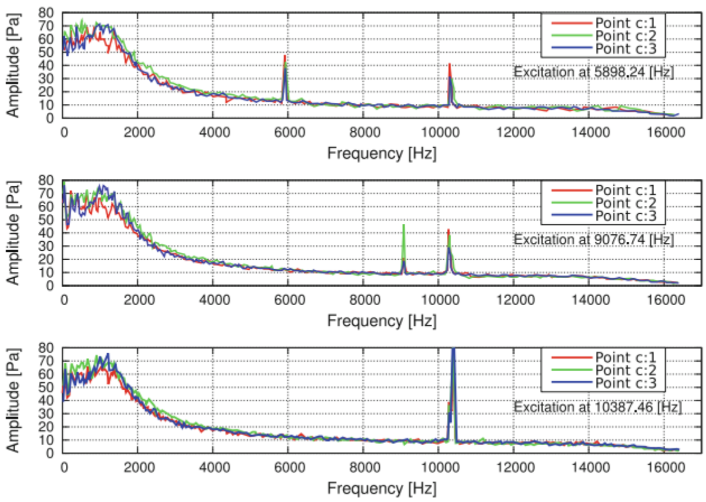

Figure 3.7: 1/2 active model WT results at Ma=0.86,PSD

assessment considering a reliable configuration (4 pinched corners).
The outputs of the research show that panel can be affected by aeroelastic instability,so the design should consider aeroelastic loads. Moreover, the assessments of the computational tool and the comparisons with the WT tests, provide a more reliable FSI computational tool that can predict flutter on complex configuration.

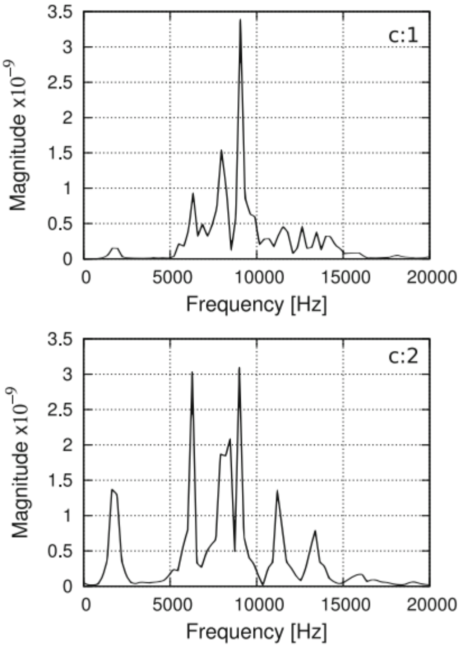

Figure 3.8: 1/2 active model CA results at Ma=0.86,PSD

Chapter 4

Structural models based on the Carrera unified formulation

4.1 Preliminates

4.1.1 Equilibrium Conditions

In the linear case,when continuous and deformable structures are introduced,stress and strain is two main performance behavior of the material when it is subjected to load force, following below is the differential indefinite dynamic equilibrium conditions along the three directions of an orthogonal Cartesian reference system and the Stress distribution in Cartesian coordinate system[121]:

$$\begin{aligned}
\frac{\partial \sigma_{xx}}{\partial x} + \frac{\partial \tau_{yx}}{\partial y} + \frac{\partial \tau_{zx}}{\partial z} &= g_x \\
\frac{\partial \tau_{xy}}{\partial x} + \frac{\partial \sigma_{yy}}{\partial y} + \frac{\partial \tau_{zy}}{\partial z} &= g_y \\
\frac{\partial \tau_{xz}}{\partial x} + \frac{\partial \tau_{yz}}{\partial y} + \frac{\partial \sigma_{zz}}{\partial z} &= g_z
\end{aligned} \tag{4.1}$$

The nine stress components including 3 normal stress and 6 shear stress are $\sigma_{xx}, \tau_{xy}, \tau_{xz}, \tau_{yx}, \tau_{yy}, \tau_{yz}, \tau_{zx}, \tau_{zy}, \sigma_{zz}$. where g_x, g_y, g_z indicate the inertial forces or weight of per unit volume. The equilibrium conditions related to rotations along the axes lead to the symmetry conditions or to the Cauchy theorem:$\tau_{xy} = \tau_{yx}, \tau_{xz} = \tau_{zx}, \tau_{yz} = \tau_{zy}$. The equilibrium equations can be rewritten in vectorial form,

$$\boldsymbol{b}^T \boldsymbol{\sigma} = \boldsymbol{g} \tag{4.2}$$

where ,Stresses vector

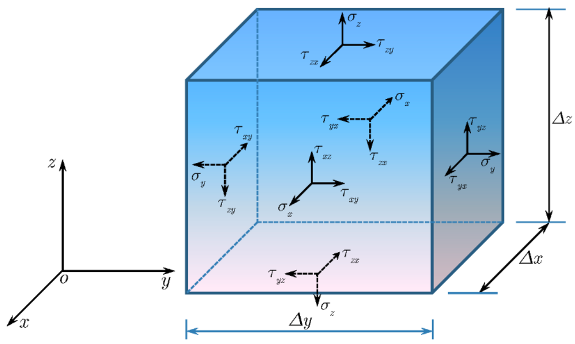

Figure 4.1: Stress in Cartesian coordinate system

$$\boldsymbol{\sigma}^T = \{\sigma_{xx}, \sigma_{yy}, \sigma_{zz}, \sigma_{xz}, \sigma_{yz}, \sigma_{xy}\} \tag{4.3}$$

strains vector

$$\boldsymbol{\varepsilon}^T = \{\varepsilon_{xx}, \varepsilon_{yy}, \varepsilon_{zz}, \varepsilon_{xy}, \varepsilon_{xz}, \varepsilon_{yz}\} \tag{4.4}$$

$$b = \begin{bmatrix} \partial/\partial x & 0 & 0 \\ 0 & \partial/\partial y & 0 \\ 0 & 0 & \partial/\partial z \\ \partial/\partial z & 0 & \partial/\partial x \\ 0 & \partial/\partial z & \partial/\partial y \\ \partial/\partial y & \partial/\partial x & 0 \end{bmatrix} \tag{4.5}$$

Loading vector g,

$$\boldsymbol{g}^T = \{g_x, g_y, g_z\} \tag{4.6}$$

Similarly,assuming p_x, p_y, p_z are the applied loading vector per unit area on S_m. So Mechanical boundary conditions must be fulfilled on S_m with normal $n = (n_x, n_y, n_z)$,

$$\begin{cases} \sigma_{xx}n_x + \sigma_{yx}n_y + \sigma_{zx}n_z = p_x \\ \sigma_{xy}n_x + \sigma_{yy}n_y + \sigma_{zy}n_z = p_y \\ \sigma_{xz}n_x + \sigma_{yz}n_y + \sigma_{zz}n_z = p_z \end{cases} \tag{4.7}$$

4.1.2 Geometrical Relations

when studying on deformed structure in linear system,strain components are related to the displacement components u_x, u_y, u_z of the displacement vector u through the following differential equations:

$$
\begin{aligned}
\varepsilon_{xx} &= \frac{\partial u_x}{\partial x} = u_{x,x}, \ \gamma_{xy} = \frac{\partial u_x}{\partial y} + \frac{\partial u_y}{\partial x} = u_{x,y} + u_{y,x} \\
\varepsilon_{yy} &= \frac{\partial u_y}{\partial y} = u_{y,y} \ , \gamma_{zx} = \frac{\partial u_x}{\partial z} + \frac{\partial u_z}{\partial x} = u_{x,z} + u_{zy} \\
\varepsilon_{zz} &= \frac{\partial u_z}{\partial z} = u_{z,z}, \ \gamma_{zy} = \frac{\partial u_y}{\partial z} + \frac{\partial u_z}{\partial y} = u_{y,z} + u_{z,y}
\end{aligned}
\tag{4.8}
$$

where a compact notation to indicate derivatives is introduced (e.g. $u_{x,x}$ indicates the derivative of u_x with respect to x). Strains can be given in vectorial form,

$$
\varepsilon = bu \tag{4.9}
$$

where matrix b is a differential operator. In explicit form,

$$
\begin{Bmatrix} \varepsilon_{xx} \\ \varepsilon_{yy} \\ \varepsilon_{zz} \\ \gamma_{yz} \\ \gamma_{yz} \\ \gamma_{xy} \end{Bmatrix} = bu = \begin{bmatrix} \partial_x & 0 & 0 \\ 0 & \partial_y & 0 \\ 0 & 0 & \partial_z \\ \partial_z & 0 & \partial_x \\ 0 & \partial_z & \partial_y \\ \partial_y & \partial_x & 0 \end{bmatrix} \begin{Bmatrix} u_x \\ u_y \\ u_z \end{Bmatrix} \tag{4.10}
$$

4.1.3 Hooke's Law for isotropic materials

So the physical relationship between stress and strain in terms of stiffness coeffcients:

$$
\sigma = C\varepsilon \tag{4.11}
$$

also in written with compliances,

$$
\varepsilon = S\sigma \tag{4.12}
$$

where C is the stiffness coefficient for isotropic materials,

$$
\boldsymbol{C} = \begin{bmatrix} C_{11} & C_{12} & C_{12} & 0 & 0 & 0 \\ C_{21} & C_{11} & C_{12} & 0 & 0 & 0 \\ C_{21} & C_{21} & C_{11} & 0 & 0 & 0 \\ 0 & 0 & 0 & C_{44} & 0 & 0 \\ 0 & 0 & 0 & 0 & C_{44} & 0 \\ 0 & 0 & 0 & 0 & 0 & C_{44} \end{bmatrix} \tag{4.13}
$$

$$
C_{11} = 2G + \lambda, \quad C_{12} = C_{21} = \lambda, \quad C_{44} = G \tag{4.14}
$$

$$
G = \frac{E}{2(1+v)}, \quad \lambda = \frac{vE}{(1+v)(1-2v)} \tag{4.15}
$$

where E is Young's modulus, G is the shear modulus and λ is Poisson's ratio.

Using matrix notation, these relations can be written as

$$\left\{\begin{array}{c}\epsilon_x\\ \epsilon_x\\ \gamma_{xy}\end{array}\right\} = \left[\begin{array}{ccc}1/E & -\nu/E & 0\\ -\nu/E & 1/E & 0\\ 0 & 0 & 1/G\end{array}\right]\left\{\begin{array}{c}\sigma_x\\ \sigma_y\\ \tau_{xy}\end{array}\right\} \tag{4.16}$$

The quantity in brackets is called the *compliancematrix* of the material, denoted $\mathbf{S}$ or $\mathbf{S_{ij}}$.It is important to grasp the physical significance of its various terms. Directly from the rules of matrix multiplication, the element in the i^{th} row and j^{th} column of $\mathbf{S_{ij}}$ is the contribution of the j^{th} stress to the i^{th} strain.

If we wish to write the stresses in terms of the strains, the matrix can be inverted to give:

$$\left\{\begin{array}{c}\sigma_x\\ \sigma_y\\ \tau_{xy}\end{array}\right\} = \frac{E}{1-\nu^2}\left[\begin{array}{ccc}1 & \nu & 0\\ \nu & 1 & 0\\ 0 & 0 & (1-\nu)/2\end{array}\right]\left\{\begin{array}{c}\epsilon_x\\ \epsilon_y\\ \gamma_{xy}\end{array}\right\} \tag{4.17}$$

where here $\mathbf{G}$ has been replaced by $\mathbf{E}/2(1+\epsilon)$. This relation can be abbreviated further as:

$$\sigma = D\varepsilon \tag{4.18}$$

where $D = S^{-1}$ is the $stiffnessmatrix$.

4.1.4 Hooke's Law for orthotropic materials

If the material is orthotropic, matrix C can be written in the material reference system as:

$$\boldsymbol{C} = \left[\begin{array}{cccccc}C_{11} & C_{12} & C_{13} & 0 & 0 & 0\\ C_{21} & C_{22} & C_{23} & 0 & 0 & 0\\ C_{31} & C_{32} & C_{33} & 0 & 0 & 0\\ 0 & 0 & 0 & C_{44} & 0 & 0\\ 0 & 0 & 0 & 0 & C_{55} & 0\\ 0 & 0 & 0 & 0 & 0 & C_{66}\end{array}\right] \tag{4.19}$$

If the material has a texture like wood or unidirectionally-reinforced fiber composites as shown figure 4.2,the modulus $\mathbf{E_1}$ in the fiber direction will typically be larger than those in the transverse directions ($\mathbf{E_2}$ and $\mathbf{E_3}$).When $\mathbf{E_1}$, $\mathbf{E_2}$, $\mathbf{E_3}$ are not equal,the material is said to be *orthotropic*.It is common, however, for the properties in the plane transverse to the fiber direction to be isotropic to a good approximation ($\mathbf{E_2} = \mathbf{E_3}$),such a material is called $transverselyisotropic$. The elastic constitutive laws must be modified to account for this anisotropy, and the following form is an extension of the usual equations of isotropic elasticity to transversely isotropic materials:

$$\left\{ \begin{array}{c} \epsilon_1 \\ \epsilon_2 \\ \gamma_{12} \end{array} \right\} = \left[\begin{array}{ccc} 1/E_1 & -\nu_{21}/E_2 & 0 \\ -\nu_{12}/E_1 & 1/E_2 & 0 \\ 0 & 0 & 1/G_{12} \end{array} \right] \left\{ \begin{array}{c} \sigma_1 \\ \sigma_2 \\ \tau_{12} \end{array} \right\} \tag{4.20}$$

The parameter ν_{12} is the $principal Poisson's ratio$.

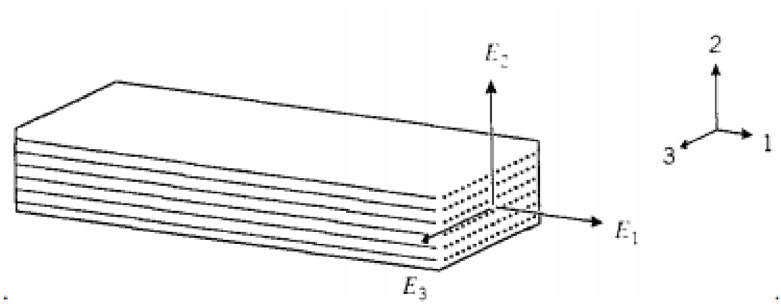

Figure 4.2: An orthotropic material

4.2 Governing equation via PVD

the PVD was used to derive the equilibrium equations of a generic point, Q, in a body D.the PVD (Principle of Virtual Displacements) is used to derive the displacement formulation for a 3D structural problem.Usually this form is called a 'strong' formulation, as it provides the exact equations of the problem in terms of displacements, stresses and strains at each point of D. They can usually only be solved for simple geometries and boundary conditions.

4.2.1 Strong Form of the Equilibrium Equations via the PVD

The use of the PVD allows one to derive the same equations, both weak and strong forms. The PVD can be written in its static case as

$$\delta L_{int} = \delta L_{ex} \tag{4.21}$$

where $\mathbf{L_{int}}$ is the internal elastic work, $\mathbf{L_{ext}}$ is the work done by the external forces and δ indicates the virtual variation. The internal work can be expressed in explicit form as

$$\delta L_{int} = \int_V \left(\sigma_{xx}\delta\varepsilon_{xx} + b_{yy}\delta\varepsilon_{yy} + \sigma_{zz}\delta\varepsilon_{zz} + \sigma_{xz}\delta\varepsilon_{xz} + \sigma_{yx}\delta\varepsilon_{yz} + \sigma_{xy}\delta\varepsilon_{xy} \right) dV \tag{4.22}$$

The same equation can be written in compact form using matrix notation:

$$\delta L_{int} = \int_V \delta\varepsilon^T \sigma dV \tag{4.23}$$

The external work on a general body D is expressed as a sum of four contributions: volume forces g, on volume V, surface forces p, on surface S, line forces q, on line l and the concentrated force P, at point Q. The formulation of the external work, introduced becomes

$$\delta L_{ent} = \int_V \delta u^T g dV + \int_S \delta u^T p dS + \int_L \delta u^T q dy + \delta u^T \big|_Q P \tag{4.24}$$

The relationship between the displacement vector u, and the strain vector ε, is obtained from the geometrical relation

$$\varepsilon = bu \tag{4.25}$$

where matrix b is a differential operator. In explicit form, the equation becomes

$$\begin{Bmatrix} \varepsilon_{xx} \\ \varepsilon_{yy} \\ \varepsilon_{zz} \\ \gamma_{xz} \\ \gamma_{yz} \\ \gamma_{xy} \end{Bmatrix} = bu = \begin{bmatrix} \partial_x & 0 & 0 \\ 0 & \partial_y & 0 \\ 0 & 0 & \partial_z \\ \partial_z & 0 & \partial_x \\ 0 & \partial_z & \partial_y \\ \partial_y & \partial_x & 0 \end{bmatrix} \begin{Bmatrix} u_x \\ u_y \\ u_z \end{Bmatrix} \tag{4.26}$$

The internal work can be written in terms of displacements as

$$\delta L_{int} = \int_V \delta(bu)^T \sigma dV = \int_V \left(\delta u^T b^T\right) \sigma dV \tag{4.27}$$

In order to obtain strong form equations, it is possible to move the differential operator from the displacements to the strains by integrating by parts,

$$\int_V \left(\delta u^T b^T\right) \sigma dV = -\int_V \delta u^T \left(b^T \sigma\right) dV + \int_S \delta u^T \left(I_n^T \sigma\right) dS \tag{4.28}$$

where $\mathbf{I_n}$ is a matrix with cosine directors. In the frst term on the right-hand side, operator b acts on the stress vector. The PVD can be written as

$$-\int_V \delta u^T \left(b^T \sigma\right) dV + \int_S \delta u^T \left(I_n^T \sigma\right) dS = \int_V \delta u^T g dV + \int_S \delta u^T p dS + \int_L \delta u^T q dy + \delta u^T \big|_Q P \tag{4.29}$$

From this equation, and using the virtual variation defnition, it is possible to derive the equilibrium equation at a generic point P on volume V of body D

$$\delta u : -b^T \sigma = g \tag{4.30}$$

From this equation, it is clear that the differential operator b must be the same for both the equilibrium and geometrical equations. The integrals on the surface give the boundary conditions, which can be expressed as

$$\delta u : I_n^T \sigma = p \tag{4.31}$$

4.2.2 Equilibrium equation in strong form

The equilibrium equations can be derived in explicit form by expanding Equation:

$$\begin{array}{ll} \delta u_x : & \frac{\partial \sigma_{xx}}{\partial x} + \frac{\partial \sigma_{xz}}{\partial z} + \frac{\partial \sigma_{xy}}{\partial y} = g_x \\ \delta u_y : & \frac{\partial \sigma_{yy}}{\partial y} + \frac{\partial \sigma_{yz}}{\partial z} + \frac{\partial \sigma_{yx}}{\partial x} = g_y \\ \delta u_z : & \frac{\partial \sigma_{zz}}{\partial z} + \frac{\partial \sigma_{zx}}{\partial x} + \frac{\partial \sigma_{zy}}{\partial y} = g_z \end{array} \tag{4.32}$$

This expansion is omitted for the sake of brevity. Hooke's law allows the equilibrium equations to be written in terms of displacements,

$$\delta u : -b^T C b u = g \tag{4.33}$$

If the material is isotropic, matrix C can be written using Lame coeffcients,

$$\boldsymbol{C} = \begin{bmatrix} \lambda + 2G & \lambda & \lambda & 0 & 0 & 0 \\ \lambda & \lambda + 2G & \lambda & 0 & 0 & 0 \\ \lambda & \lambda & \lambda + 2G & 0 & 0 & 0 \\ 0 & 0 & 0 & G & 0 & 0 \\ 0 & 0 & 0 & 0 & G & 0 \\ 0 & 0 & 0 & 0 & 0 & G \end{bmatrix} \tag{4.34}$$

where

$$\lambda = \frac{Ev}{(1+v)(1-2v)}, \quad G = \frac{E}{2(1+v)} \tag{4.35}$$

The equilibrium equations can be written, in strong form, by introducing a matrix k that originates from the previous matrix multiplication,

$$\delta u : ku = g \tag{4.36}$$

where

$$\boldsymbol{k} = -\boldsymbol{b}^T \boldsymbol{C} \boldsymbol{b} \tag{4.37}$$

above all, with isotropic and homogeneous materials and, for the sake of simplicity, matrix C is assumed to be constant in V. Matrix k is a 3 X 3 matrix and it contains nine differential operators,

$$\boldsymbol{k} = \begin{bmatrix} k_{xx} & k_{xy} & k_{xz} \\ k_{yx} & k_{yy} & k_{yz} \\ k_{zx} & k_{zy} & k_{zz} \end{bmatrix} \tag{4.38}$$

which, in explicit form, become

$$\begin{aligned}
k_{xx} &= -(\lambda + 2G)\partial_x\partial_x - G\partial_y\partial_y - G\partial_z\partial_z \\
k_{xy} &= -\lambda\partial_x\partial_y - G\partial_y\partial_x \\
k_{xz} &= -\lambda\partial_x\partial_z - G\partial_z\partial_x \\
k_{yx} &= -\lambda\partial_y\partial_x - G\partial_x\partial_y \\
k_{yy} &= -(\lambda + 2G)\partial_y\partial_y - G\partial_x\partial_x - G\partial_z\partial_z \\
k_{yz} &= -\lambda\partial_y\partial_z - G\partial_z\partial_y \\
k_{zx} &= -\lambda\partial_z\partial_x - G\partial_x\partial_z \\
k_{zy} &= -\lambda\partial_z\partial_y - G\partial_y\partial_z \\
k_{zz} &= -(\lambda + 2G)\partial_z\partial_z - G\partial_x\partial_x - G\partial_y\partial_y
\end{aligned} \tag{4.39}$$

The symbol ∂_x means partial differentiation with respect to x. The derivatives in Equation (4.39) appear in pairs, where the first derivative is due to a virtual variation of the strains, while the second is due to the stresses. Since the displacements are continuous functions, it is possible to state that

$$\partial_y\partial_x = \partial_x\partial_y = \partial_{yx}, \quad \partial_z\partial_x = \partial_x\partial_z = \partial_{zx}, \quad \partial_z\partial_y = \partial_y\partial_z = \partial_{zy} \tag{4.40}$$

Therefore Equation (4.39) can be written as

$$\begin{aligned}
k_{xx} &= -(\lambda + 2G)\partial_{xx} - G\partial_{yy} - G\partial_{zz} \\
k_{xy} &= -(\lambda + G)\partial_{xy} \\
k_{xz} &= -(\lambda + G)\partial_{xz} \\
k_{yx} &= -(\lambda + G)\partial_{yx} \\
k_{yy} &= -(\lambda + 2G)\partial_{yy} - G\partial_{xx} - G\partial_{zz} \\
k_{yz} &= -(\lambda + G)\partial_{yz} \\
k_{zx} &= -(\lambda + G)\partial_{zx} \\
k_{zy} &= -(\lambda + G)\partial_{zy} \\
k_{zz} &= -(\lambda + 2G)\partial_{zz} - G\partial_{xx} - G\partial_{yy}
\end{aligned} \tag{4.41}$$

Finally, the equilibrium equations can be written in terms of displacements,

$$
\begin{aligned}
\delta u_x :& -(\lambda + 2G)\left(\frac{\partial^2 u_x}{\partial x^2}\right) - G\left(\frac{\partial^2 u_z}{\partial y^2} + \frac{\partial^2 u_x}{\partial z^2}\right) \\
& -(\lambda + G)\left(\frac{\partial^2 u_y}{\partial x \partial y} + \frac{\partial^2 u_z}{\partial x \partial z}\right) = g_x \\
5u_y :& -(\lambda + 2G)\left(\frac{\partial^2 u_y}{\partial y^2}\right) - G\left(\frac{\partial^2 u_y}{\partial x^2} + \frac{\partial^2 u_y}{\partial z^2}\right) \\
\delta u_z :& -(\lambda + 2G)\left(\frac{\partial^2 u_z}{\partial z^2}\right) - G\left(\frac{\partial^2 u_z}{\partial x^2} + \frac{\partial^2 u_z}{\partial y^2}\right) \\
& -(\lambda + G)\left(\frac{\partial^2 u_x}{\partial y \partial x} + \frac{\partial^2 u_z}{\partial y \partial z}\right) = g_y \\
& -(\lambda + G)\left(\frac{\partial^2 u_z}{\partial z \partial x} + \frac{\partial^2 u_y}{\partial z \partial y}\right) = g_z
\end{aligned}
\tag{4.42}
$$

4.2.3 Fundamental nucleus in strong form

Although there are 9 terms in matrix k, only 2 terms have a different structure, let us consider the following two

$$k_{xx} = -(\lambda + 2G)\partial_{xx} - \lambda\partial_{zz} - \lambda\partial_{yy} \tag{4.43}$$

$$k_{xy} = -\lambda\partial_{xy} - G\partial_{yx} \tag{4.44}$$

It is evident that the other components of matrix k can be obtained in a similar form of k_{xx} and k_{xy}. The elements on the diagonal have the form of k_{xx}, therefore the terms k_{yy} and k_{zz} have the same form of k_{xx} with the indexes permuted. The elements out of the diagonal come from a permutation of the indexes of k_{xy} in fact k_{xz}, k_{yz}, k_{yx}, k_{zx} and k_{zy} can be obtained by permuting the indexes in k_{xy}.

4.2.4 Extension to composite material

If composite material are considered the formulation of the fundamental nuclei cannot be reduced at only two terms but all the 9 terms should be considered:

$$
\begin{aligned}
k_{xx} &= \partial_x C_{11} \partial_x + \partial_y C_{61} \partial_x + \partial_z C_{44} \partial_z + \partial_x C_{16} \partial_y + \partial_y C_{66} \partial_y \\
k_{xy} &= \partial_x C_{12} \partial_y + \partial_y C_{62} \partial_y + \partial_z C_{45} \partial_z + \partial_x C_{16} \partial_x + \partial_y C_{66} \partial_x \\
k_{xz} &= \partial_x C_{13} \partial_z + \partial_y C_{63} \partial_z + \partial_z C_{44} \partial_x + \partial_z C_{45} \partial_y \\
k_{yz} &= \partial_y C_{21} \partial_y + \partial_x C_{61} \partial_y + \partial_z C_{54} \partial_z + \partial_y C_{26} \partial_y + \partial_x C_{66} \partial_y \\
k_{yy} &= \partial_y C_{22} \partial_y + \partial_x C_{62} \partial_y + \partial_z C_{55} \partial_z + \partial_y C_{26} \partial_x + \partial_x C_{66} \partial_x \\
k_{yz} &= \partial_y C_{23} \partial_z + \partial_y C_{13} \partial_z + \partial_z C_{54} \partial_x + \partial_z C_{55} \partial_y \\
k_{zx} &= \partial_z C_{31} \partial_x + \partial_x C_{44} \partial_z + \partial_y C_{45} \partial_z + \partial_z C_{36} \partial_y \\
k_{zy} &= \partial_z C_{32} \partial_y + \partial_x C_{45} \partial_z + \partial_y C_{55} \partial_z + \partial_z C_{36} \partial_x \\
k_{zz} &= \partial_z C_{33} \partial_z + \partial_x C_{44} \partial_x + \partial_y C_{54} \partial_x + \partial_x C_{45} \partial_y + \partial_y C_{55} \partial_y
\end{aligned}
\tag{4.45}
$$

It is possible to see that the form of the nucleus elements is similar at the isotropic case. In this case the 9 terms have to be written in explicit form because the material constants cannot be written in terms of Lamé parameters.

4.3 Carrera Unified Formulation

CUF is based on a displacement field obtained in a unified manner, and then every theory order can be reached, which allows FE matrices/vectors to be derived in terms of fundamental nuclei. The CUF is introduced by extending the index notation (indexes i and j), which is often used in FE procedures, to the theory of structures (indexes τ and s). As a result, a fundamental nucleus (FN), expressed in terms of four indexes (τ, s, i and j), is obtained.

4.3.1 CUF Assembly Technique

The use of the CUF makes the assembly of the matrices a trivial operation that can be easily implemented in computer code. The assembly of the matrix consists of four loops on indexes i, j, τ and s, and an FN is calculated for each combination of these indexes. A representation of this procedure is shown in Figure 4.3. The diagram shows how it is possible to build a matrix of the node, of the element and finally, of the global stiffness matrix by exploiting the nucleus. The general form of the stiffness matrix is as follows:
Then,the main feature of the unified formulation is the possibility of arbitrarily choosing the kind of expansion and the number of terms.This section presents 2D flat elements based on Taylor expansions of the displacement variables. First of all, classical models (by Kirchhoff and Reissner–Mindlin) will be briefly described together with the more general complete linear expansion case.

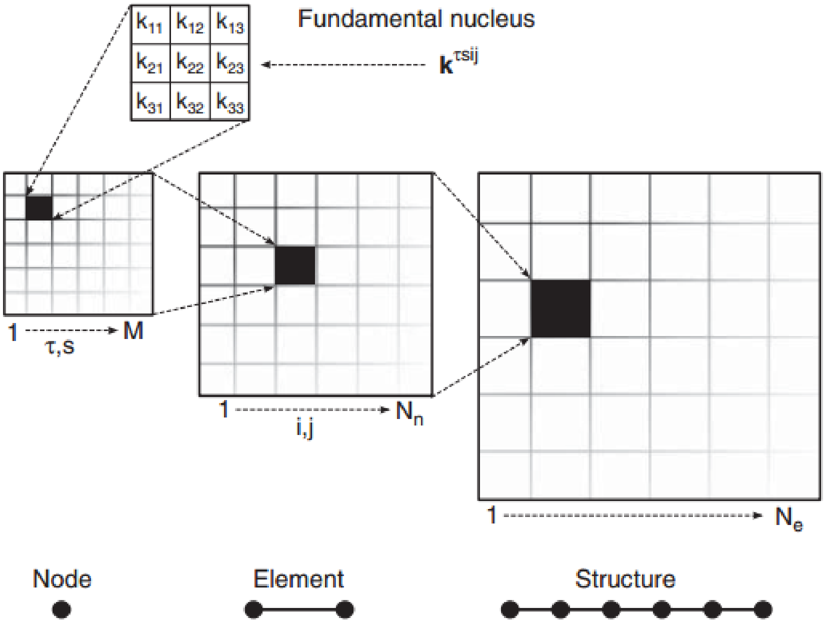

Figure 4.3: Representation of the assembly procedure: the FN is the core, the loops on τ and s build the matrix for a given pair of i and j, the loops on i and j give the matrix of the elements, and the loop on the elements gives the global stiffness matrix

$$
\begin{array}{ll|ccccccc}
 & & \multicolumn{3}{c}{\overbrace{\qquad\qquad\qquad}^{i=1}} & & \multicolumn{3}{c}{\overbrace{\qquad\qquad\qquad}^{i=N_{NE}}} \\
 & & \tau=1 & \cdots & \tau=M & & \tau=1 & \cdots & \tau=M \\
\multirow{3}{*}{$j=1$} & s=1 & \boldsymbol{k}^{1111} & \cdots & \boldsymbol{k}^{1M11} & & \boldsymbol{k}^{111N_n} & \cdots & \boldsymbol{k}^{1M1N_n} \\
 & \vdots & \vdots & & \vdots & \cdots & \vdots & & \vdots \\
 & s=M & \boldsymbol{k}^{M111} & \cdots & \boldsymbol{k}^{MM11} & & \boldsymbol{k}^{M11N_n} & \cdots & \boldsymbol{k}^{MM1N_n} \\
 & & & \vdots & & \ddots & & \vdots & \\
\multirow{3}{*}{$j=N_n$} & s=1 & \boldsymbol{k}^{11N_n1} & \cdots & \boldsymbol{k}^{1MN_n1} & & \boldsymbol{k}^{11N_nN_n} & \cdots & \boldsymbol{k}^{1MN_nN_n} \\
 & \vdots & \vdots & & \vdots & \cdots & \vdots & & \vdots \\
 & s=M & \boldsymbol{k}^{M1N_n1} & \cdots & \boldsymbol{k}^{MMN_n1} & & \boldsymbol{k}^{M1N_nN_n} & \cdots & \boldsymbol{k}^{MMN_nN_n}
\end{array}
$$

Figure 4.4: Each FN is reported as $k^{\tau sij}$ and it works as the core of the matrix construction. The indexes indicate the nucleus position in the global matrix.

4.4 2D Plate elements FEM formulation and discrezation

Plates are 2D structures in which one dimension, in general the thickness h, is at least one order of magnitude lower than the in-plane dimensions a and b Figure 4.5. This permits the reduction of the 3D problem to a 2D one. Such a reduction can be seen as a transformation of the problem defined at each point $Q_V(x, y, z)$ of the 3D continuum plate into a problem defned at each point $Q_\omega(x, y)$ of the plate surface ω. The elimination of the z coordinate can be performed through several methodologies that lead to a signifcant number of approaches and techniques. For instance, the unknown variables can be axiomatically assumed along z. This means that, for a given point $Q_\omega(x, y)$ in the plane, the distribution of the unknowns along the thickness will be given by a polynomial expansion in z.

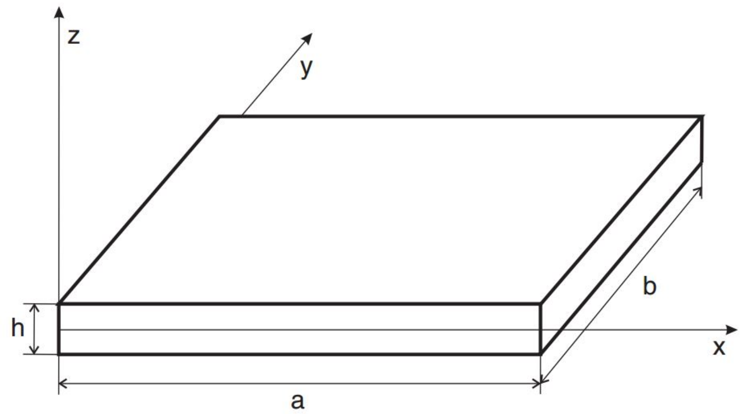

Figure 4.5: panel configuration

4.4.1 Classical Plate Theory

The Kirchhoff plate model, hereafter referred to as CPT (Classical Plate Theory), was derived from the following a priori assumptions:
1. Straight lines perpendicular to the mid-surface (i.e. transverse normals) before deformation remain straight after deformation.
2. The transverse normals do not experience elongation (i.e. they are inextensible).
3. The transverse normals rotate such that they remain perpendicular to the mid-surface after deformation.
According to the first hypothesis, the in-plane displacements u_x and u_y are

linear versus the thickness coordinate z

$$\begin{aligned} u_x(x,y,z) &= u_{x0}(x,y) + \phi_x(x,y)z \\ u_y(x,y,z) &= u_{y0}(x,y) + \phi_y(x,y)z \end{aligned} \tag{4.46}$$

where ϕ_x and ϕ_y are the rotations of a transverse normal about the y- and x-axes, respectively.The notation where ϕ_x denotes the rotation of a transverse normal about the y-axis and ϕ_y denotes the rotation about the x-axis may be a little confusing, and they do not follow the right-hand rule. However, the notation has been used extensively in the literature, and we will not depart from it. If (β_x, β_y) denote the rotations about the x- and y-axes that respectively, follow the right-hand rule, then

$$\beta_x = \phi_y, \quad \beta_y = -\phi_x \tag{4.47}$$

On the basis of the second hypothesis, the transverse displacement u_z is independent of the transverse (or thickness) coordinate and the transverse normal strain ε_{zz} is disregarded:

$$u_z(x,y,z) = u_{z0}(x,y) \Rightarrow \varepsilon_{zz} = \frac{\partial u_z}{\partial z} = 0 \tag{4.48}$$

On the basis of the third hypothesis and according to the defnition of shear strains, shear deformations γ_{xz} and γ_{yz} are disregarded:

$$\gamma_{xz} = \gamma_{yz} = 0 \tag{4.49}$$

Equations (4.46), (4.48) and (4.49) allow the rotation angles to be obtained as functions of the derivatives of the transverse displacement

$$\begin{cases} \gamma_{xz} = \frac{\partial u_z}{\partial x} + \frac{\partial u_x}{\partial z} = \frac{\partial u_{z0}}{\partial x} + \phi_x = 0 \\ \gamma_{xz} = \frac{\partial u_z}{\partial y} + \frac{\partial u_y}{\partial z} = \frac{\partial u_{z0}}{\partial y} + \phi_y = 0 \end{cases} \Rightarrow \begin{cases} \phi_x = -\frac{\partial u_{z0}}{\partial x} \\ \phi_y = -\frac{\partial u_{z0}}{\partial y} \end{cases} \tag{4.50}$$

The displacement feld of CPT is then

$$\begin{aligned} u_x &= u_{x0} - \frac{\partial u_{z0}}{\partial x} z \\ u_y &= u_{y0} - \frac{\partial u_{z0}}{\partial y} z \\ u_z &= u_{z0} \end{aligned} \tag{4.51}$$

where (u_{x0}, u_{y0}, u_{z0}) are the displacements along the coordinate lines of a material point on the xy-plane. Note that the form of the displacement feld in Equation (4.50) allows the reduction of the 3D problem to one of studying the deformation of the reference plane $z = 0$ (or midplane). Once the midplane displacements (u_{x0}, u_{y0}, u_{z0}) are known, the displacements of any arbitrary point (u_x, u_y, u_z) in the 3D continuum can be determined using Equation (4.50).
According to the kinematic hypotheses, CPT accounts for the in-plane strains only. On the basis of their defnition, and of the CPT displacement feld, these

strains are

$$
\begin{aligned}
\varepsilon_{xx} &= \frac{\partial u_x}{\partial x} = \frac{\partial u_{x_0}}{\partial x} - \frac{\partial^2 u_{z_0}}{\partial x^2} z = k_x^x + k_{xx^2}^z z \\
\varepsilon_{yy} &= \frac{\partial u_y}{\partial y} = \frac{\partial u_{y_0}}{\partial y} - \frac{\partial^2 u_{z_0}}{\partial y^2} z = k_y^y + k_{yy^2}^z z \\
\gamma_{xy} &= \frac{\partial u_x}{\partial y} + \frac{\partial u_y}{\partial x} = \frac{\partial u_{x_0}}{\partial y} + \frac{\partial u_{y_0}}{\partial x} - 2\frac{\partial^2 u_{z_0}}{\partial xy} z = k_y^x + k_x^y + 2k_{xy}^z z^2
\end{aligned}
\tag{4.52}
$$

k_x^x, k_y^y, k_x^y have the physical meaning of membrane deformation, whereas k_{xx}^z ,k_{yy}^z and k_{xy}^z ,being the second-order derivatives of the transverse displacement, represent the curvatures in the case of infnitesimal deformations and small rotations. The corresponding in-plane stresses are obtained by means of the reduced constitutive equations

$$
\left\{ \begin{array}{c} \sigma_{xx} \\ \sigma_{yy} \\ \tau_{xy} \end{array} \right\} = \frac{E}{1-v^2} \left[\begin{array}{ccc} 1 & v & 0 \\ v & 1 & 0 \\ 0 & 0 & (1-v)/2 \end{array} \right] \left\{ \begin{array}{c} \varepsilon_{xx} \\ \varepsilon_{yy} \\ \gamma_{xy} \end{array} \right\}
\tag{4.53}
$$

4.4.2 First-Order Shear Deformation Theory

In the Reissner–Mindlin theory, also called first-order shear deformation theory (FSDT), the third part of Kirchhoff's hypothesis is removed, therefore the transverse normals do not remain perpendicular to the mid-surface after deformation. In this way, transverse shear strains γ_{xz} and γ_{yz} are included in the theory. However, the inextensibility of the transverse normal remains,so displacement u_z is constant in the thickness direction z. The displacement field in the case of FSDT is

$$
\begin{aligned}
u_x(x,y,z) &= u_{x_0}(x,y) + \phi_x(x,y)z \\
u_y(x,y,z) &= u_{y_0}(x,y) + \phi_y(x,y)z \\
u_z(x,y,z) &= u_{z_0}(x,y)
\end{aligned}
\tag{4.54}
$$

The quantities (u_{x0}, u_{y0},u_{z0},ϕ_x,ϕ_y) will be the unknowns. For thin plates, i.e. when the plate in-plane characteristic dimension-to-thickness ratio is of the order of 50 or more, the rotation functions ϕ_x and ϕ_y should approach the respective slopes of the transverse deflection $\frac{\partial u_{z0}}{\partial x}$ and $\frac{\partial u_{z0}}{\partial y}$. Figure 4.6 shows the typical distribution of displacement components according to FSDT: linear for ux and uy and constant for uz. Also the physical meaning of the rotations, ϕ_x and ϕ_y, is represented.
The strain components are obtained by substituting the displacement field in the geometrical relations. Only strain ε_{zz} is zero, therefore the non-null strains are

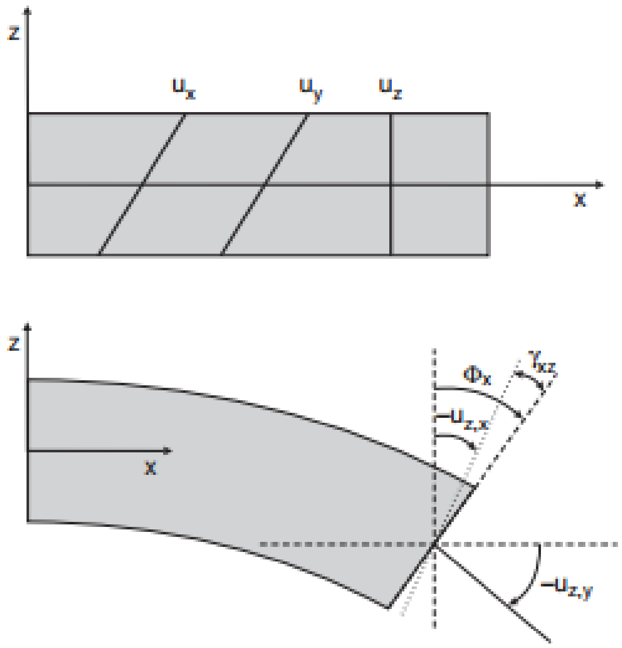

Figure 4.6: Distribution of displacements in FSDT

$$
\begin{aligned}
\varepsilon_{xx} &= \frac{\partial u_x}{\partial x} = u_{x_0 x} + \phi_{x_r x^2} \\
\varepsilon_{yy} &= \frac{\partial u_y}{\partial y} = u_{y_0 y} + \phi_{yy^z} \\
\gamma_{xy} &= \frac{\partial u_x}{\partial y} + \frac{\partial u_y}{\partial x} = u_{x_0 y} + u_{y_0 x} + \phi_{x_0} z + \phi_{y,x^2} z \\
\gamma_{xz} &= \frac{\partial u_x}{\partial z} + \frac{\partial u_z}{\partial x} = \phi_x + u_{z_0 x} \\
\gamma_{xy} &= \frac{\partial u_x}{\partial y} + \frac{\partial u_y}{\partial x} = \phi_y + u_{z_0 y}
\end{aligned}
\tag{4.55}
$$

The constitutive relations are used to obtain the in-plane stresses and the shear stress components

$$
\begin{aligned}
&\left\{ \begin{array}{c} \sigma_{xx} \\ \sigma_{yy} \\ \tau_{xy} \end{array} \right\} = \frac{E}{1-v^2} \begin{bmatrix} 1 & v & 0 \\ v & 1 & 0 \\ 0 & 0 & (1-v)/2 \end{bmatrix} \left\{ \begin{array}{c} \varepsilon_{xx} \\ \varepsilon_{yy} \\ \gamma_{xy} \end{array} \right\} \\
&\tau_{xz} = \kappa G \gamma_{xz}, \quad \tau_{yz} = \kappa G \gamma_{yz}
\end{aligned}
\tag{4.56}
$$

where κ is the shear correction factor.

4.4.3 FEM model

The FEM approximation can be introduced using the two-dimensional shape function, N_i:

$$\boldsymbol{u}_\tau(x, y) = N_i \boldsymbol{u}_{\tau i} \tag{4.57}$$

The displacement field therefore becomes

$$\boldsymbol{u}(x, y, z) =| N_i(x, y) F_\tau(z) \boldsymbol{u}_{\tau i} \tag{4.58}$$

As for the three-dimensional model, the virtual variation of the displacement can be written as:

$$\boldsymbol{u}(x, y, z) = N_j(x, y) F_s(z) \boldsymbol{u}_{js} \tag{4.59}$$

4.4.4 FE Approximation in the CUF

Use of the FEM allows the displacement field to be written as the sum of the known functions multiplied by a constant. In the simple case introduced with an eight-node element was considered, and the displacement field can therefore be written as

$$\boldsymbol{u} = u_1 N_1 + u_2 N_2 + u_3 N_3 + u_4 N_4 + u_5 N_5 + u_6 N_6 + u_7 N_7 + u_8 N_8 \tag{4.60}$$

The same displacement feld can be written in index form,If i is the index used for the displacement,

$$\boldsymbol{u} = N_i \boldsymbol{u}_i \tag{4.61}$$

The virtual variation of the displacements can be written in the same form using index j,

$$\delta u = N_j \delta u_j \tag{4.62}$$

The strains, and their virtual variations, can also be written in this compact form,

$$\begin{aligned} \varepsilon &= bN_i u_i \\ \delta\varepsilon &= bN_j \delta u_j \end{aligned} \tag{4.63}$$

In the same way, the stresses become

$$\sigma = CbN_i u_i \tag{4.64}$$

Indexes i and j can vary according to the number of nodes of the element.

4.4.5 Stiffness matrix

The governing equation of the two-dimensional problem can be derived using the PVD. The indicial notation allows the eruptions to be written in terms of fundamental nuclei.The virtual variation of the internal work in compact form is

$$\delta L_{\text{int}} = \delta \boldsymbol{u}_{js} \left(\int_V N_j F_s \boldsymbol{b}^T \boldsymbol{C} \boldsymbol{b} N_i F_\tau dV \right) \boldsymbol{u}_{\tau i} \tag{4.65}$$

The plate model used herein is based on the Mixed interpolation of Tensorial Components formulation, therefore the matrix b assume a more complex formulation with respect the Equation:4.26, now introduce the 3 x 3 matrix $K^{\tau sij}$

$$\delta L_{int} = \delta u_j K^{\tau sij} u_i \tag{4.66}$$

Matrix $K^{\tau sij}$ is the fundamental nucleus of the stiffness matrix and is a 3 x 3 matrix,as shown in the following formula

$$K^{\tau sij} = \int_V \left[N_j \underbrace{\overbrace{\begin{bmatrix} 3 \times 6 \end{bmatrix}}^{\boldsymbol{b}^T} \overbrace{\begin{bmatrix} 6 \times 6 \end{bmatrix}}^{\boldsymbol{C}} \overbrace{\begin{bmatrix} 6 \times 3 \end{bmatrix}}^{\boldsymbol{b}}}_{\begin{bmatrix} 3 \times 3 \end{bmatrix}} N_i \right] dV = \begin{bmatrix} k_{xx}^{\tau sij} & k_{xy}^{\tau sij} & k_{xz}^{\tau sij} \\ k_{yx}^{\tau sij} & k_{yy}^{\tau sij} & k_{yz}^{\tau sij} \\ k_{zx}^{\tau sij} & k_{zy}^{\tau sij} & k_{zz}^{\tau sij} \end{bmatrix}$$

$$\begin{aligned}
k_{xx}^{\tau sij} &= (\lambda + 2G) \int_V N_{i,x} N_{j,x} F_\tau F_s dV + G \int_V N_{i,y} N_{j,y} F_\tau F_s dV + G \int_V N_i N_j F_{\tau,z} F_{s,z} dV \\
k_{xy}^{\tau sij} &= \lambda \int_V N_{i,y} N_{j,x} F_\tau F_s dV + G \int_V N_{i,x} N_{j,y} F_\tau F_s dV \\
k_{xz}^{\tau sij} &= \lambda \int_V N_i N_{j,x} F_{\tau,z} F_s dV + G \int_V N_{i,x} N_j F_\tau F_{s,z} dV \\
k_{yz}^{\tau sij} &= \lambda \int_V N_{i,x} N_{j,y} F_\tau F_s dV + G \int_V N_{i,y} N_{j,x} F_\tau F_s dV \\
k_{\text{yy}}^{\tau sij} &= (\lambda + 2G) \int_V N_{i,y} N_{j,y} F_\tau F_s dV + G \int_V N_{i,x} N_{j,x} F_\tau F_s dV + G \int_V N_i N_j F_{\tau,z} F_{s,z} dV \\
k_{yz}^{\tau sij} &= \lambda \int_V N_i N_{j,y} F_{\tau,z} F_s dV + G \int_V N_{i,y} N_j F_\tau F_{s,z} dV \\
k_{zx}^{\tau sij} &= \lambda \int_V N_{i,x} N_j F_\tau F_{s,z} dV + G \int_V N_i N_{j,x} F_{\tau,z} F_s dV \\
k_{zy}^{\tau sij} &= \lambda \int_V N_{i,y} N_j F_\tau F_{s,2} dV + G \int_V N_i N_{j,y} F_{\tau,z} F_s dV \\
k_{zz}^{\tau sij} &= (\lambda + 2G) \int_V N_i N_j F_{\tau,z} F_{s,z} dV + G \int_V N_{i,x} N_{j,x} F_\tau F_s dV + G \int_V N_{i,y} N_{j,y} F_\tau F_s dV
\end{aligned} \tag{4.67}$$

4.4.6 Mass matrix

The virtual variation of the inertial work, as well as the internal work, can be expressed in terms of displacements. If the displacements are expressed in compact formulation, the inertial work becomes

$$\delta L_{\text{ine}} = \boldsymbol{\delta u}_j \left(\int_V N_j F_s \boldsymbol{I} \rho \boldsymbol{I} F_\tau N_i dV \right) \boldsymbol{u}_i \tag{4.68}$$

The identity matrix $\mathbf{I}$ is introduced and the fundamental nucleus of the mass matrix is

$$\delta L_{\text{ine}} = \delta u_{js} M^{\tau sij} \ddot{u} \tag{4.69}$$

where

$$\boldsymbol{m}^{ij} = \int_V N_j \boldsymbol{I} \rho \boldsymbol{I} N_i dV \tag{4.70}$$

Matrix m^{ij} is a 3 x 3 matrix. It only has 3 elements on the diagonal that are not 0,

$$\begin{aligned} m_{xx}^{\tau sij} &= \int_V N_j F_s \rho N_i F_\tau dV \\ m_{yy}^{\tau sij} &= \int_V N_j F_s \rho N_i F_\tau dV \\ m_{zz}^{Tsij} &= \int_V N_j F_s \rho N_i F_\tau dV \end{aligned} \tag{4.71}$$

While the elements outside the diagonal are null,

$$m_{yz}^{\tau sij} = m_{zx}^{\tau sij} = m_{zy}^{\tau sij} = m_{xy}^{\tau sij} = m_{xz}^{\tau sij} = m_{yx}^{\tau sij} = 0 \tag{4.72}$$

The assembly of the global mass matrix follows the same rules as those of the stiffness matrix. The loops on the indices i and j give the mass matrix of the elements. The mass matrix of the structure can be assembled by superimposing the masses of the shared nodes.

4.4.7 Loading vector

The loading vector can be derived using the formulation of the virtual variation of the external work.The virtual variation of the displacements in Equation (4.62) can be used to express the virtual variation of the external work in the CUF framework.

The virtual variation of the external work can be written as:

$$\delta L_{cxt} = \int_V \delta \boldsymbol{u}^T \boldsymbol{g} dV + \int_S \boldsymbol{\delta u}^T \boldsymbol{p} dS + \int_L \boldsymbol{\delta u}^T \boldsymbol{q} dy + \boldsymbol{\delta u}_j^T \boldsymbol{P} \tag{4.73}$$

were g are the volume forces, p are the surface forces, q are the line forces and P are the concentrated loads. The external loads are usually applied as surface loads, or as a concentrated load.
Each contribution of the external load can be written in the indicial form. The volume loads become

$$\delta L_{cxt} = \int_V \delta \boldsymbol{u}^T \boldsymbol{g} dV = \delta \boldsymbol{u}_{js}^T \int_V N_j F_s \boldsymbol{g} dV \tag{4.74}$$

The surface load are

$$\delta L_{ext} = \int_S \delta \boldsymbol{u}^T \boldsymbol{p} dS = \delta \boldsymbol{u}_{js}^T \int_S N_j F_s \boldsymbol{p} dS \tag{4.75}$$

The line loads becomes

$$\delta L_{ext} = \int_l \delta \boldsymbol{u}^T \boldsymbol{q} dl = \delta \boldsymbol{u}_{js}^T \int_l N_j F_s \boldsymbol{q} dl \tag{4.76}$$

Where l is the line where the load is applied. Finally the concentrated loads are

$$\delta L_{ext} = \delta \boldsymbol{u}^T P = \delta \boldsymbol{u}_{js}^T N_j F_s P \tag{4.77}$$

The load vector can be written as the sum of the previous contributions

$$\boldsymbol{P}^{sj} = \int_V N_j F_s \boldsymbol{g} dV + \int_S N_j F_s p dS + \int_I N_j F_s \boldsymbol{q} dl + N_j F_s P \tag{4.78}$$

The load vector of the element can be assembled following the same procedure that was introduced for the stiffness matrix. In this case, only a loop on j and s gives the load vector of the element. The global vector can be derived by summing the loads in the shared nodes.

Chapter 5

Piston theory

Piston theory has been used broadly to a number of aerodynamic models which describe the pressure on a point of a body through analogy to the motion of a piston in a 1-dimensional cylinder. As a result, a number of flavours of piston theory exist, with variations in the basis of the pressure equation and in the reference frame used. However, all the variations assume supersonic flow at the point under consideration, with various limits of validity depending on the basis of the theory. In all cases, piston theory provides a quasi-steady, point-function relationship between the surface downwash and aerodynamic pressure at a point on a body. This renders piston theory a computationally inexpensive aerodynamic model.[122]

5.1 Developments in Piston Theory

5.1.1 Lightill's Classical Piston Theory

Piston theory was originally developed by Lighthill, on the basis of the extension of Tsien's hypersonic similitude by Hayes.Under the condition that the basic principles and assumptions of aerodynamics are satisfied, When the aircraft is flying at hypersonic speed, the Mach Angle of the airflow is very small, and the disturbance on the surface only propagates along the normal direction.When the aerodynamic model is built, the influence of each point on other is ignored and the following assumptions are made:The relationship between the downwash and the pressure on the surface is a point function,in other words, the local velocity corresponding to the direction perpendicular to the incoming flow is directly proportional to the local pressure on the surface.This can be simulated as the relation between the pressure acting on the piston in a unitary pipe and the piston moving speed.

The gas in the pipe is an ideal gas, w(t) is the moving velocity of the piston, which $P_\infty(P_0)$,ρ_∞,$a_\infty(a_0)$ are seperately the undisturbed pressure,density and speed of sound. In the case of w(t)$< a_\infty$ the moving velocity of the piston, the piston is equivalent to a small disturbance. When the gas in the pipe moves,

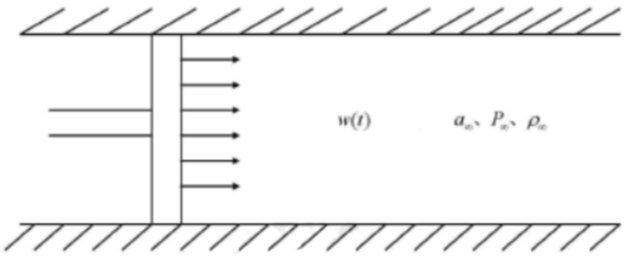

Figure 5.1: movement of Piston

it satisfies the motion equation, the continuous equation and the adiabatic equation, namely the following three equationseq. (5.1),eq. (5.2),eq. (5.3):

$$\frac{\partial w}{\partial t} + w\frac{\partial w}{\partial z} = -\frac{1}{\rho}\frac{\partial P}{\partial z} \tag{5.1}$$

$$\frac{\partial \rho}{\partial t} + \frac{\partial(\rho w)}{\partial z} = 0 \tag{5.2}$$

$$\frac{P}{\rho'} = \frac{P_\infty}{\rho'_\infty} \tag{5.3}$$

reorganized those equations,then:

$$\frac{\partial w}{\partial t} + w\frac{\partial w}{\partial z} + \frac{1}{\rho}\frac{\partial P}{\partial \rho}\frac{d\rho}{dw}\frac{\partial w}{\partial z} = 0 \tag{5.4}$$

$$\frac{\partial \rho}{\partial w}\frac{\partial w}{\partial t} + \frac{\partial(\rho w)}{\partial w}\frac{\partial w}{\partial z} = 0 \tag{5.5}$$

Compute partial equation then

$$\frac{d\rho}{dw} = \frac{\rho}{a} \tag{5.6}$$

$$a = \sqrt{\frac{\gamma P}{\rho}} = \sqrt{\frac{\gamma P_\infty}{\rho_\infty}} \rho^{\frac{\gamma-1}{2}} \tag{5.7}$$

γ is the specific heat ratio.

$$dw = \sqrt{\frac{\gamma P_\infty}{\rho'_\infty}} \rho^{\frac{\gamma-1}{2}} d\rho \tag{5.8}$$

Take the product of both sides of above equation,we obtain

$$w = \frac{2}{\gamma - 1} \sqrt{\frac{\gamma P_\infty}{\rho_\infty}} \rho^{\frac{\gamma-1}{2}} + c \tag{5.9}$$

which is equal with eq. (5.9)

$$w = \frac{2}{\gamma - 1} a + c \tag{5.10}$$

When U ia equal to Zero,a=a_∞,c=$\frac{2}{\gamma-1}a_\infty$,we could get w=$\frac{2}{\gamma-1}a - a_\infty$, a=$a_\infty(\frac{P}{P_\infty})^{\frac{\gamma-1}{2\gamma}}$
Then we obtain,

$$w = \frac{2}{\gamma - 1} a_\infty [(\frac{P}{P_\infty})^{\frac{\gamma-1}{2\gamma}} - 1] \tag{5.11}$$

So we get from the above equation

$$\frac{P}{P_\infty} = (1 + \frac{\gamma - 1}{2} \frac{w}{a_\infty})^{\frac{2\gamma}{\gamma-1}} \tag{5.12}$$

eq. (5.12) also could be written into

$$\frac{P}{P_0} = (1 + \frac{\gamma - 1}{2}\frac{u_z}{a_0})^{\frac{2\gamma}{\gamma-1}} \tag{5.13}$$

in which , u_z is the same as w.The above formula is an expression for the immediate pressure generated on the piston surface.
because of w«a_∞, then Taylor expansion in the above equation,after that the linear piston theory can be obtained

$$P - P_\infty = P_\infty a_\infty w \tag{5.14}$$

Lighthill [122] recommended the use of the third-order binomial expansion of the equation, given in eq. (5.15). The influence of entropy is of third-order in flow deflection; the series expansions of the pressure equations for oblique shocks and Prandlt-Meyer expansions differ in their third-order terms. Lighthill noted that the pressure given by third-order truncation,eq. (5.15), was bounded by results from eq. (5.13) and from oblique shock theory; hence the third-order expansion of the simple wave equation was deemed sufficiently accurate to use for both expansion and compression flows.

$$\frac{P}{P_0} = [1 + \gamma(\frac{u_z}{a_0}) + \frac{\gamma(\gamma+1)}{4}(\frac{u_z}{a_0})^2 + \frac{\gamma(\gamma+1)}{12}(\frac{u_z}{a_0})^3] \tag{5.15}$$

The assumptions inherent in the model were considered to be a good approximation to the flow physics, provided that the piston velocity did not exceed the speed of sound in the freestream. The range of validity set by Lighthill was for piston motions conforming for Mach numbers in the range of M>4. Lightill noted that enforcing the limits of validity allowed the piston pressure to be modeled as dependent on only the instantaneous piston velocity, neglecting the history of piston motion.
Lighthill's original development of piston theory has been dubbed "classical piston theory"(CPT). In CPT, both the steady pressure distribution (due to airfoil shape and mean incidence) and the unsteady pressure distribution (due to airfoil motion and surface deformations) are computed.

5.1.2 Further Developments of Classical Piston Theory

The widely cited review of piston theory by Ashley and Zartarian [29] summarises the work of Hayes [123] and Lighthill[28], and considers the application to a number aeroelastic problems,including airfoil flutter, wing flutter, and

panel flutter. In the review by Ashley and Zartarian,linearized piston theory as applied to "small motions of thin airfoils" was determined to be valid [29]for any of the conditions.
The three available conditions of piston theory are: $\omega^{*2}Ma^2 >> 1$,$\omega^* Ma >> 1$, $Ma^2 >> 1$(ω^* Is the reduction frequency,Ma Is the Mach number of airflow).
Whilst no extensions to the formulation of piston theory were made in the review by Ashley and Zartarian [29], the applications of contemporary research were covered. This was shortly followed by the work of Chawla [124], which was significant in conducting a parametric study of airfoil flutter at high Mach numbers using piston theory.
The theoretical basis for piston theory was revisited by Bird [125], who noted that the limiting assumptions on high Mach number and small airfoil thickness may be avoided in certain special flow cases. Bird noted that the equations of motion of two-dimensional steady flow reduce identically to those of one-dimensional unsteady flow when the velocity component of the flow in any direction remains constant throughout the flow field. Bird noted that for these special cases, the piston acts perpendicular to the direction of constant velocity, rather than perpendicular to the freestream velocity, and provided an amendeded equation for the convective component of the piston downwash. Of significance is Bird's recommendation to define the cylinder orientation as perpendicular to the surface, this recommendation was followed in many subsequent applications of piston theory
Rodden et al [126] used third-order CPT to extract aerodynamic influence coefficients for an aerodynamic modeling routine for swept wings. The formulation represented an extension of the application of piston theory, with a sweep correction being introduced. Of particular interest is the generalized formulation of the equation for the pressure coefficient in CPT, first put forward by Rodden as:

$$C_p = \frac{2}{M_\infty^2}\left[c_1\left(\frac{w}{a_\infty}\right) + c_2\left(\frac{w}{a_\infty}\right)^2 + c_3\left(\frac{w}{a_\infty}\right)^3\right] \tag{5.16}$$

C_p is Pressure coefficient,It was noted that both Lighthill's CPT and Van Dyke's second-order theory could be described by eq. (5.16), with the coefficients c1, c2, and c3 being defined by which theory was implemented.
Classical piston theory is a mature aerodynamic method. However, a number of formulations exist, with differences in the coefficients used and in the definition of the downwash and the direction of the piston action. The works cited here are representative of the main developments to CPT as applied to airfoils.

5.1.3 Local Piston Theory

The method was first suggested by Morgan [127] towards the end of the 1950s as "local-flow piston theory".
Based on the first-order piston theory, the analytical expression of aerodynamic force on two-dimensional panels can be obtained as follows:

$$p - p_\infty = -\frac{2q}{\sqrt{Ma^2 - 1}} \left(\frac{\partial w}{\partial x} + \frac{Ma^2 - 2}{Ma^2 - 1} \frac{1}{V} \frac{\partial w}{\partial t} \right) \tag{5.17}$$

of which $q = \rho_a V^2/2$ is dynamic pressure, ρ_a is air density, $V$is airflow velocity. It can be seen from the formula eq. (5.17) that the first term in the aerodynamic expression is proportional to the Angle of attack of the plate relative to the airflow, and the second term is proportional to the lateral vibration velocity of the plate. Therefore, the first-order piston theory belongs to the linear quasi-steady aerodynamic theory. In case $Ma >> 1$,the formula eq. (5.17) The linear aerodynamic force can be simplified as

$$p - p_\infty = -\frac{2q}{Ma} \left(\frac{\partial w}{\partial x} + \frac{1}{V} \frac{\partial w}{\partial t} \right) \tag{5.18}$$

The first-order piston theory is applicable to the analysis of aerodynamic forces on airflow plates at supersonic speeds ($\sqrt{2} < Ma < 5$). If the Mach number of the airflow on the panel exceeds 5 and enters the hypersonic stage, the first-order piston theory cannot truly reflect the aerodynamic nonlinear effect that increases significantly with the Mach number. Piston theory of aerodynamic force of the influence of nonlinear term on the panel flutter force with the foregoing, to the contrary, the influence of the internal forces in the panel flutter system play a "soft spring" effect, which with the increase of vibration amplitude aerodynamic force of the nonlinear item of the equivalent stiffness of the panel flutter system is reduced, which results in the decrease of the flutter critical velocity of the plate, so with the analysis of hypersonic flutter characteristics of airflow in the panel, enough attention to the nonlinear effect of aerodynamic force needed focused.At the hypersonic stage of $Ma > 5$, the third-order piston theory can better reflect the nonlinear effect of aerodynamic force. The analytical expression of unsteady aerodynamic force of two-dimensional panels obtained by the third-order piston theory is:

$$
\begin{aligned}
p - p_\infty = -\tfrac{2q}{Ma} \Big[& C_{1t} \tfrac{1}{V} \tfrac{\partial w}{\partial t} + C_{1x} \tfrac{\partial w}{\partial x} + \\
& \tfrac{\gamma+1}{4} Ma \left(C_{2t} \tfrac{1}{V} \tfrac{\partial w}{\partial t} + C_{2x} \tfrac{\partial w}{\partial x} \right)^2 + \\
& \tfrac{\gamma+1}{12} Ma^2 \left(C_{3t} \tfrac{1}{V} \tfrac{\partial w}{\partial t} + C_{3x} \tfrac{\partial w}{\partial x} \right)^3 \Big]
\end{aligned}
\tag{5.19}
$$

In the formula, γ is the specific heat ratio. By taking the parameter value $C_{it}, C_{ix} (i = 1,2,3)$ of 0 or 1, the nonlinear term of aerodynamic force can be selected or rejected. When all parameters C_{it}, C_{ix} are equal to 1, eq. (5.19) becomes the formula for calculating the aerodynamic force of the whole third order.

5.2 Aeroelastic model

In the study of panel flutter, many researchers have proposed various aerodynamic computational models in order to better simulate the actual aerodynamic change process.Commonly used aerodynamic calculation models include piston theory, linear potential theory, Newton theory, and some unsteady aerodynamic model based on the solution of Euler equation or N-S equation.Among them, the application scope of various theoretical models is different. In terms of computational precision, the aerodynamic model based on equation or equation solution is more consistent with the actual situation. However, the shortcoming of this aerodynamic model lies in the consideration of more complex boundary conditions, so the solution process of the equation is quite complex.The piston theory is the most widely used in the analysis of the actual panel flutter problem.Because this method can not only simulate the aerodynamic change process more accurately, but also its calculation process is relatively easy to realize.fig. 5.2 is 2D aeroelastic model, U is incoming airflow. fig. 5.3 shows the reference system used in the following formulation.

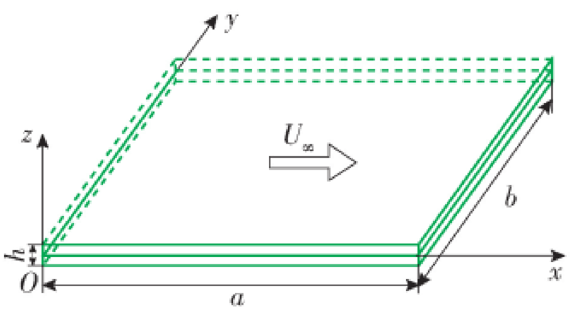

Figure 5.2: Composite 2D laminated plate in airflow

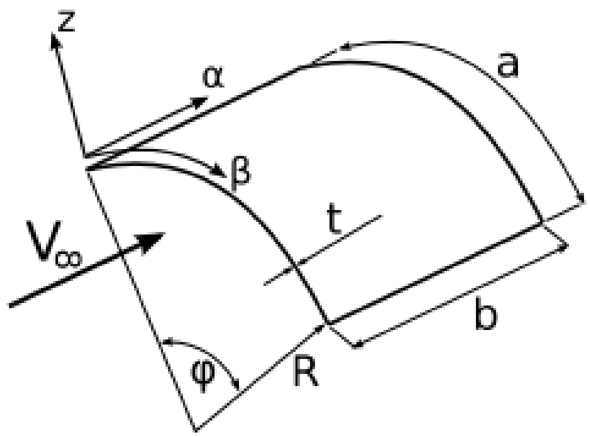

Figure 5.3: Reference system used in the two-dimensional aeroelastic model

5.2.1 Aerodynamic Stiffness Matrix

The aerodynamic stiffness matrix may be derived evaluating the work $\delta\mathbf{L_{aer}}$, made by a differential pressure Δp, due to the slope of the surface in the flow direction.

$$\delta L^{A}_{\text{acr}} = \int_{\Lambda} \left(\delta \mathbf{u}^{k} \Delta p^{A} \right) d\Lambda \tag{5.20}$$

where the index **A** indicates that only the contribution of the slope is considered,and Λ is the surface where the pressure is acting. Considering the formulation proposed in eq.5.17,and introducing the displacement formulation .the differential pressure can be written as:

$$\Delta p^{A} = A \frac{\partial u_z}{\partial \alpha} = A \cdot I_{\Delta p} \frac{\partial N_i}{\partial \alpha} F_{\tau} q^{k}_{i\tau} \tag{5.21}$$

Where:

$$I_{\Delta p} = \begin{bmatrix} 0 & 0 & 0 \\ 0 & 0 & 0 \\ 0 & 0 & 1 \end{bmatrix} \tag{5.22}$$

Being $d\Lambda = d\alpha \cdot d\beta$ and substituting eq.5.21 in eq.5.20, the virtual work of the differential pressure can be written as:

$$\delta L^{A}_{\text{acr}} = \delta q^{k^{T}}_{js} \left[A \left(F_{\text{s}} F_{\tau} \right) \int_{\Lambda} N_j \frac{\partial N_i}{\partial \alpha} I_{\Delta p} d\alpha d\beta \right] q^{k}_{i\tau} = \delta q^{k^{T}}_{js} k^{kij\tau s}_{a} q^{k}_{i\tau} \tag{5.23}$$

Where $k^{kij\tau s}_{a}$ is the aerodynamic stiffness matrix and it may be written in the form:

$$k_a^{\text{kijrs}} = \frac{2q}{\sqrt{M^2-1}} F_\tau F_s \begin{bmatrix} 0 & 0 & 0 \\ 0 & 0 & 0 \\ 0 & 0 & \int_\Lambda N_j \frac{\partial N_i}{\partial \alpha} d\alpha d\beta \end{bmatrix} \tag{5.24}$$

5.2.2 Aerodynamic Damping Matrix

The aerodynamic damping matrix may be derived evaluating the work $\delta \mathbf{L_{aer}}$, made by a differential pressure Δp, due to the vertical displacement velocity of the surface.

$$\delta L_{acr}^B = \int_\Lambda \left(\delta \mathbf{u}^k \Delta p^B \right) d\Lambda \tag{5.25}$$

where the index B indicates that only the contribution of the vertical displacement velocity is considered. Considering the formulation proposed in eq.5.17 and introducing the displacement formulation ,the differential pressure can be written as:

$$\Delta p^B = B \frac{\partial u_2^k}{\partial t} = B \cdot F_\tau N_i I_{\Delta p} \frac{\partial q_{i\tau}^k}{\partial t} \tag{5.26}$$

$$\delta L_{acr}^B = \delta q_{js}^{kT} \left[B \left(F_\tau F_s \right) \int_\Lambda N_i N_j I_{\Delta p} d\alpha d\beta \right] \frac{\partial q_{i\tau}^k}{\partial t} = \delta q_{js}^{kT} d_a^{kij\tau s} \frac{\partial q_{i\tau}^k}{\partial t} \tag{5.27}$$

$D_a^{ij\tau s}$ is the aerodynamic damping matrix and it may be written in following form:

$$\boldsymbol{d}_a^{kij\tau s} = \frac{2q}{\sqrt{M^2-1}} \frac{1}{V_\infty} \left(\frac{M^2-2}{M^2-1} \right) \int_x \left(F_\tau F_s \right) dx \begin{bmatrix} 0 & 0 & 0 \\ 0 & 0 & 0 \\ 0 & 0 & \int_\Lambda N_i N_j d\alpha d\beta \end{bmatrix} \tag{5.28}$$

5.2.3 Solution of the aeroelastic problem

The FEM aeroelastic problem is formulated such as a second order dynamic system:

$$\left([\boldsymbol{K}] + [\boldsymbol{K}_a] \right) \{\boldsymbol{q}\} + \left([\boldsymbol{D}] + [\boldsymbol{D}_a] \right) \{\dot{\boldsymbol{q}}\} + ([\boldsymbol{M}])\{\ddot{\boldsymbol{q}}\} = 0 \tag{5.29}$$

In which, the structure is represented by the matrix K, D and M, that are the stiffness, damping and mass matrix, respectively. The aerodynamic forces are expressed in terms of Ka and Da. If the structural damping is negligible the eq.5.29 can be reduced to:

$$\left([K] + [K_a] \right) \{q\} + \left([D_a] \right) \{\dot{q}\} + ([M])\{\bar{q}\} = 0 \tag{5.30}$$

For a linear problem it is possible to assume a periodic solution:

$$\begin{array}{l} \{q\} = \{\bar{q}\}e^{i\omega t} \\ \{\dot{q}\} = i\omega\{\bar{q}\}e^{i\omega t} \\ \{\ddot{q}\} = -\omega^2\{\bar{q}\}e^{i\omega t} \end{array} \tag{5.31}$$

Substituting eq.4.30 in eq.4.29 the FE formulation becomes:

$$\{\bar{q}\}e^{i\omega t}\left[([K]+[K_a]) + ([D_a])\, i\omega - ([M])\omega^2\right] = 0 \tag{5.32}$$

Eq.5.32 represents a quadratic eigenvalues problem (QEP). The eigenvalues are in general complex number, the imaginary part is related to the natural frequencies, the real part to the damping of the aeroelastic system and represent the exponential decay of the oscillation, usually expressed in [1/s].

5.2.4 Quadratic eigenvalues problem (QEP) solution

Quadratic eigenvalues problem is not a classical lienar eigenvalue problem. A possible solution can be made by switching the QEP of a generic the number of degrees of freedom in a classic 'linear' eigenvalues problem of order 2 x R. To make it, the following 'trick' can be used:

$$\begin{cases} ([\boldsymbol{K}]+[\boldsymbol{K}_a])\,\{\boldsymbol{q}\} + ([\boldsymbol{D}_a])\,\{\dot{\boldsymbol{q}}\} + ([\boldsymbol{M}])\{\overline{\boldsymbol{q}}\} = 0 \\ -\{\dot{\boldsymbol{q}}\} + \{\dot{\boldsymbol{q}}\} = 0 \end{cases} \tag{5.33}$$

now, by introducing:

$$\begin{array}{l} \{Q\} = \begin{Bmatrix} \{\boldsymbol{q}\} \\ \{\dot{\boldsymbol{q}}\} \end{Bmatrix} \\ \{\dot{\boldsymbol{Q}}\} = \begin{Bmatrix} \{\dot{\boldsymbol{q}}\} \\ \{\overline{\boldsymbol{q}}\} \end{Bmatrix} \end{array} \tag{5.34}$$

it is possible to obtain the following form:

$$[R]\{\dot{Q}\} + [T]\{Q\} = 0 \tag{5.35}$$

Where:

$$\begin{array}{l} [R] = \begin{bmatrix} [D_a] & [M] \\ [I] & [0] \end{bmatrix} \\ [T] = \begin{bmatrix} ([K]+[K_a]) & [0] \\ [0] & -[I] \end{bmatrix} \end{array} \tag{5.36}$$

by switching the problem in the term of frequency the eq. 5.35 assumes the form:

$$\frac{[R]}{[T]} - \frac{1}{\omega}[I] = 0 \tag{5.37}$$

Where:

$$[T]^{-1}[R] = \begin{bmatrix} ([K]+[K_a])^{-1}[D_a] & ([K]+[K_a])^{-1}[M] \\ -[I] & [0] \end{bmatrix} \tag{5.38}$$

The problem in eq.5.37 is in the classical form and it can be solved with the standard eigensolvers.

Chapter 6

Numerical results

Preliminary study on the effect of Mesh generation on Displacement.The mesh is to divide the model into many small elements, which is the most important part of the pre-processing of finite element analysis. The matching degree between mesh generation and calculation target and the quality of mesh determine the quality of later finite element calculation.At present, the methods and techniques of mesh generation are becoming more and more mature, and a large number of CAD software have independent functions of mesh generation. The simple model generation platform built by MUL2 based on this theory is more convenient for more beginners to learn and understand the principle of grid generation.

6.1 MUL^2 code introduction

- Input files description
- MUL^2 code discretization

6.2 meshing based on «MUL^2 code user manual»

The number of meshes will affect the accuracy and scale of the calculation results. Generally speaking,with the increase of the number of grids,the calculation accuracy will be improved, but at the same time,the calculation scale will also increase. Therefore,when determining the number of grids,two factors should be considered comprehensively.

At present,the initial research only focuses on both Static Analysis and Free vibration Analysis.In static analysis, if only the deformation of the structure is calculated, the number of meshes can be less.Using low order elements can be met the precision requirements,either TE(Taylor expansion) or LE(Lagrange expansion),its character number is equal to 1.figure 6.1 shows the different geometrical modelling approaches,TE model vs LE model.

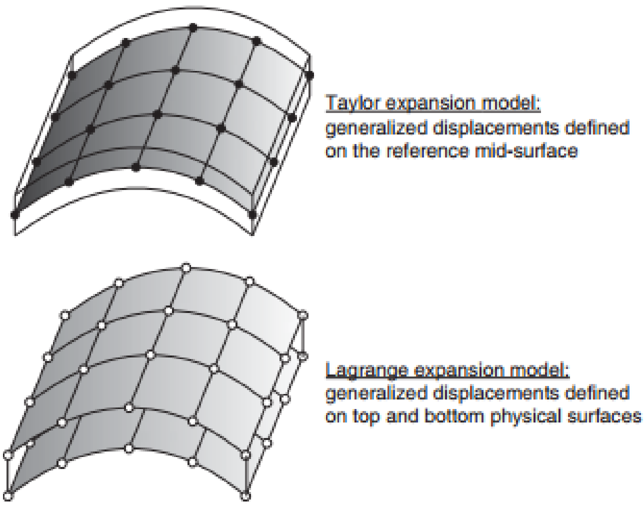

Figure 6.1: Different geometrical modelling approaches TE model vs LE model

Because the research object is 2D panel, the chosen element type is quadrilateral plate Q4 and Q9 at initial research,represent Four-node Quadrilateral plate and Nine-node Quadrilateral plate respectively.this type has characteristics:
1. Simple meshing
2. Easy to retain model details
3. The computational cost is low with the same number of grids.
Disadvantage: Computational accuracy is relatively poor.

6.3 B.C issues on modeling by Elements Combination

There are countless combinations of elements to build models. When the order of element is fixed, increasing the number of meshing elements can improve the accuracy of calculation.In order to compare the influence of different element combinations on displacement, assuming the dimension of length, width and height(a,b,h) along local reference system are (1,1,0.1) respectively, figure 6.2 shows Plate geometry and reference system.The analyses presented in the following sections have been performed using different structural models.The models based on Lagrange expansion are indicated with Lagrange Expansion nth order (LEn), where n stands for the order of the theory;for example, LE3 represents a third-order Lagrange expansion model. The models based on Taylor expansion are indicated with TE.

The material used in all the analyses is an isotropic material and the properties are those of aluminium alloy.Young's modulus equal to 70 GPa, Poisson's ratio equal to 0.3,and density equal to 2700 kg/m^3.figure 6.3

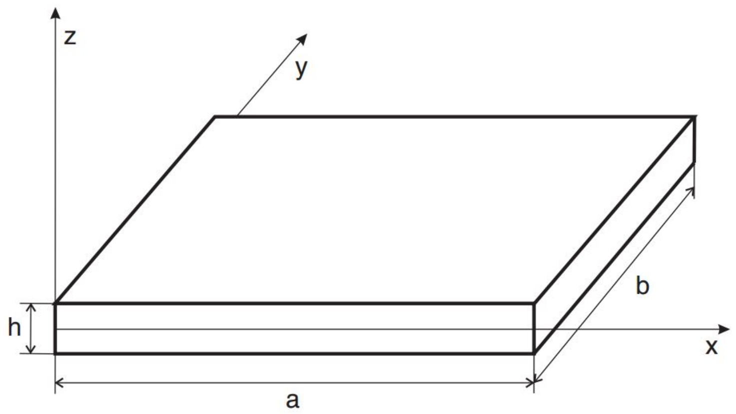

Figure 6.2: Plate geometry and reference system

```
ISO-M   1   70.0D9     0.30D0     2.7D3
```

Figure 6.3: The material used is an isotropic material and the properties

If the analysis of structures only contains elastic and external forces,the problem becomes a static response problem . When the system includes elastic and inertial forces, the problem becomes to be free vibration analysis. If all three contributions are considered, including inertial, elastic and external forces, a dynamic response analysis is needed to study.The internal work originates from the deformation of the structure. The external work comes from the loads applied to the structure. In «MUL^2 code user manual»,code 101,103 represent Static Analysis and Free vibration Analysis respectively.At the initial phase, we mainly study on the displacement deformed shape of plate and stress distribution from *pareview*. Similarly, the performance study on both the natural frequency and at least 30 different modal shape was obtained during Free vibration Analysis. No matter what case is assuming, the general BC is set as following commands,an trival demo case is illustrated as following table 6.1:

where D-PLANE use to impose the displacement in the nodes that stay on a plane,F-POINT use to impose a force in one node.when the BC is applied in one plane(X-PLANE)the same BC is applied in all the nodes that satisfy the

BC.type	ID.BC	(A,B,C,D)	Magnitude of force in(x,y,z)
D-PLANE	1	0.0D0 1.0D0 0.0D0 0.0D0	0.0D0 0.0D0 0.0D0
D-PLANE	2	1.0D0 0.0D0 0.0D0 -1.0D0	0.0D0 0.0D0 0.0D0
F-POINT	3	0.0D0 1.0D0 0.05D0 0.0D0	0.0D0 -1.000D+2

Table 6.1: BC.dat file data

N.Mesh	I	II	III	IV
Mesh	2x2Q4+2LD1	2x2Q9+2LD1	2x2Q9+LD2	2x2Q4+4LD2
	V	VI	VII	VIII
	8Q9+2LD2	2Q9+2LD2	2x2Q9+4LD2	2x2Q9+8LD2
	IX	X	XI	XII
	4x4Q16+2LD1	8Q16+LD2	2Q16+4LD2	10x10Q16+4LD2

Table 6.2: Mesh approximations corresponding to the Roman numeral number

same equation:

$$Ax + By + Cz + D \quad = \quad 0 \tag{6.1}$$

There are many works in literature on panel flutter based on classical boundary conditions. When beam models are used for the structural side, it is common practice to assume that the panels are simply supported. To assess the present aeroelastic model, a simply supported panel,clamped panel and one centrial forced panel have already been investigated in the following sections and the results have been compared with those from literature Carrera and Zappino [128],[129, 130].

6.4 Modelling results based on MUL^2

A total number of 12 groups new combinations have been made by combining the «MUL^2 code user manual» with the paraview tool. Those displacement results of these different combinations are shown in the table 6.2.

As the number of different combination increases, the finer the meshes are, the more concentrated the influence of the point force is near the stress point, and the more accurate the displacement is.

Therefore,The type of analysis data should be considered when deciding the number of mesh element. In static analysis,as in the same case, if only the deformation of the structure is calculated *displacement*, the number of meshes can be less. If the stress needs to be calculated, a relatively large number of meshes should be taken under the same accuracy requirements. Similarly, in response calculation, the number of meshes for calculating stress response should be more than that for calculating displacement.When calculating the inherent dynamic characteristics of structures, if only a few low-order modes are calculated, fewer meshing grids can be selected, and if the calculated modal order is higher, more meshing grids should be selected.

6.5 Static Response Analysis on 2D plate structure

The continuous and deformable structures are simulated by BC in *paraview* with both point force P and constrains along x-axis and y-axis. The internal work originates from the deformation of the structure, while the external work comes from the loads applied to the structure.when only refer to the elastic contribution,the use of the PVD allows the problem to be described in terms of work. There are three main contributions to the work balance of a system in classical structural problems: internal work,external work and inertial work.
The internal work and the external work can be seperately expressed as

$$\delta L_{int} = \delta U^T K U \tag{6.2}$$

$$\delta L_{ext} = \delta U^T P \tag{6.3}$$

In a static response analysis includes the effects of elastic forces and external loads. The PVD in the static case states that

$$\delta L_{int} = \delta L_{ext} \tag{6.4}$$

which in the PVD states

$$\delta \boldsymbol{U}^T \boldsymbol{K} \boldsymbol{U} = \delta \boldsymbol{U}^T \boldsymbol{P} \tag{6.5}$$

which can be reduced to the classic form

$$\boldsymbol{K} \boldsymbol{U} = \boldsymbol{P} \tag{6.6}$$

6.5.1 Static analysis

table 6.3 shows all those vertical displacements on the loading place for different loading values.the obvious results is the same as we originally imaged on the mesh grids size and the DOF quanties, the refined meshes were, the larger quanties of each structual modal, and the more caculating time cost.Also we could see from those results ,as we divided different external loads,the vertical deformation on the model were quiet enlarger the values we seen from the computational modals. table 6.4 shows stress[MPa] distributions at different models with the same loading values.

N.Approximation	Mesh	DOFs	F=-100N	F=-500N	F=-1KN
I	2x2Q4	81	-2.5e-9	-1.3e-8	-2.5e-8
II	2x2Q9	225	4.3e-23	2.1e-22	4.2e-22
III	2x2Q9	225	4.1e-23	2.1e-22	4.0e-22
IV	2x2Q4	81	-2.7e-9	-1.4e-8	-2.7e-9
V	8Q9	675	4.0e-23	4.0e-22	2.0e-22
VI	2Q9	225	4.0e-23	2.0e-22	4.0e-22
VII	2x2Q9	675	1.8e-23	9.3e-23	1.9e-22
VIII	2x2Q9	1275	5.0e-24	2.6e-23	5.3e-23
IX	4x4Q16	1521	5.1e-11	2.6e-10	5.1e-10
X	8Q16	3265	4.2e-10	2.6e-9	4.0e-10
XI	2Q16	756	-3.1e-8	-1.5e-7	-3.1e-7
XII	10x10Q16	25947	7.3e-6	3.4e-5	6.8e-5

Table 6.3: Vertical displacements on the loading place for different loading values

In the analysis of table 6.4,in order to assesse the obtained aeroelastic model, those four-sides simply supported panel on different structural model were displayed.as we know before disscusssing,D-PLANE is used to impose the displacements in the nodes that stay on a plane. and the panel's geometry is the same as we selected. The model is made of $16Q_{16}$ x $2LD1$ elements. Well,in table 6.4,all those 12 combinations vertical displacement,3 normal stress and 3 shear stress is caculated in the table.in static analysis field,we could get to learn that only elastic and external forces were taken into accounted.In order to obtain a higher accuracy,those models need a larger and refined meshed,in which is corrisponded to the table.

6.6 Free vibrations analysis

A free vibration analysis investigates the equilibrium between elastic forces and inertial forces.The PVD in the dynamic case is written as

$$\delta L_{int} = -\delta L_{ine} \tag{6.7}$$

In order to introduce free vibration analysis, a description of the inertial forces is given. Details of this contribution will be given in the following chapters.The virtual variation of inertial work can be written as

$$\delta L_{ine} = \int_V \delta u \rho \ddot{u} dV \tag{6.8}$$

where ρ is the density of the material and $\ddot{u}$ is the acceleration. Introducing the FEM approximation, the variation of the inertial work assumes the form

Mesh	$U_z[10^{-3}mm]$	σ_{xx}	σ_{xy}	σ_{xz}	σ_{yy}	σ_{yz}	σ_{zz}
I	-2.5e-9	-6.2e1	5.6e-16	1.4e2	-6.2e1	1.4e2	-1.3e2
II	4.3e-23	1.2e3	1.1e2	5.1e2	1.2e3	7.8e2	5.0e2
III	4.1e-23	2.8e3	1.0e2	1.1e2	1.0e3	6.2e2	3.6e2
IV	-2.7e-9	-5.6e1	4.6e-16	1.0e2	-5.6e1	1.0e2	-2.2e2
V	4.0e-23	1.3e3	2.3e2	9.9e2	2.0e3	6.5e2	9.7e2
VI	4.0e-23	4.6e2	5.0e1	1.1e2	1.9e2	3.0e2	1.7e2
VII	1.8e-23	1.1e3	1.4e2	8.7e2	1.1e3	8.7e2	5.4e2
VIII	5.0e-24	1.1e3	1.4e2	8.7e2	1.1e3	8.7e2	5.5e2
IX	5.1e-11	5.3e4	6.8e3	1.0e4	5.8e4	1.2e4	2.9e4
X	4.2e-10	6.2e5	2.6e4	6.7e5	4.6e5	8.0e5	5.2e5
XI	-3.1e-8	2.4e5	9.0e3	5.2e3	1.2e5	6.4e4	7.7e3
XII	7.3e-6	9.5e7	1.6e7	1.3e7	6.6e7	2.5e7	2.4e7

Table 6.4: Stress$[MPa]$ distributions at different models with the same loading values

$$\delta L_{ine} = \delta \boldsymbol{U}^T \boldsymbol{M} \overrightarrow{\boldsymbol{U}} \tag{6.9}$$

It is possible to write the equilibrium equations

$$\delta L_{\text{ine}} + \delta L_{\text{int}} = 0 \tag{6.10}$$

$$\delta \boldsymbol{U}^T \boldsymbol{M} \ddot{\boldsymbol{U}} + \delta \boldsymbol{U}^T \boldsymbol{K} \boldsymbol{U} = 0 \tag{6.11}$$

$$\boldsymbol{M} \boldsymbol{U} + \boldsymbol{K} \boldsymbol{U} = 0 \tag{6.12}$$

The solution of 6.25 gives the vector U that satisfes this equilibrium condition. The problem constitutes a homogeneous system and the solution must be calculated by solving an eigenvalue problem. The problem can be easily solved if the solution is considered to be harmonic. In this case, the displacement, the velocity and the acceleration become

$$\begin{aligned} \boldsymbol{U} &= \overline{\boldsymbol{U}} e^{i\omega t} \\ \dot{\boldsymbol{U}} &= i\omega \overline{\boldsymbol{U}} e^{i\omega t} \\ \overrightarrow{\boldsymbol{U}} &= -\omega^2 \overline{\boldsymbol{U}} e^{ict} \end{aligned} \tag{6.13}$$

where $\overline{\boldsymbol{U}}$ is the amplitude of the displacements and ω is the angular frequency. 6.25 can be rewritten in the frequency domain, as

$$-\boldsymbol{M}\omega^2 \overline{\boldsymbol{U}} e^{i\omega t} + \boldsymbol{K} \overline{\boldsymbol{U}} e^{i\omega t} = 0 \tag{6.14}$$

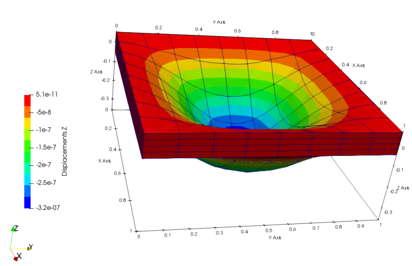

(a) vertical deformed displacement U_z

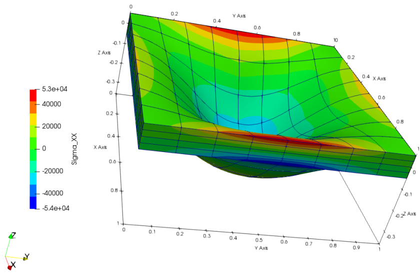

(b) Normal stress σ_{xx}

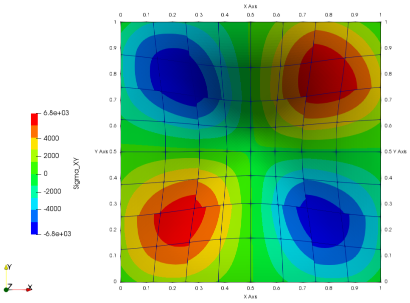

(c) Shear stress σ_{xy}

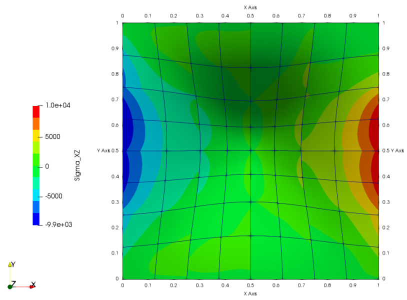

(d) Shear stress σ_{xz}

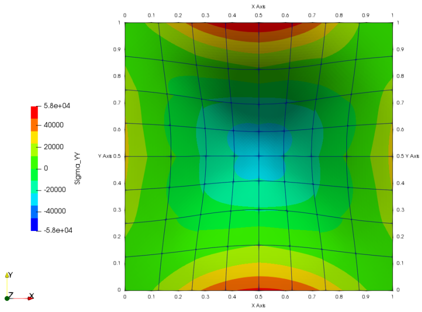

(e) Normal stress σ_{yy}

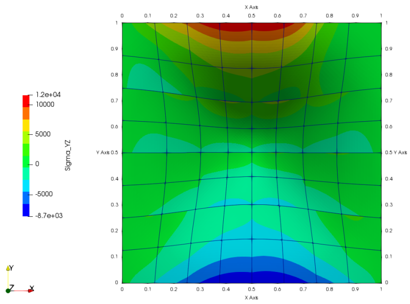

(f) Shear stress σ_{yz}

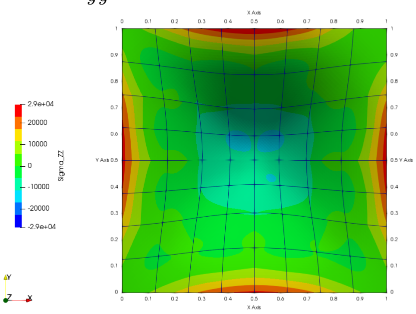

(g) Normal stress σ_{zz}

Figure 6.4: Stress distributions of Model 16Q16+2LD1

This equation can be reduced to a standard eigenvalue problem

$$
\begin{aligned}
\overline{\boldsymbol{U}}e^{i\omega t}\big(-\boldsymbol{M}\omega^2 + \boldsymbol{K}\big) = 0 \\
-\boldsymbol{M}\omega^2 + \boldsymbol{K} = 0
\end{aligned}
\tag{6.15}
$$

The eigenvalue problem that has to be solved becomes

$$
\begin{aligned}
K^{-1}M - \tfrac{1}{\omega^2}I = 0 \\
\omega^2 I - M^{-1}K = 0
\end{aligned}
\tag{6.16}
$$

The natural frequencies can be obtained from the eigenvalues

$$f = \frac{\omega}{2\pi} \tag{6.17}$$

Each frequency gives an eigenvector that is the vector $\boldsymbol{U}$ which satisfes

$$K^{-1}MU = \frac{1}{\omega^2}U \tag{6.18}$$

6.6.1 natural frequency and mode shape

Given i and j, integer numbers of flexural halfwaves in x and y directions respectively,the deformation can be expressed, according to the expansion theorem, as the eq. (6.19) sum of modal deformations:

$$u = \Sigma_i \Sigma_j A_{ij} q_{ij} \sin\left(2\pi f_{ij} t + \phi_{ij}\right) \tag{6.19}$$

For any i and j where a vibration mode exists, we can define:Amplitude A_{ij} ,Mode shape q_{ij},Natural frequency f_{ij},Phase angle ϕ_{ij}. The exact natural frequencies eq. (6.20) of the plate are given by the expression:

$$F_{ij} = \frac{\lambda_{ij}^2}{2\pi a^2}\left[\frac{Eh^3}{12\gamma\left(1 - v^2\right)}\right]^{1/2} \tag{6.20}$$

where λ_{ij} parameter depends on mode indices i and j, plate geometry and aspect ratio,boundary conditions, and v weekly on Poisson ratio eq. (6.21).An approximated closed form solution for frequencies exists,obtained using Rayleigh energy method and assuming beam mode shapes eq. (6.22), where coefficients G, H and J for each couple of edges (index 1 when referring to sides of width, index 2 for sides of length) are tabulated as function of B.C. and mode indexes i and j.

$$\lambda_{ij} = \lambda_{ij}\left(\frac{a}{b}, b, c, , v\right) \tag{6.21}$$

$$f_{ij} = \frac{\pi}{2}\left[\frac{G_1^4}{a^4} + \frac{G_2^4}{b^4} + \frac{2J_1J_2 + 2v\left(M_1M_2 - J_1/_2\right)}{a^2b^2}\right]^{1/2}\left[\frac{Eh^3}{12\gamma\left(1-v^2\right)}\right]^{1/2} \tag{6.22}$$

Since a general analytical form for mode shapes of a plate with generic boundary condition doesn't exist, an approximation involving a series of beam mode shapes eq. (6.23) eq. (6.24) $\tilde{q}_m$ and $\tilde{q}_n$:

$$q_{ij}(x, y) = \sum_m \sum_n \tilde{q}_m(x)\tilde{q}_n(y) \tag{6.23}$$

$$q_{ij}(x, y) \approx \tilde{q}_m(x)\tilde{q}_n(y) \tag{6.24}$$

For boundary conditions with certain patterns, the first term alone is sufficient to approximate the mode shapes. If the plate has two opposite free edges, there will be a mode in which$\tilde{q}_n \approx 1$, i.e. the halfwave in that direction is basically flat,If two opposite edges are simply supported, the beam mode shape in this direction will be exactly $\tilde{q}_n(x) = \sin\left(\frac{\ln x}{a}\right)$, resulting in the plate mode shape eq. (6.25),if all the four edges are simply supported, the mode shape is eq. (6.26).

$$q_{ij}(x, y) = \sin\left(\frac{i\pi x}{a}\right)\tilde{q}_m(y) \tag{6.25}$$

$$q_{ij} = \sin\left(\frac{\text{tax}}{a}\right)\sin\left(\frac{i\pi y}{b}\right) \tag{6.26}$$

As the boundary conditions become less regular, for example if there is not even a couple of opposite supported edges, the expression eq. (6.24) is no longer enough to describe the mode shapes, and a higher order expansion of eq. (6.23) is needed. A typical example is the completely free plate, where the deformations along directions x and y intermingle in more complex patterns.

table 6.5 shows the first 20 natural frequencies of different models.In the free vibration analysis, the system included elastic and inertial forces.In each structual modal,the more refined mesh grids, the larger mode frequency,which means the higher critical instability speed could be obtained.Also in genellay, the more complex combinational elments, it costs more time to run those results,and in turn more larger its DOF needed.which means, we could find the accurate critical instability speed by modifing the combinations, also by BC,structual ratio,temperature differences and laminational angles.So in the following section, some modifing test were taken and been disscussed. Figure 6.5 shows mode shapes for the different model considered the first 6 modes was simulinked from mode $16Q_{16}$ x $2LD1$. the same as before,in order to assesse the obtained aeroelastic model, those four-sides simply supported panel on different structural model were displayed.From the simple computaional results, we could learn that in $16Q_{16}$ x $2LD1$ model,the flutter mode for it is instability bending modes.

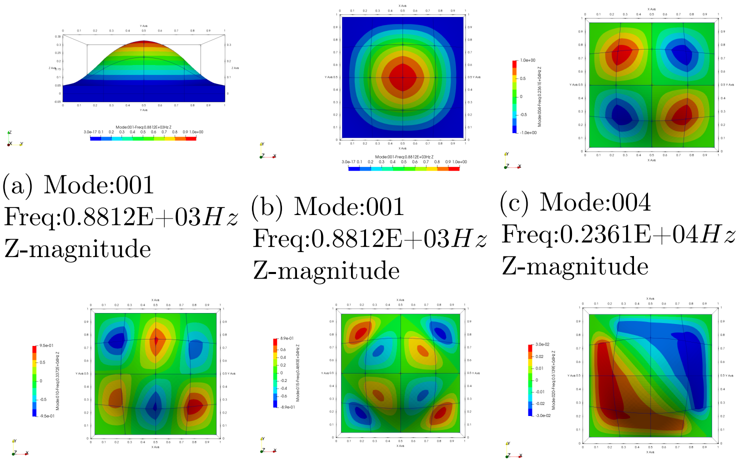

(a) Mode:001 Freq:0.8812E+03Hz Z-magnitude

(b) Mode:001 Freq:0.8812E+03Hz Z-magnitude

(c) Mode:004 Freq:0.2361E+04Hz Z-magnitude

(d) Mode:010 Freq:0.3372E+04Hz Z-magnitude

(e) Mode:015 Freq:0.4693E+04Hz Z-magnitude

(f) Mode:020 Freq:0.5139E+04Hz Z-magnitude

Figure 6.5: Mode shapes for the different model considered , first 6 modes was simulinked from mode 16Q16+2LD1

6.7 Dynamic Response Analysis

If all inertial, elastic and external work contributions are considered, the problem that has to be solved can be written, through the PVD, in the form

$$\delta L_{\text{ine}} + \delta L_{\text{int}} = \delta L_{\text{exd}} \tag{6.27}$$

In FE form, the problem becomes

$$\delta \boldsymbol{U}^T \boldsymbol{M} \ddot{\boldsymbol{U}} + \delta \boldsymbol{U}^T \boldsymbol{K} \boldsymbol{U} = \delta \boldsymbol{U}^T \boldsymbol{P} \tag{6.28}$$

$$\boldsymbol{M} \ddot{\boldsymbol{U}} + \boldsymbol{K} \boldsymbol{U} = \boldsymbol{P} \tag{6.29}$$

The last equation above is written in the time domain. The solution of this equation in the time domain requires the use of a numerical technique. Three

N.Mesh	I	II	III	IV
DOFs	81	225	225	81
1	2.520 kHz	1.267 kHz	1.324 kHz	1.324 kHz
2	3.960 kHz	2.447 kHz	1.586 kHz	3.465 kHz
3	3.960 kHz	2.447 kHz	3.557 kHz	2.345 kHz
4	18.25 kHz	3.251 kHz	3.557 kHz	1.343 kHz
5	18.25 kHz	3.871 kHz	1.345 kHz	14.36 kHz
6	35.85 kHz	3.286 kHz	1.345 kHz	34.53 kHz
7	35.46 kHz	3.286 kHz	4.876 kHz	34.56 kHz
8	35.85 kHz	4.762 kHz	4.532 kHz	35.65 kHz
9	70.78 kHz	5.475 kHz	4.631 kHz	38.54 kHz
10	4.008 GHz	5.508 kHz	5.438 kHz	56.33 kHz
11	4.008 GHz	5.711 kHz	5.783 kHz	6.352 GHz
12	3.848 GHz	6.328 kHz	5.438 kHz	3.454 GHz
13	3.848 GHz	8.950 kHz	7.903 kHz	3.543 GHz
14	3.848 GHz	7.740 kHz	7.436 kHz	3.656 GHz
15	4.712 GHz	5.889 kHz	9.873 kHz	4.677 GHz
16	4.712 GHz	5.889 kHz	4.893 kHz	4.677 GHz
17	4.909 GHz	6.106 kHz	8.476 kHz	5.767 GHz
18	4.909 GHz	6.106 kHz	3.894 kHz	4.768 GHz
19	5.441 GHz	11.40 kHz	12.43 kHz	6.785 GHz
20	5.772 GHz	7.062 kHz	8.346 kHz	6.467 GHz
	V	VI	VII	VIII
DOFs	675	225	675	1275
1	1.083 kHz	1.842 kHz	1.253 kHz	1.253 kHz
2	1.832 kHz	2.751 kHz	2.421 kHz	2.421 kHz
3	2.344 kHz	3.351 kHz	2.421 kHz	2.421 kHz
4	2.831 kHz	3.613 kHz	3.214 kHz	3.214 kHz
5	3.184 kHz	4.583 kHz	3.871 kHz	3.871 kHz
6	3.200 kHz	5.643 kHz	3.286 kHz	3.286 kHz
7	3.271 kHz	6.125 kHz	3.286 kHz	3.286 kHz
8	3.794 kHz	6.669 kHz	4.761 kHz	4.761 kHz
9	3.885 kHz	11.46 kHz	5.472 kHz	5.472 kHz
10	4.551 kHz	16.62 kHz	5.502 kHz	5.502 kHz
11	4.706 kHz	16.59 kHz	5.710 kHz	5.710 kHz
12	5.090 kHz	16.85 kHz	6.327 kHz	6.327 kHz
13	5.327 kHz	17.45 kHz	7.664 kHz	7.664 kHz
14	5.452 kHz	17.45 kHz	7.739 kHz	7.739 kHz
15	5.512 kHz	19.91 kHz	5.876 kHz	5.876 kHz
16	5.672 kHz	31.81 kHz	5.876 kHz	5.876 kHz
17	6.015 kHz	31.84 kHz	6.106 kHz	6.106 kHz
18	6.224 kHz	32.47 kHz	8.948 kHz	8.948 kHz
19	6.258 kHz	36.25 kHz	7.061 kHz	7.061 kHz
20	6.752 kHz	35.82 kHz	7.061 kHz	7.061 kHz

	IX	X	XI	XII
DOFs	1521	3265	756	25947
1	0.8812 kHz	2.355 kHz	1.559 kHz	1.681 kHz
2	1.684 kHz	1.576 kHz	1.865 kHz	1.681 kHz
3	1.684 kHz	3.546 kHz	1.973 kHz	0.4216 kHz
4	2.361 kHz	3.565 kHz	2.067 kHz	0.4216 kHz
5	2.791 kHz	2.566 kHz	2.855 kHz	1.745 kHz
6	2.819 kHz	2.791 kHz	2.979 kHz	1.745 kHz
7	3.159 kHz	2.791 kHz	3.673 kHz	2.038 kHz
8	3.687 kHz	5.677 kHz	3.237 kHz	2.038 kHz
9	3.159 kHz	5.678 kHz	3.537 kHz	2.535 kHz
10	3.372 kHz	4.677 kHz	3.918 kHz	2.535 kHz
11	3.371 kHz	3.435 kHz	3.975 kHz	2.654 kHz
12	4.259 kHz	2.234 kHz	5.490 kHz	3.270 kHz
13	4.591 kHz	1.434 kHz	4.942 kHz	2.800 kHz
14	4.646 kHz	2.657 kHz	6.230 kHz	3.554 kHz
15	4.693 kHz	2.354 kHz	5.340 kHz	3.554 kHz
16	4.194 kHz	1.465 kHz	5.693 kHz	3.094 kHz
17	4.194 kHz	3.565 kHz	6.520 kHz	3.266 kHz
18	5.191 kHz	3.565 kHz	7.787 kHz	3.266 kHz
19	5.139 kHz	4.565 kHz	8.225 kHz	3.295 kHz
20	5.139 kHz	4.672 kHz	8.195 kHz	3.343 kHz

Table 6.5: First 20 natural frequencies of different models

different numerical approaches can be used in a dynamic response analysis:the mode superposition method;the explicit direct integration method;the implicit direct integration method.

6.8 Different boundry condition on 2D plate Numerial results

6.8.1 Different panel Loads

Natural frequencies and modal shapes have been computed analytically, implementing a procedure on *Paraview*. The computation has been carried out for 7 different boundary condition constrains configurations,which is showed

Figure 6.6. Take $y = 1$ plane as the first digit, and so on in the clockwise direction, a total of four sides.

•B.C type a :all four edges of plate in all the nodes on plane were simply supported (x =0,x =1,y =0,y =1) ,additional with a pressure on plane. 'ssss' boundry condition configuration.

•B.C type b:two edges in all the nodes of y_axis(y =0,y =1) on plane were simply supported,other two displacements in the nodes on which stay on plane(y =0.25,y =0.75),additional with a pressure on plane. 'sfsf' boundry condition configuration. f means free B.C

•B.C type c: all four edges of plate in all the nodes on plane were simply supported (x =0,x =1,y =0,y =1),without any force o pressure.

•B.C type d:two edges in all the nodes in x_axis and y_axis(x =1,y =0) were on plane were simply supported, additional with a force in one node(0,1,0.05). 'fssf' boundry condition configuration.

•B.C type e: all four edges of plate in all the nodeson plane were simply supported (x =0,x =1,y =0,y =1),other two displacements in the nodes on which stay on plane (x =0.5,y =0.5),without any force o pressure.

•B.C type f: two edges in all the nodes of y_axis(y =0,y =1) were on plane were simply supported,other two displacements in the nodes on which stay on plane(y =0.25,y =0.75)with z_axis.

•B.C type g: two edges in all the nodes of y_axis(y =0,y =1) were on plane were simply supported,additional with a pressure on plane. sfsf' boundry condition configuration.

Figure 6.8 shows the static analysis models from modeMesh: 16Q16+2LD1 ,for All 7 B.C Types,each figure selected was changed by its model static displacement-Z ,stress σ_{xx} ,stress σ_{xz},stress σ_{yy},stress σ_{xy} ,stress $\sigma_{zz}$and its scale factor.Those different flutter modes shows mainly in bending modes ,and the stress distribution on each corriding modes is evenly distributed on each same livel deformations values,and the distribution shows a symmetric division

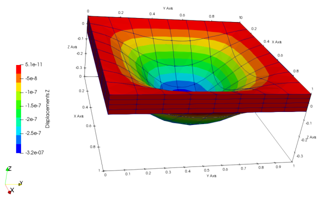

(a) B.C type: a ,displacement z

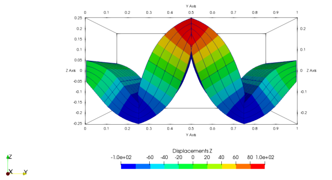

(b) B.C type: b ,displacement z

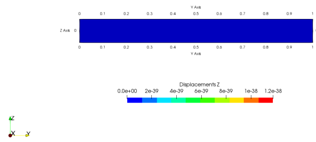

(c) B.C type: c ,displacement z

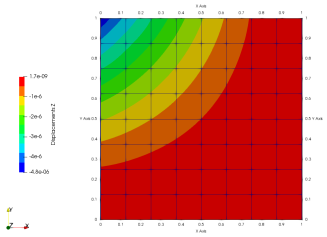

(d) B.C type: d ,displacement z

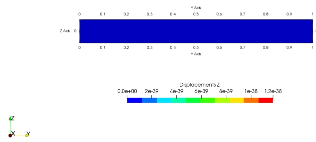

(e) B.C type: e ,displacement z

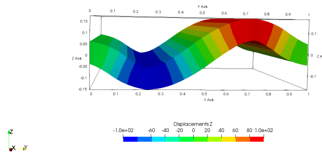

(f) B.C type: f ,displacement z

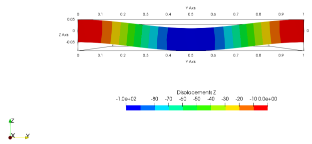

(g) B.C type: g ,displacement z

Figure 6.6: 7 different Boundry condition configurations

on the panel.Those symmetric deformation on plane is mainly belonging to the fact that we initially set a symmetric B.C and the material propeties we used is isotropic one.Test has been identified that the panel flutter was also largely influenced by B.Cs,we also disscussed in following section in which the results we obtained from above different boundary condition has a good compromise with those from literatures.All those different boundary conditions were analysis from the panel elements 16Q16+2LD1.In such way ,only boundary conditions need to be take int account.The results of the modal analysis of each panel are reported also in the below Table. The natural frequencies evaluated by means of the present model compared with those from Carrera and Zappino's literature ,the 2-D model are also reported below for each panel.

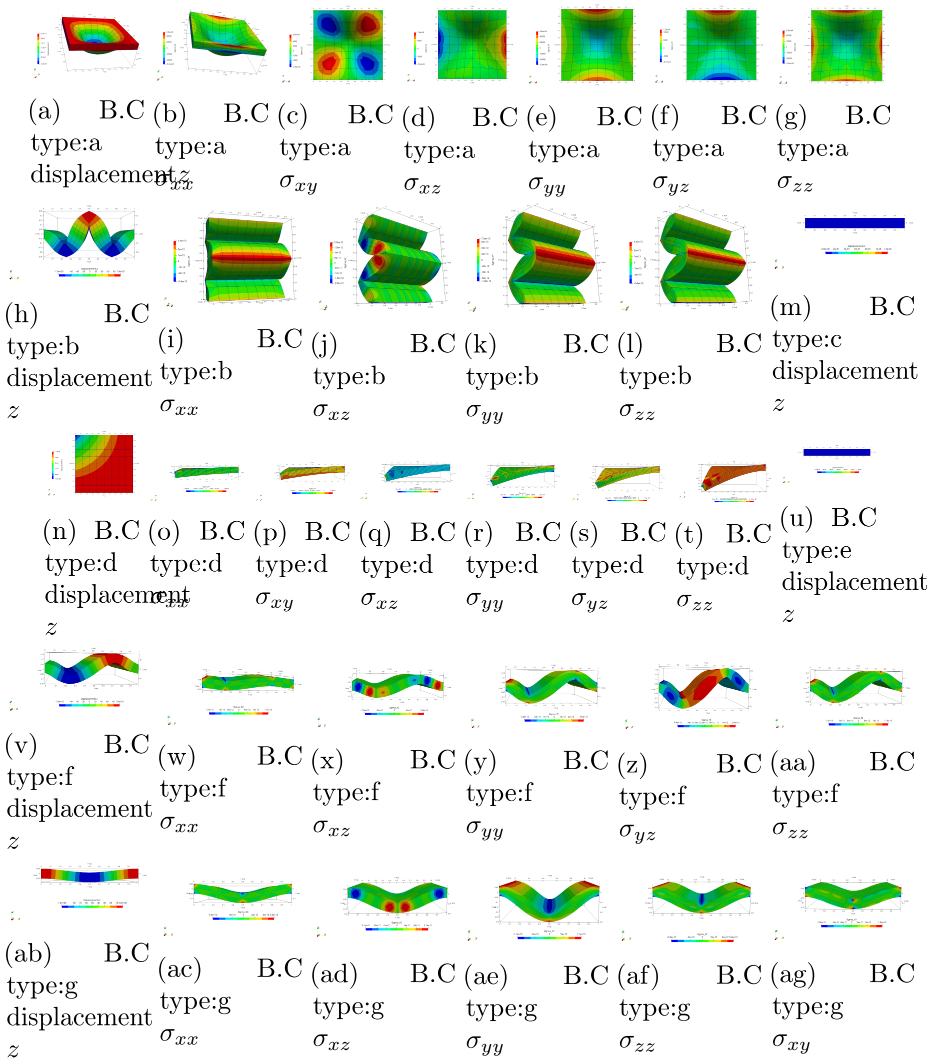

(a) B.C type:a displacement z (b) B.C type:a σ_{xx} (c) B.C type:a σ_{xy} (d) B.C type:a σ_{xz} (e) B.C type:a σ_{yy} (f) B.C type:a σ_{yz} (g) B.C type:a σ_{zz}

(h) B.C type:b displacement z (i) B.C type:b σ_{xx} (j) B.C type:b σ_{xz} (k) B.C type:b σ_{yy} (l) B.C type:b σ_{zz} (m) B.C type:c displacement z

(n) B.C type:d displacement z (o) B.C type:d σ_{xx} (p) B.C type:d σ_{xy} (q) B.C type:d σ_{xz} (r) B.C type:d σ_{yy} (s) B.C type:d σ_{yz} (t) B.C type:d σ_{zz} (u) B.C type:e displacement z

(v) B.C type:f displacement z (w) B.C type:f σ_{xx} (x) B.C type:f σ_{xz} (y) B.C type:f σ_{yy} (z) B.C type:f σ_{yz} (aa) B.C type:f σ_{zz}

(ab) B.C type:g displacement z (ac) B.C type:g σ_{xx} (ad) B.C type:g σ_{xz} (ae) B.C type:g σ_{yy} (af) B.C type:g σ_{zz} (ag) B.C type:g σ_{xy}

Figure 6.7: static analysis models from modeMesh: 16Q16+2LD1 ,for All 7 B.C Types,each figure selected was changed by its model static displacement-Z ,stress σ_{xx} ,stress σ_{xz},stress σ_{yy},stress σ_{xy} ,stress $\sigma_{zz}$and scale factor

Those displacement and stress values of these different B.C combinations are shown in the Figure table 6.6. And Figure 6.9 shows the modal shapes of the different panels. It is clear that the phenomenon is strongly 2-D and is different from the classical configuration used in the panel flutter analysis. Also 6.10,6.11,6.12 show the first 6,8,8,6,6 individual modal shapes for its each model. From the results, it appears that the present model is able to illustrate the dynamic behavior of the simply supported panel in the such configurations.

B.C	Dynamic element				
	Frequency $[Hz]$		Magnitude $[10^{-3}mm]$		
	First frequency	Last frequency	U_x	U_y	U_z
a	0.8812E3	0.5139E4	1.3e-1	1.3e-1	1.0e+00
b	0.5702E4	0.6421E4	1.2e-1	5.4e-14	9.5e-1
c	0.8812E3	0.5139E4	2.4e-1	3.4e-1	9.9e-1
d	0.1711E3	0.3650E4	4.8e-1	4.8e-1	5.5e-2
e	0.1156E4	0.5652E4	2.3e-1	2.3e-1	1.0e00
f	0.1932E4	0.5846E4	1.2e-1	1.2e-1	4.4e-16
g	0.1932E4	0.4871E4	1.2e-1	1.8e-1	1.8e-2
	Static element				
	Displacement $[10^{-3}mm]$	Stress $[MPa]$			
	U_z	σ_{xx}	σ_{xz}	σ_{yy}	σ_{zz}
a	5.1e-11	5.3e4	1.0e4	5.8e4	2.9e4
b	1.0e2	3.4e+13	2.0e+12	7.0e+13	3.4e+13
c	1.2e-38	1.2e-38	1.2e-38	1.2e-38	1.2e-38
d	1.7e-9	7.5e4	6.8e4	7.5e4	5.0e4
e	1.2e-38	1.2e-38	1.2e-38	1.2e-38	1.2e-38
f	1.0e2	1.7e+13	1.0e+12	3.5e+13	1.7e+13
g	0.00e+00	5.4e+12	3.1e+11	1.1e+13	5.4e+12

Table 6.6: Displacements and stress evaluated by different Boundry conditions

6.9 Instability analysis

In general, to study the aeroelastic stability of composite laminate structure under different airflow, in order to analyze it by solving the generalized eigenvalue problem through aeroelastic properties. And generally by calculating the natural frequency of the laminate structure at different incoming flow speeds, the critical instability velocity of the laminate structure under the action of airflow is obtained, because the rigidity of the laminate structure decreases, resulting in the structure instability.
Through the eigenvalue equation presented in the previous Chapter 3, the natural frequencies of the structure at different incoming flow speeds can be obtained. It can be seen from the stiffness matrix that when the aerodynamic pressure is considered, the stiffness of the structure system includes the aerodynamic stiffness term, and the With the gradual increase in speed, the stiffness of the structural system will gradually decrease, which will cause the natural frequencies of the system to gradually decrease. When the fundamental frequency of the structure is reduced to 0, the structure will be in

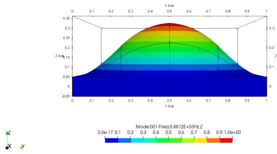

(a) B.C type:a, Mode:001-Freq:0.8812E+03 Hz Z

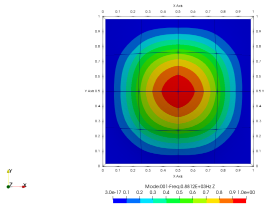

(b) B.C type:a ,Mode:001-Freq:0.8812E+03 HzZ

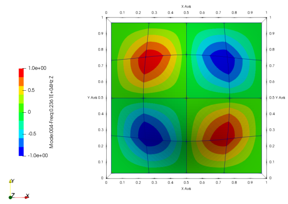

(c) B.C type:a ,Mode:004-Freq:0.2361E+04 HzZ

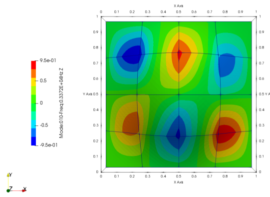

(d) B.C type:a ,Mode:010-Freq:0.3372E+04 HzZ

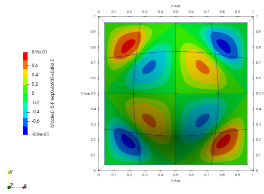

(e) B.C type:a ,Mode:015-Freq:0.4693E+04 HzZ

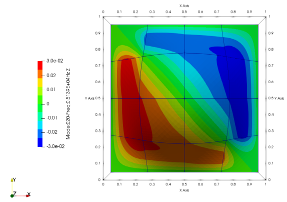

(f) B.C type:a ,Mode:020-Freq:0.5139E+04 HzZ

Figure 6.8: 6 Mode shapes for from mode 16Q16+2LD1 of B.C Type: a ,each figure selected was changed by its model dynamic frequency ,magnitude Z and scale factor

a critical instability state. The corresponding incoming flow velocity is the critical instability velocity. Therefore, in practical applications, the structural parameters should be reasonably designed according to the mechanical environment of the composite laminate structure to avoid structural instability problems under the action of airflow.

6.9.1 critical instability speed caculated by different structual configurations

This thesis compares the calculation results using the method in this paper with the results of the existing literature to verify the rationality of the aerodynamic model and structural motion equation established in this paper, as well as the correctness of the numerical algorithms and procedures.
In the literarure [131],The Kirchhoff plate theory is used to simulate the displacement field of the structure, and for the composite material laminated structure, the fiber direction of each single-layer plate is not necessarily consistent with the coordinate axis direction in the global coordinate system. In order to obtain the material parameters in the global coordinate system The constitutive relationship requires coordinate conversion. From this, the material parameter matrix, the bending stiffness matrix, the strain energy of the structure, and the virtual work of the external force after the coordinate conversion are obtained, and the simply supported boundary conditions of the

SC.type		results			Literature [58]
panel width $b/[m]$	1	3	10	30	infinte
critical speed $U/[s]$	167.29	98.22	90.87	90.21	90.14

Table 6.7: Critical instability velocities of the plate with different structural configurations

four sides of the panel are set to obtain the subsurface The three-dimensional sonic aerodynamic model and the motion equation of the fluid-solid coupling structure system are used to obtain the natural frequencies of the structure at different incoming flow speeds. This idea is completely consistent with that presented in this paper.

In the literarure [131],By discussing the change of the natural frequency of the system with the incoming flow speed, the influence of different structural modes configurations and lamination angles changes on the aeroelastic stability of the laminated structure is analyzed. The material and structure parameters are taken as $E = 70\ GPa$, $\mu = 0.3$, flow density equal to 1.29 $kg/\ m^3$, length $a = 1\ m$.table 6.7The critical instability speed of the plate under different structural parameters calculated by the method in this paper is given, and compared with the results in the literature.

6.9.2 critical instability speed caculated by different lamination angles

With the gradual increase of the plate width b, the critical instability speed of the plate gradually decreases. When b is equal to 30 m, the critical instability speed differs from the result of literature [58] by less than 0.1%, which verifies the research method in this paper. And the validity of the calculated results.And The flutter speed of the panel increases with the increase of the Boundary layer thickness,but even though from fig. 2.13,thus "linear relationship" Hashimoto demonstrates that it is not always true,we could see from above figure.

fig. 6.13 and fig. 6.14shows the change of the natural frequency of the laminate angle of 30 degree with the incoming flow velocity.It can be seen from fig. 6.13 that as the incoming flow speed increases, the fundamental frequency of the structure gradually decreases. When the fundamental frequency decreases to 0, the corresponding incoming flow speed at this time is the critical instability speed of the structure. Critical instability rate Approximately 168 m/s. It can be seen from fig. 6.14 that when the width of the laminate is $b = 1$, 3, 10 and 30 m, the critical instability speed of the structure is 168, 104, 98, 98 $m/\ s$. The comparison shows that when the width of the laminate becomes larger,The closer it is to the two-dimensional plate, b becomes infinite large, then the three-dimensional thin plate is further degenerated into a two-dimensional plate.the critical instability rate of the structure lower,the structure tends to be easier to lose stability.When the lamination angle is 0 degree, 30 degree, 45 degree, 60 degree, 90 degree, the natural frequency of the laminate structure changes with the incoming flow velocity. As the lamination angle of the laminate gradually increases, the critical instability speed of the panel initially increase and then decrease, this conclusion can also be obtained. it can be seen that there is an optimal lamination angle. The optimal lamination angle of the laminate is related to its own structural configurations. Therefore, it can be boldly inferred that the critical speed can be calculated accrding to the curve of the instability flow velocity to determine the optimal lamination angle.

6.9.3 critical dynamic pressure caculated by number of pinched points

In literature [128], unconventional boundary conditions are analyzed,The geometry of the panel is shown as: The dimensions a and b are equal to 0.5 m and the thickness h is equal to 0.002 m. The boundary conditions of the four panels are given in fig. 6.15, The four panels have two (panel 1), three (panel 2), four (panel 3), and infinite (panel 4) pinched points, respectively. with infinite pinched points representing the classic case in which the edges are fully constrained.

The flutter critical condition was investigated by means of the piston theory adopting the structural model used in the assessments.The flow direction has reported in chapter3 in aeroelastic model section.The critical dynamic pressure is reported in fig. 6.16 for a wide range of Mach numbers.It is possible to evaluate the altitude using the standard atmosphere model starting from a Mach number and a dynamic pressure.The results show that, by increasing the number of pinched points,it is possible to increase the critical dynamic pressure up to the limit value given by the full clamped configuration (panel 4).By fixing the Mach number, it is possible to define the limit altitude. The panel is stable for higher altitude because of the decrease in the air density. The panel is not stable for lower altitude. By fixing the altitude, it is possible to investigate the critical value of the Mach number.The effect of BC is reported in fig. 6.17 The Mach number was considered constant and equal to 3. The critical dynamic pressure increases as the number of pinched points increases up to the limit value given by the full clamped configuration (panel 4).

6.9.4 critical dynamic pressure caculated by Flow Conditions

In this section,the flow is considered constant and the Mach number is considered variable.A fixed altitude was chosen in order to define the flow condition. The structural model is the same as that used in the preceding analyses. critical Mach number and frequency, are reported in fig. 6.18,and fig. 6.19, fig. 6.20,fig. 6.21,fig. 6.22 show the frequencies and the damping evolution for different Mach regimes.From the results, it is possible to see that instability occurs when two frequencies merge together. This coalescence produces a positive branch in the damping, which means that the oscillation is self-excited. The presence of the coalescence is not sufficient to produce instability. The P-4 instability of panel 2 fig. 6.20 in fact shows coalescence of the frequencies, but the damping remains negative. The coalescence may disappear with an increase in the Mach number. Panel2 fig. 6.20 shows that P-2 instability arises at Mach is equal to 4.95, but stabilities when above Mach is equal to 9.5. The boundary conditions affect the nature of the instabilities to a great extent. There is only one coalescence P-1 for panel1 fig. 6.19, panel 3 fig. 6.21, and panel4 fig. 6.22, whereas panel 2 fig. 6.20 shows four coalescences.

In literature [128], Panel flutter is a common aeronautical phenomena. Most of the published works have studied it at a constant altitude and have been devoted to investigating the critical flight speed. However, the pinched configuration is a typical space configuration and is common in launcher structure in which some panels have to be ejected after atmospheric flight. A simulation of a standard mission has been carried out in this section.The flight data were extrapolated from [130]. The flow data are reported in fig. 6.23,The table shows the data from an altitude of 9500 m, where the Mach number is large enough to justify the use of the piston theory, up to 36,500 m, where the density of the air is so low that the aerodynamic loads are negligible.fig. 6.24 shows the magnitude of the constants of the piston theory. Term A is related to aerodynamic stiffness and decreases because of the decrease in the density. Term B is related to aerodynamic damping and has a maximum at 75 s. It is dominated in the first part by an increase in the Mach number, whereas the decrease in the density in the second part reduces the aerodynamic influence, even in terms of damping. The third line shows the dynamic pressure, which has a maximum between 75 and 80 s. The dynamic pressure indicates the magnitude of the aerodynamic forces. Therefore, the most critical phenomena can be expected in the first part of the evaluated range.

A first approach to this analysis is to overlap the mission profiles in terms of dynamic pressure.All four panels were analyzed in fig. 6.25 in which it can be seen that panels 2, 3 and 4 have a critical dynamic pressure that is much greater than the mission profile. Panel 1 has a lower critical dynamic pressure than that of the mission profile in the first part of the mission. This panel, therefore, seems unstable in the first part of the Mach range.To investigate the nature of the flutter and to confirm this instability in the first part of the mission, an analysis was carried out of the whole mission profile. The evolution of the frequencies and the damping was investigated, point by point, over the whole range. fig. 6.26 shows the results of the analysis. The first two frequencies were merged in the first part of the mission and the damping was positive. The instability occurred up to 85 s, where the two frequencies split and the damping went back to being negative. If the time is increased, the damping becomes smaller and smaller due to the decrease in the density of the air.The results show that the variable flow conditions can affect the aeroelastic instabilities to a great extent.

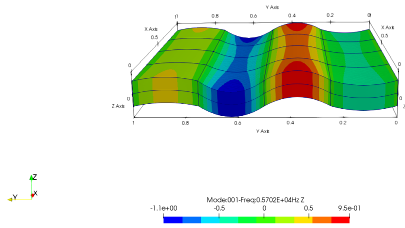

(a) B.C type:b
Mode:001-Freq:0.5702E+04Hz
Z-magnitude

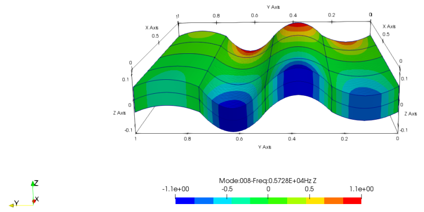

(b) B.C type:b
Mode:008-Freq:0.5728E+04Hz
Z-magnitude

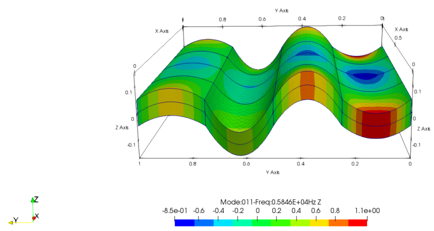

(c) B.C type:b
Mode:011-Freq:0.5846E+04Hz
Z-magnitude

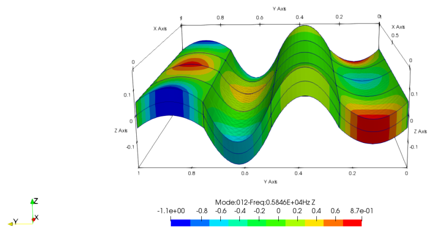

(d) B.C type:b
Mode:012-Freq:0.5846E+04Hz
Z-magnitude

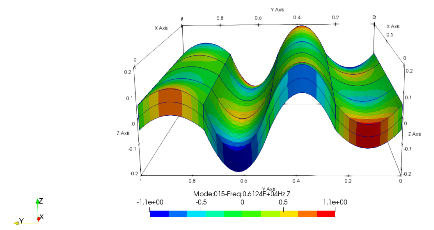

(e) B.C type:b
Mode:015-Freq:0.6124E+04Hz
Z-magnitude

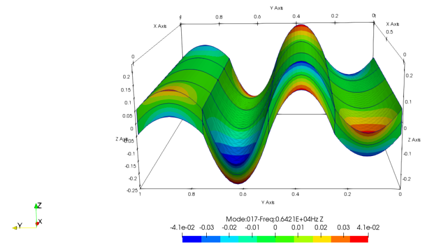

(f) B.C type:b
Mode:017-Freq:0.6421E+04Hz
Z-magnitude

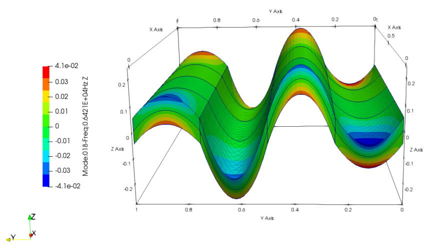

(g) B.C type:b
Mode:018-Freq:0.6421E+04Hz
Z-magnitude

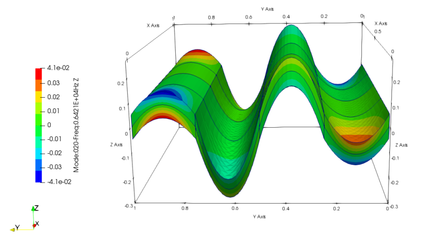

(h) B.C type:b
Mode:020-Freq:0.6421E+04Hz
Z-magnitude

Figure 6.9: 8 Mode shapes for from mode 16Q16+2LD1 of B.C Type: b ,each figure selected was changed by its model dynamic frequency ,magnitude Z and scale factor

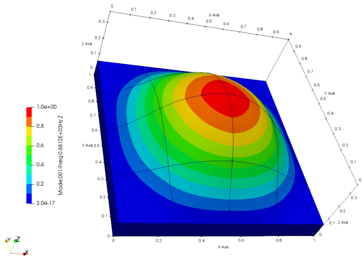

(a) B.C type:c
Mode:001-Freq:0.8812E+03Hz
Z-magnitude

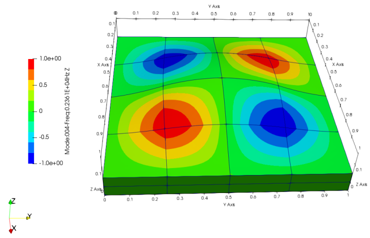

(b) B.C type:c
Mode:004-Freq:0.2361E+04Hz
Z-magnitude

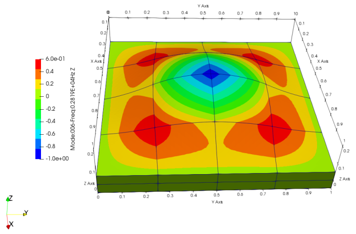

(c) B.C type:c
Mode:006-Freq:0.2819E+04Hz
Z-magnitude

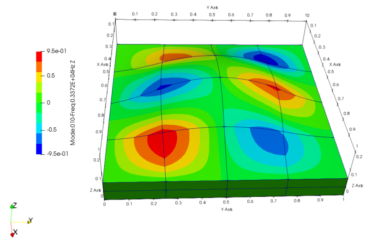

(d) B.C type:c
Mode:010-Freq:0.3372E+04Hz
Z-magnitude

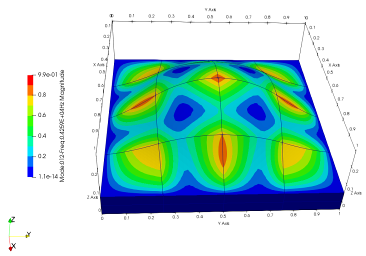

(e) B.C type:c
Mode:012-Freq:0.4259E+04Hz
Z-magnitude

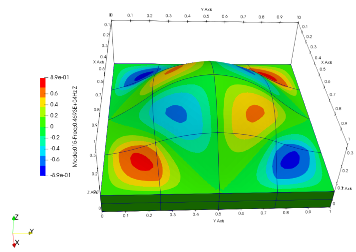

(f) B.C type:c
Mode:015-Freq:0.4693E+04Hz
Z-magnitude

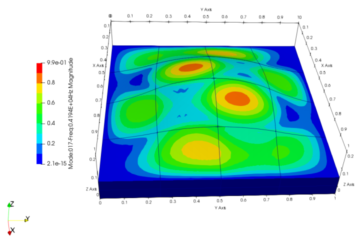

(g) B.C type:c
Mode:017-Freq:0.4194E+04Hz
Z-magnitude

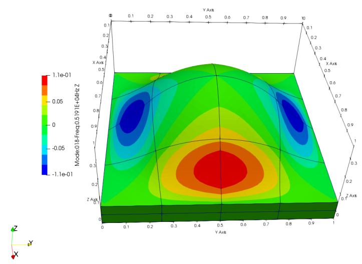

(h) B.C type:c
Mode:018-Freq:0.5191E+04Hz
Z-magnitude

Figure 6.10: 8 Mode shapes for from mode 16Q16+2LD1 of B.C Type: c ,each figure selected was changed by its model dynamic frequency ,magnitude Z and scale factor

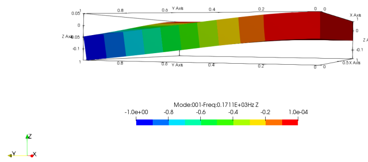

(a) B.C type:d
Mode:001-Freq:0.1711E+03Hz
Z-magnitude

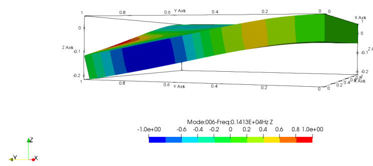

(b) B.C type:d
Mode:006-Freq:0.1413E+04Hz
Z-magnitude

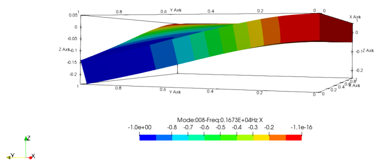

(c) B.C type:d
Mode:008-Freq:0.1673E+04Hz
Z-magnitude

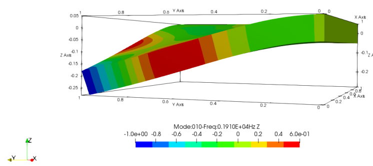

(d) B.C type:d
Mode:010-Freq:0.1910E+04Hz
Z-magnitude

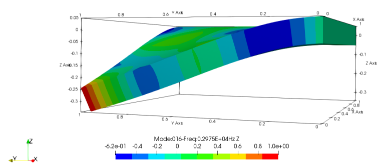

(e) B.C type:d
Mode:016-Freq:0.2975E+04Hz
Z-magnitude

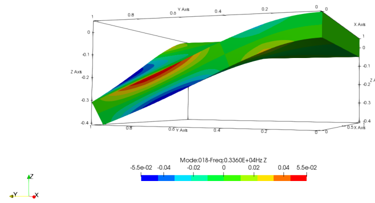

(f) B.C type:d
Mode:018-Freq:0.3360E+04Hz
Z-magnitude

Figure 6.11: 6 Mode shapes for from mode 16Q16+2LD1 of B.C Type: d ,each figure selected was changed by its model dynamic frequency ,magnitude Z and scale factor

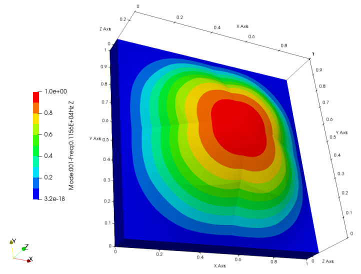

(a) B.C type:e
Mode:001-Freq:0.1156E+04Hz
Z-magnitude

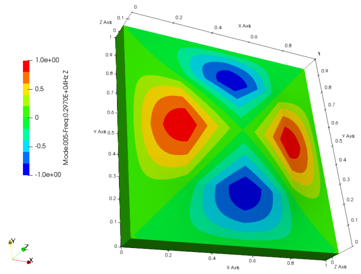

(b) B.C type:e
Mode:005-Freq:0.2970E+04Hz
Z-magnitude

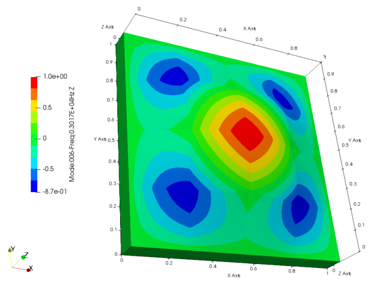

(c) B.C type:e
Mode:006-Freq:0.3017E+04Hz
Z-magnitude

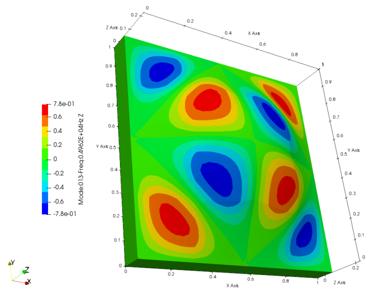

(d) B.C type:e
Mode:013-Freq:0.4962E+04Hz
Z-magnitude

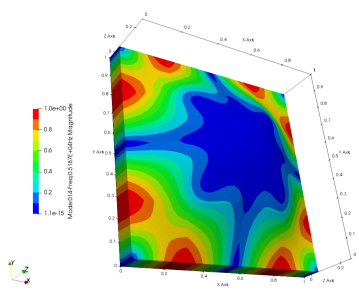

(e) B.C type:e
Mode:014-Freq:0.5187E+04Hz
Z-magnitude

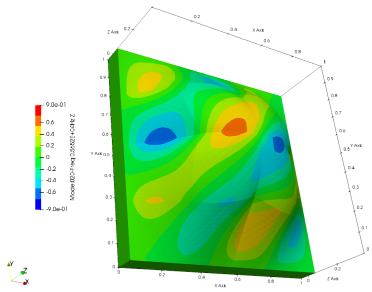

(f) B.C type:e
Mode:020-Freq:0.5652E+04Hz
Z-magnitude

Figure 6.12: 6 Mode shapes for from mode 16Q16+2LD1 of B.C Type: e ,each figure selected was changed by its model dynamic frequency ,magnitude Z and scale factor

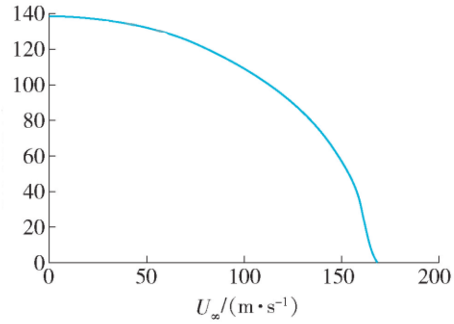

Figure 6.13: natural frequencies with respect to the flow velocity

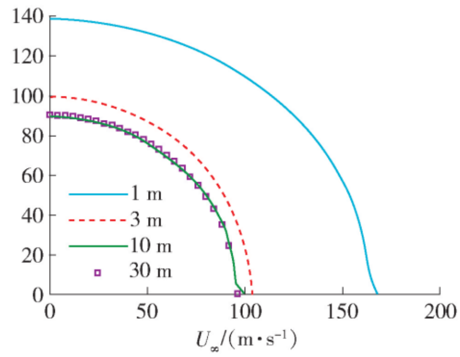

Figure 6.14: natural frequencies with respect to the flow velocity of different panel width

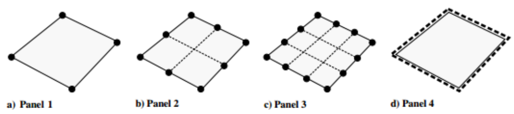

Figure 6.15: Boundary condition configurations

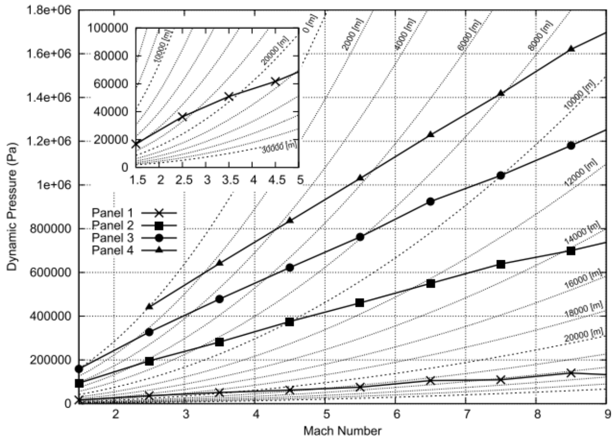

Figure 6.16: Flutter boundaries for the different panels. defined as $q = \frac{1}{2}\rho_{\text{now}} V_{\infty}^2$

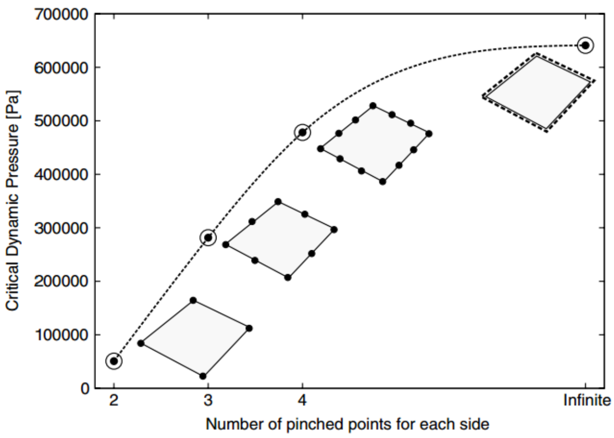

Figure 6.17: Effect of the number of pinched points on the flutter boundary

Instability point	Panel 1 (20,000 m)		Panel 2 (8000 m)		Panel 3 (8000 m)		Panel 4 (8000 m)	
	Mach	Frequency, Hz	Mach	Frequency, Hz	Mach	Frequency, Hz	Mach	Frequency, Hz
P-1	3.95	30.39	3.37	85.08	5.68	108.86	7.69	135.15
P-2	-	-	4.95	175.33	-	-	-	-
P-3	-	-	5.53	135.94	-	-	-	-
P-4	-	-	6.25	419.10	-	-	-	-

Figure 6.18: Critical Mach number and flutter frequencies for the different panels

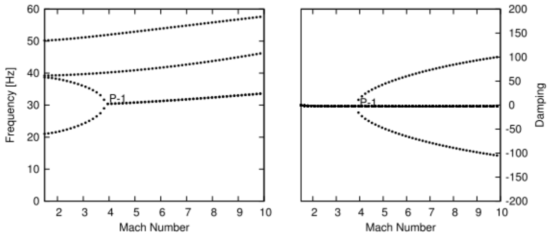

Figure 6.19: Panel 1 frequencies and damping at different Mach numbers at 20,000 m

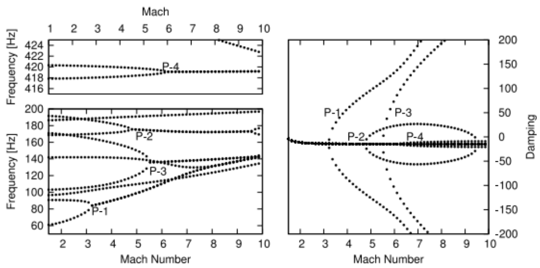

Figure 6.20: Panel 2 frequencies and damping at different Mach numbers at 8000 m

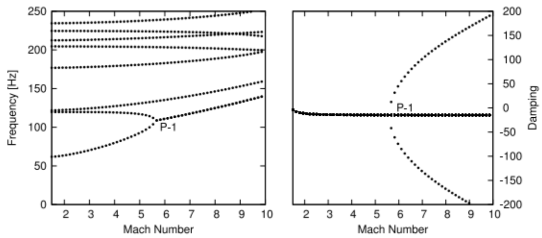

Figure 6.21: Panel 3 frequencies and damping at different Mach numbers at 8000 m

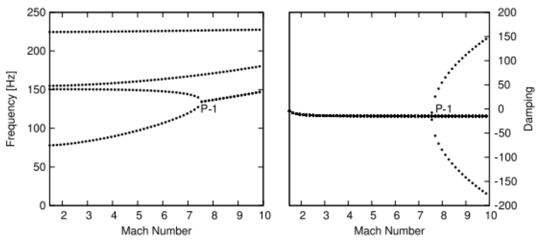

Figure 6.22: Panel 4 frequencies and damping at different Mach numbers at 8000 m

Time	Mach	Temperature, K	Density, kg/m^3	Sound speed, m/s	Altitude, m	Dynamic pressure, Pa
70.0	1.5	226.4	0.4389	301.6	9,500	44,924
73.3	1.83	216.65	0.3363	295.0	11,500	49,028
76.7	2.15	216.65	0.2454	295.0	13,500	49,382
80.0	2.48	216.65	0.1790	295.0	15,500	47,926
83.3	2.81	216.65	0.1306	295.0	17,500	44,892
86.7	3.14	216.65	0.0953	295.0	19,500	40,904
90.0	3.46	218.15	0.0691	296.0	21,500	36,261
93.3	3.79	220.15	0.0501	297.4	23,500	31,834
96.7	4.12	222.15	0.0365	298.7	25,500	27,656
100.0	4.45	224.15	0.0266	300.1	27,500	23,724
103.3	4.77	226.15	0.0195	301.4	29,500	20,161
106.7	5.10	228.15	0.0143	302.7	31,500	17,051
110.0	5.43	232.85	0.0104	305.9	33,500	14,347
113.3	5.75	238.45	0.0076	309.5	35,500	12,039
115.0	5.92	241.25	0.0065	311.3	36,500	11,042

Figure 6.23: Flow properties during the mission profile

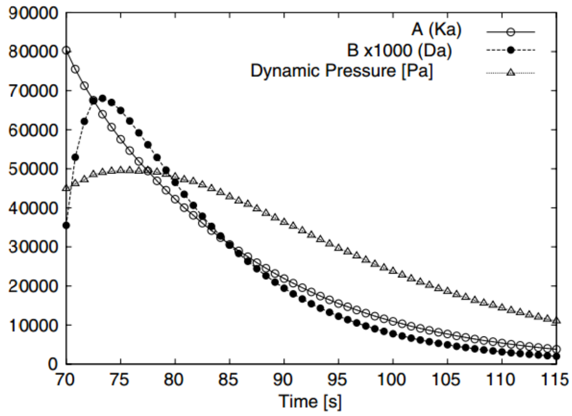

Figure 6.24: Piston theory parameter during the mission profile

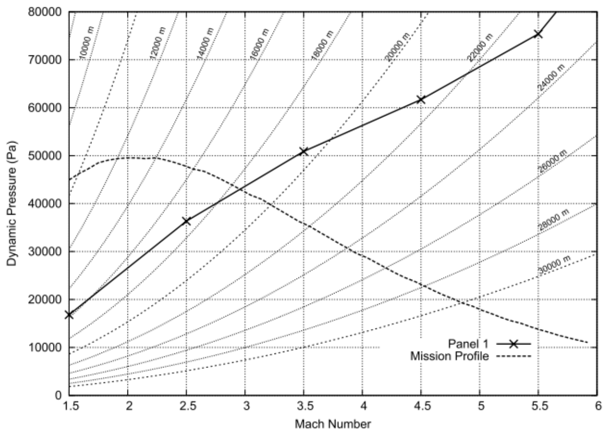

Figure 6.25: Mission profile and flutter boundary

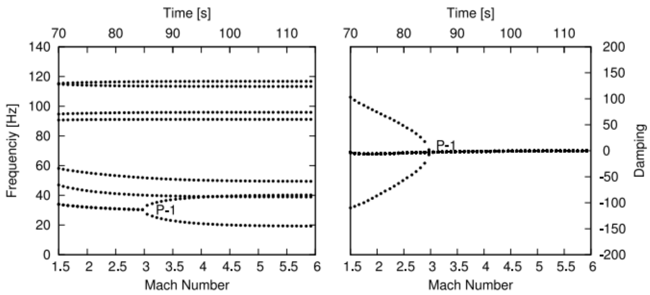

Figure 6.26: Panel 1 evolution of the frequencies and damping during the mission

Chapter 7

Conclusion and Outlook

In this paper, a two-dimensional models have been used in the derivation of refined aeroelastic models able to predict panel flutter of advanced structure in supersonic range with Piston theory.On the other hand,Carrera Unified Formulation (CUF) is used to perform theoritical analysis for composite laminates.
As the classical beam and plates theories have several limitations in the prediction of high order effects or in-plane deformations.Due to Carrera Unified Formulation allows any models to be derived using a compact and unified formulation. The high-efficiency of the CUF tool allows any order model to be derived.Chapter 2 the state of art illustrates the research methhos backgroud in those past years on panel flutter.simply list a comparasion on potential flow theory,Piston theory,N-S equation method,CFD methods.Also there are many methods of solving panel flutter conventional and unconventional differential equations,it depends the condition in real paractice.To tudy the aeroelastic stability of composite laminate structure under different airflow, in order to analyze it by solving the generalized eigenvalue problem through aeroelastic properties,and many parameters have been considered to investigate their effects on flutter boundaries.
In future ,a further study on hypersonic panel could be needed,because it needs much higher requirement under the higher speed, greater pressure load, higher temperature and thermal load, and the large deflection of the composite.In chapter 3,tunnel tests is disscussed ,because it is an important task for aeroelastic researchers to learn from previous experimental results and design more optimized wind tunnel tests to verify the theoretical analysis of panel flutter,and in study it is effected by boundary layer effects and amplitudes, stresses, and frequency of the flutter oscillation. Also high-Mach number flows are the most difficult to simulate properly because of the high temperatures and low dynamic pressures.
In chapter 4, an introduction of the Carrera Unified Formulation and the derivation of the characteristic matrices of the FEM for two-dimensional

models,the fundamental nuclei allow the matrices to be derived using an automatic procedure.A strong form solutions and the finite element approximation of the proposed CUF models. The Finite Element Method (FEM) still deserves important attentions due to its versatility and numerical efficiency. The various problems of the mechanics have been addressed, including static, free vibration and dynamic response problems of chapter 6,which is the bae of solving aeroelastic instability of composite laminate structure under different airflow, in order to analyze it by solving the generalized eigenvalue problem through aeroelastic properties in Chapter 4.
The results from the structural analyses and aeroelastic modes in chapter 6,they have highlighted the following key-features:The aeroelastic structural model used in the present thesis provide accurate results and are computationally respect to classical models in static analysis,free vibration analysis and dynamic response analysis.The CUF offers a reliable tool to derive any structural model using an efficient and compact formulation.Firstly,in the critical instability speed anaysis, all influencce factor including different structual configurations and different lamination angles are analyzed.A simple summary is:As the width of the plate increases along the b direction, the width of the three-dimensional plate increases,The critical instability speed approaches the two-dimensional plates'. As the velocity of the incoming flow increases,the natural frequency of the structural system decreases as the natural frequency decreases as small as zero, the laminated structural modes will be unstable, mainly due to airflow caused the stiffness of the structure is changed. As the lamination angle increases of panel gradually, the critical instability speed of the structure increases first and then decreases, and there is an optimal lamination angle.Therefore, the method presented in this paper can be used to calculate the optimal lamination angle of 3D composite laminates panel with any structual configuration.Secondly,according to literature the summaries as belows:The BC configuration had an important effect on the panel flutter phenomena. The flutter boundary increased with the number of pinched points and the modes involved in the instabilities were different for each configuration. All the flow parameters affected the flutter boundary. In the mission analysis, it was evident that the aeroelastic instabilities affected the space structure at low Mach numbers because of the high air density, whereas the aerodynamic forces were lower in the high Mach number regimes due to the low flow density.
Future outlook:Regarding the structural formulation, the most promising developments deal with the extension to more complex composite aircraft structures, non-linear analysis, including both large strains and displacements,and more complex specific configurations and composite panels of different Mach regions and flow conditions,as illustrated above of the influences by those parameters when studing on aeroelastic instability analysis.

Bibliography

[1] Earl H Dowell. *Aeroelasticity of plates and shells*, volume 1. Springer Science & Business Media, 1974.

[2] Liviu Librescu. *Elastostatics and kinetics of anisotropic and heterogeneous shell-type structures*, volume 43. Springer Science & Business Media, 1976.

[3] Xianzong Meng, Zhengyin Ye, Kun Ye, and Cheng Liu. Analysis on location of maximum vibration amplitude in panel flutter. *Proceedings of the Institution of Mechanical Engineers, Part G: Journal of Aerospace Engineering*, 234:095441001987652, 09 2019.

[4] Dewey Hodges and G. Pierce. *Introduction to Structural Dynamics and Aeroelasticity*. 01 2011.

[5] Toru Nishimura. Hiroaki Katori. Vibration and dynamic stability of anisotropic plates : Free vibration and panel flutter,58(546):330-334 January 1992TRANSACTIONS OF THE JAPAN SOCIETY OF MECHANICAL ENGINEERS,1992. DOI:10.1299/kikaic.58.330.

[6] Z.-C Yang, W. Xia, and R.-L Zhang. The effects of thermal distribution on the composite panel flutter. 31:850–854, 03 2010.

[7] Guoyong Zheng and Yiren Yang. Chaotic motions and limit cycle flutter of two-dimensional wing in supersonic flow. *Acta Mechanica Solida Sinica - ACTA MECH SOLIDA SINICA*, 21:441–448, 10 2008.

[8] James Njuguna. Flutter prediction, suppression and control in aircraft composite wings as a design prerequisite: A survey. *Structural Control and Health Monitoring*, 14:715 – 758, 08 2007.

[9] Shore C P. Gray C E, Mei C. A finite element method for large amplitude two-dimentional panel flutter at hypersonic speed,29(2):290-298,AIAA Journal,1991.

[10] Mei C. Xue D Y. finite element nonliear panel flutter with arbitrary temperature in supersonic flow,31(1):154-162,AIAA Journal,1993.

[11] Dowell E H. Nonlinear flutter of curved plates,7(3):424-431,AIAA Journal,1969.

[12] Weifang Z. Yuying H. Analysis of large elastic-plastic deformation of anisotropic medium thickness plate and shell,12(3):77-85,AIAA Journal,1995.

[13] Raj Bharati, M. Filippi, Prashanta K Mahato, and Erasmo Carrera. Flutter analysis of laminated composite structures using carrera unified formulation. *Composite Structures*, 253:112759, 08 2020.

[14] Zhansheng L. Yunfeng Z. Analysis of nonlinear flutter hysteresis of viscous wall panel,26(7):101-105,Vibration and shock,2007.

[15] Sameer Mulani. Nonlinear aeroelastic analysis of in-plane functionally graded metal nanocomposite thin panels in supersonic flow, 03 2019.

[16] Chonghui S. Huagang L. Nonlinear flutter and random response of composite panel embedded in shape memory alloy in thermal-aero-acoustic coupled field,Aerospace Science and Technology,2020.

[17] Dengqing C. Research on thermal buckling and flutter of composite panel with sma wire laying in supersonic flow,2015.

[18] Dowell E H. Nonlinear oscillation of a fluttering plate,4(7):1267-1275,AIAA Journal,1966.

[19] Kamal Hassan. Linear solution of the problem of panel flutter. *Mechanics Based Design of Structures and Machines - MECH BASED DES STRUCT MECH*, 22:37–47, 01 1994.

[20] Yushu C. Yinshan L. Nonlinear vibration of orthotropic circular plate,23(2):148-151,Mechanical strength,2001.

[21] Yuji Matsuzaki and Shigeo Kobayashi. Nonlinear analysis of supersonic panel flutter of circular cylindrical shells. *Journal of the Japan Society for Aeronautical and Space Sciences*, 18:103–111, 01 1970.

[22] Sergey Shitov and Vasily Vedeneev. Flutter of rectangular simply supported plates at low supersonic speeds. *Journal of Fluids and Structures*, 69:154–173, 02 2017.

[23] Chad Gibbs, Ivan Wang, and E.H. Dowell. Theory and experiment for flutter of a rectangular plate with a fixed leading edge in three-dimensional axial flow. *Journal of Fluids and Structures*, 34:68–83, 10 2012.

[24] Huagang Lin, D.Q. Cao, and Yuqian Xu. Vibration characteristics and thermoelastic analysis of the supersonic composite laminated panel with arbitrary elastic boundaries. *Proceedings of the Institution of Mechanical Engineers, Part G: Journal of Aerospace Engineering*, 233:095441001878148, 06 2018.

[25] Dowell E H. Nonlinear oscillation of a fluttering plates,5(10):1856-1862,AIAA Journal,1967.

[26] Johnson E H. Rodden W P. Msc/nastran aeroelastic analysis user's guide,1994.

[27] Chen R. Mei C, Abdel Motagaly K. Review of nonlinear panel flutter at supersonic and hypersonic speed,52(10):321-332,Applied Mechanics Review,1999.

[28] Lighthill M J. Oscillating airfoils at high mach numbers,20(6): 402-406,Journal of Aeronautical Science,1953.

[29] Zartarian G. Ashley H. Piston theory a new aerodynamic tool for the aeroelastician,23(10): 1109-1118,Journal of Aeronautical Science,1956.

[30] Cao J. Chen J S. An approximate calculation method for unsteady aerodynamic forces of supersonic and hypersonic airfoils,1990.

[31] Song W L. Yang B Y. The aerodynamic force expression of flutter on lifting surface with high angle of attack is presented by applying the local flow piston theory,1999.

[32] Ye zhengyin. Zhang W. Research on aeroelastic calculation method based on local flow piston theory,2005.

[33] Yang B Y. Liu C F, Li D H. The flutter calculation of the fuselage,wing,rudder assembly with hypersonic variable attack angle,32(8): 1663-1669,Journal of Astronautics,2011.

[34] Zhang Z. Guo J. Nonlinear aeroelastic analysis of wall panels based on piston theory,STRUCTURE ENVIRONMENT ENGINEERING,2018.

[35] Fithen R. Gordnier R E. Coupling of a nonlinear finite element structural method with a navier-stokes solver,81: 75-89,Computers and Structurals,2003.

[36] Friedmann P P. Nydick. Hypersonic panel flutter studies on curved panels,1995.

[37] King P I. Lucia D J, Beran P S. Reduced order modeling of an elastic panel in transonic flow,2002.

[38] Debortoli A L. Aeroelastic analysis of panels in compressible flows,20:189-195,Journal of fluids and structures,2005.

[39] Zheng Q. Selvam R P, Qu Z Q. Three dimentional nonlinear panel flutter at supersonic euler flow,2002.

[40] Visbal M R. Gordnier R E. Development of a three dimentional viscous aeroelastic solver for nonlinear panel flutter,16(4):497-527,Journal of fluids and structures,2002.

[41] Gordnier R E. Visbal M R. Numerical simulation of the interaction of a transitional boundary layer with a 2d flexible panel in the subsonic regime,19:881-903,Journal of fluids and structures,2004.

[42] Jordan P F. The physical nature of panel flutter,72:34-38,Aero Digest,1956.

[43] Dowell E H. A review of the aeroelastic stability of plates and shells,8:385-399,AIAA Journal,1970.

[44] Mei C. Cheng G F. Flow angle,temperature and aerodynamic damping on supersonic panel flutter stability boundary,2002.

[45] Marzocca P. Librescu L. Linear/nonlinear supersonic panel flutter in a high temperature field,41(4):918-924,Journal of Aircraft,2004.

[46] Udrescu R. Surace G. Finite element analysis of the fluttering panels excited by external forces,224(5):917-935,Journal of Sound and Vibration,1999.

[47] Mei C. Gray C E. A finite element method for large amplitude 2d panel flutter at hypersonic speed,29(2):290-298,AIAA Journal,1991.

[48] Mcintosh S C. Effect of hypersonic nonlinear aerodynamic loading on panel flutter,11(1):29-32,AIAA Journal,1973.

[49] Mcintosh S C. Eastep F E. Analysis of nonlinear panel flutter and response under random excitation or noonlinear aerodynamic loading,9(3):411-418,AIAA Journal,1971.

[50] Powell K G. Mcnamara J J, Friedmann P P. Three dimentional aeroelastic and aerothermoelastic behavior in hypersonic flow,2005.

[51] Li W L. Vibration analysis of rectangular plates with general elastic boundary supports,273(3):619-635,Journal Sound and vibration,2004.

[52] Su J P. zhou K. Aerothermoelastic flutter analysis of supersonic moderately thick orthotropic plates with general boundary conditions,141:46-57,International Journal of Mechanical Science,2018.

[53] Chen R R. Ho M T. Wind tunnel testing of panel flutter control using piezoelectric actuation and iterative gain tuning,1997.

[54] Li F M. Song Z G. Aerothermoelastic analysis of lattice sandwich composite panels in supersonic airflow ,51: 877-891,2016.

[55] Haddadpour H. Mahmoudkhan S, Sadeghmanesh M. Aero-thermo-elastic stability analysis of sandwich viscoelastic cylindrical shells in supersonic airflow,147: 185-196,Composite Structures,2016.

[56] Vedeneev V V. Flutter of a wide strip plate in a supersonic gas flow,40(5):805-817,Fluid Dynamics,2005.

[57] Halfman R L. Bisplinghoff R L, Ashley H. Aeroelasticity,285-326,Cambridge University Press,1995.

[58] Perkin B. Dugundji J, Dowell E H. Subsonic flutter of panels on continuous elastic foundations,5(1): 1146-1154,AIAA Journal,1963.

[59] Dowell E H. Tang D M. Limit cycle oscillations of two-dimensional panels in low subsonic flow,37(7):1199-1209,International Journal of Non-Linear Mechanics,2002.

[60] Tang L. Zhao W, Paidoussis M P. Theoretical and experimental investigations of the dynamics of cantilevered flexible plates subjected to axial flow,331(3): 575-587,Journal of Sound and Vibration,2012.

[61] Uali E. Korbahti B. Vibrations of an anisotropic plate under fluid flow in a channel,13(8): 1191-1204,Journal of Vibration and Control,2007.

[62] Li F M. Yao G. Nonlinear vibration of a two dimensional composite laminated plate in subsonic airflow,21(4):662-669,Journal of Vibration and Control,2015.

[63] PERKIN B. DUGUNDJI J, DOWELL E H. Subsonic flutter of panels on continuous elastic foundations ,5(1): 1146-1154, AIAA Journal,1963.

[64] Bergman L A. Lee Y S, Vakakis A F. Suppressing aeroelastic instability using broadband passive targeted energy transfers ,45(3):693—711, AIAA Journal,2007.

[65] Bergman L A. Lee Y S, Vakakis A F. Enhancing the robustness of aeroelastic instability suppression using multi-degree-of-freedom nonlinear energy sinks,46(6):1371-1394, AIAA Journal,2008.

[66] Qatu MS. Recent research advances in the dynamic behavior of shells,applied mechanics reviews,55:325-350,2002.

[67] Reddy JN. Exact solutions of moderately thick laminated shells,110:794-809,Journal of Engineering,1984.

[68] Vlachoutsis S. Shear correction factors for plates and shells,33:1537-1552,1992.

[69] Chate A. Rikards R. Vibration and damping analysis of laminated composite and sandwich shells,4:209-232,1997.

[70] Masud A Kapania RK. Yang HTY, Saigal S. A survey of recent shell finite elements,47:101-127,2000.

[71] Mei C. Dixon I.R. Finite element analysis of large amplitude panel flutter of thin laminates,31:701-707,AIAA Journal,1993.

[72] Mei C. Gray J, C. Large amplitude finite element flutter analysis of composite panels in hypersonic flow,31:1090-1099,AIAA Journal,1993.

[73] Mei C Shore C.P. Gray J, C. Finite element method for large amplitude two dimensional panel flutter at hypersonic speed,29(2):290-298,AIAA Journal,1991.

[74] Gibson F. Jehad F.A, Ibrahim R.A. Nonlinear flutter of orthotropic composite panel under aerodynamic heating,31(8):1478-1488,AIAA Journal,1993.

[75] Guran A. Kouchakzadeh M.A, Rasekn M. Nonlinear flutter of three dimentional general laminated composite plates,2007.

[76] Haddadpour H. Kouchakzadeh M.A, Rasekn M. Panel flutter analysis of general laminated composite plates,92(12):2906-2915,composite structure,2010.

[77] Mei C. Abdel motaglay K, Chen R. Nonlinear flutter of composite panels under yawed supersonic flow with finite element method,37(9):1025-1032,AIAA Journal,1999.

[78] Ganapathi M. Singha M K. A parametric study on supersonic flutter behavior of laminated composite skew flat panel,69(1):55-63,Composite structure,2005.

[79] Xia W. Yang Z C, Tang G H. Thermal flutter analysis of composite panel with uncertain parameter,29(3):1047-1052,Journal of Astronautics,2008.

[80] Yang Z C. Gao Y. Effects of flow yaw angle on thermal flutter characteristic of composite panels with differet shapes,33(11):65-69,Journal of Vibration and Shock,2014.

[81] J. A. Cockburn. An experimental program for the investigation of panel instabilities caused by shock waves, NASA-CR-100354,1968,Contractor Report (CR). https://ntrs.nasa.gov/api/citations/19690010614/downloads/19690010614.pdf. Accessed: 2020-12-20.

[82] H. L. Bohon. Panel flutter tests on full scale x-15 lower vertical stabilizer at mach number of 3.0, NASA TN D-1385,1962. Accessed: 2020-12-20.

[83] R. L. Rich. Preliminary skin panel flutter tests. the boeing company, Document D2-8148,1962.

[84] R. L.; Mortvedt and R. T. Wagner. Transonic, supersonic panel flutter test. the boeing company, Document D2-81095,1964.

[85] T. R. Golden, C. T.; Hager and L. L. Sherman. Orthotropic panel flutter analysis correlation, x-20. the boeing company, D2-8 1301,1964.

[86] Anon. 624a panel flutter analysis. u.s. air force, space systems division,CR-64-87,May 1964.

[87] J . J. Nichols. Final report: Saturn v, s-ivb panel flutter qualification test,NASA TN D-5439,1969.

[88] Anon. Natural vibration modal analysis,NASA Space Vehicle Design Criteria (Structures)NASA SP-8012,1968.

[89] Anon. Structural vibration prediction,NASA Space Vehicle Design Criteria(Structures)NASA SP-8050,1970.

[90] Carrera Erasmo and Zappino Enrico. Aeroelastic analysis of versatile thermal insulation (vti) panels with pinched boundary conditions,2013.

[91] Davis John G. Tenney, Darrel R. Nasa role in development of advanced composite materials for aircraft and space structures,nasa/cr-2019-220267,2019.

[92] et al. Odegard, G. M. Equivalent continuum modeling of nano-structured materials,62:1869-1880,Composites Science and Technology,2002.

[93] R. B. Pipes and P. Hubert. Helical carbon nanotube arrays: Mechanical properties,63(3):419-428,Composites Science and Technology,2002.

[94] P. Hubert R. B. Pipes, S. J. V. Frankland and E. Saether. Self-consistent properties of the swcn and hexagonal arrays as composite reinforcements,63(10):1349-1358,Composites Science and Technology,2003.

[95] R. B. Pipes and P. Hubert. Scale effects in carbon nanostructures: Self-similar analysis,nano letter 3(2):239-243,Composites Science and Technology.

[96] R. B. Pipes and P. Hubert. Helical carbon nanotube arrays: Mechanical properties,62(3):418-28,Composites Science and Technology,2002.

[97] R. B. Pipes and P. Hubert. Helical carbon nanotube arrays: Thermal expansion,63(11):1571-79,Composites Science and Technology,2003.

[98] P. J. F. Harris. Carbon nanotubes and related structures,Cambridge University Press.

[99] Terry M Harris. Aeroelasticity research at wright—patterson air force base from 1953—1993,Journal of Aircraft,40(5):813—819,2003.

[100] Frederick W Gibson. Flutter investigation of models having the planform of the north american x-15 airplane wing over a range of mach number from 0.56 to 7.3,NASA-TM-X-460,1961.

[101] Homer G Morgan. Flutter tests of some simple models at 8 mach number of 7.2 in helium flow ,NASA MEMO 4-8-59L,1959.

[102] Robert C Goetz. Hypersonic flutter analysis using measured static aerodynamic derivatives, and comparison with experiment,NASA-TN-13-5233,1969.

[103] Perry W Hanson. Aerodynamic effects of some configuration variables on the aeroelastic characteristics of lifting surfaces at mach numbers from 0.7 to 6.86,NASA-TN-D-984,1961.

[104] Lou S Young. Effects of angle of attack and thickness ratio on the flutter of a rigid unswept diamond-airfoil-section wing at a mach number of 10.0,NASA-TN-D-1380,1962.

[105] A Gerald Rainey. Aeroelastic research at high speeds,NASA-TM-X-326,1960.

[106] Robert C Goetz. Effects of leading—edge bluntness on flutter characteristics of some square-plahform double-wedge airfoils at a mach number of 15.4,NASA-TN-D-1487,1962.

[107] Robert C Goetz. Effects of leading—edge sweep on flutter characteristics of some delta-planform surfaces at a mach mumber of 15.4,NASA-TN-D-2360,1964.

[108] Robert V Doggett Jr. Experimental flutter investigation of some simple models of a boost-glide-vehicle wing at mach numbers of 3.0 and 7.3,NASA-TM-X-37,1959.

[109] Robert C Goetz. Experimental flutter study of a wing-fuselage configuration at a mach number of 15.4 and comparison with theory,NASA-TN-D-3046,1965.

[110] Moeijo S Hong. Evaluation of cfl3d for unsteady pressure and flutter predictions,AIAA-2003-1923,2003.

[111] Arslan A E. Hartwich P M, Dobbs S K. Navier-stokes computations of limit cycle oscillations for a b-1 like configuration,Journal of Aircraft,38(2):239—247,2001.

[112] Ericsson L E. Comment on navier-stokes computations of limit cycle oscillations for a b-1 like configuration,Journal of Aircraft,39(3): 519,2002.

[113] Arslan A E. Hartwich P M, Dobbs S K. Comment on navier-stokes computations of limit—cycle oscillations for a b-1 like configuration,Journal of Aircraft,39(3): 519, 520,2002.

[114] E. H. Dowell. Panel flutter, NASA-SP-8004,1972,Special Publication (SP). https://ntrs.nasa.gov/api/citations/19730003205/downloads/19730003205.pdf. Accessed: 2020-12-20.

[115] Laura. Vernon. In-flight investigation of a rotating cylinder-based structural excitation system for flutter testing, NASA-TM-4512,1993.

[116] Martin J. Brenner and Eric Feron. Wavelet analysis of f/a-18 aeroelastic and aeroservoelastic flight test data, NASA-TM-4793,1997.

[117] D.T.Grossman. H.Katz, F.G.Foppe. F-15 flight flutter test program,413-431, NASA-SP-415,1976.

[118] J.T.Weissenberger. N.H.Zimmermann. Prediction of flutter onset speed based on flight testing at subcritical speed,190-202, Journal of Aircraft,1964.

[119] B.H.K.Lee. S.J.Price. Evaluation and extension of the flutter margin methods for flight flutter prediction,30(3):395-402, Journal of Aircraft,1993.

[120] J.R.Wright M.J.Schofield. J.E.Cooper, P.R.Emmett. Envelope function a tool for analyzing flutter data,30(3):785-790, Journal of Aircraft,1993.

[121] Erasmo Carrera, Maria Cinefra, Marco Petrolo, and Enrico Zappino. Finite element analysis of structures through unified formulation,2014.

[122] Laurent Dala Marius-Corné Meijer. A generalized formulation and review of piston theory for airfoils,2016.

[123] W. D. Hayes. On hypersonic similitude,pp. 105–106,1947.

[124] J. P. Chawla. Aeroelastic instability at high mach number,pp. 246-258,Journal of the Aerospace Sciences,1958.

[125] J. P. Chawla. Aeroelastic instability at high mach number,pp. 246-258,Journal of the Aerospace Sciences,1958.

[126] Malcom H. Rodden W. P, Farkas E. F. Aerodynamic influence coefficients from piston theory: Analytical development and computational procedure,tdr-169(3230-11)tn-2,1962.

[127] Huckel V. Morgan H. G, Runyan H. L. Theoretical considerations of flutter at high mach numbers,pp:371–381,Journal of the Aerospace Sciences,1958.

[128] Erasmo Carrera and Enrico Zappino. Aeroelastic analysis of pinched panels in supersonic flow changing with altitude. *Journal of Spacecraft and Rockets*, 51, 12 2013.

[129] H. Krause. Flattern flacher schalen bei uberschallanstromung,1998.

[130] Saturn v flight manual,NASA Rept. MSFC-MAN-503,1968.

[131] Ren Tao and Zhao Lei. Analysis of aeroelastic stability of composite laminated plate structure in subsonic air flow,2018.